TÉCNICO LISBOA

Cancer therapies based on Optimal Control methods

Elisa Susana Martins Pacheco

Thesis to obtain the Master of Science Degree in

Biomedical Engineering

Supervisor(s): Prof. Dr. João Manuel Lage de Miranda Lemos
Prof. Dr. Luís Marques da Costa

Examination Committee

Chairperson: Prof. Dr. João Miguel Raposo Sanches
Supervisor: Prof. Dr. João Manuel Lage de Miranda Lemos
Member of the Committee: Prof. Dr. Susana de Almeida Mendes Vinga Martins

December 2017

Mother, more than anyone I must be thankful to, you are the one who deserves it the most. This is not my accomplishment, it is yours. Everything I am, is because of you! With all my love.

Acknowledgments

I would like to express my gratitude to my master thesis advisor Prof. João Miranda Lemos for all the wise guidance, support and extensive knowledge. Throughout this long ride, Prof.Lemos managed to keep me motivated and was always there whenever I ran into a trouble or had a question. It has been a pleasure to work under your advice! A sincere thanks for this opportunity!

Several other people have been important, in a way or another, to the completeness of this challenging master thesis. A sincere thanks to Prof.Irina Alho and Juliet Ribot, who have helped me with some though questions regarding cancer immunology. I would also like to thank my laboratory colleagues, specially Francisco Teles, who have helped me with SIMULINK^{TM} and gave me some advice regarding my Matlab^{TM} code, and Gonçalo Afonso, who have ran my model in the algorithm developed during his master thesis. I also would like to thank my close friends Fabiana Silva, for all the medical advice and for her valuable corrections in my master thesis introduction, and to Patrícia Ferreira, who besides having followed all the steps of this entire master thesis, have been an incalculable help to overcome the several obstacles that have arisen. Patrícia Ferreira, thank you with all my heart! Finally, I would like to thank Cristiano Domingos for his help with Illustrator and Hugo Magalhães for his advice on optimal control numerical methods.

A special thank goes to the stackexchange and mathworks community for their help with questions regarding Latex and Matlab and to IST and INESC-ID for the material support.

I must express my very profound gratitude to my friends and brothers-in-arms Vanessa Lopes, José Portela, Mariana Elyseu, Joana Capacete and to my brother and friend Jaime Pacheco, who have always supported me. None of this would have been possible without you all! Last but not least, I would like to acknowledge my family, particularly my mother Glória Frade for her unfailing support and continuous encouragement not only during the course of this mater thesis, but also during my whole life. I will always be grateful for your love!

This master thesis has been performed in the framework of the task 7 of the project PERSEIDS – Personalizing cancer therapy through integrated modeling and decision PTDC/EMS-SIS/0642/2014 and funded by the Portuguese Foundation of Science and Technology (FCT).

Resumo

Actualmente o cancro é uma das principais causas de morte no mundo. Estima-se que a sua incidência aumente devido ao envelhecimento global da população. Relativamente às terapêuticas anticancerígenas, o insucesso da quimioterapia é ainda o desenvolvimento de resistência por parte das células tumorais. O planeamento de protocolos terapêuticos não é adaptado ao doente, mas sim um resultado de tentativa e erro. Existe, pois, uma necessidade evidente do uso de técnicas de modelação matemática e optimização destes protocolos terapêuticos *in silico*.

Nesta dissertação é proposto pela primeira vez um modelo matemático de crescimento tumoral que combina quimioterapia, desenvolvimento de resistência proporcional à concentração sanguínea de quimioterapia, imunoterapia e resposta imune. Uma versão modificada da hipótese de Norton-Simon é também sugerida. Posteriormente, os problemas de controlo óptimo são formulados e dois índices de desempenho (linear e quadrático no controlo) são otimizados usando métodos numéricos baseados no princípio de Pontryagin. As equações de estado e adjunta são integradas e o Hamiltoniano é otimizado em função das variáveis de controlo. Para este fim, dois métodos numéricos são adaptados e melhorados. Finalmente, são apresentadas simulações numéricas assim como os protocolos ótimos de tratamento para quimioterapia, imunoterapia e terapia combinada. Esta última erradica tumores impossíveis de serem eliminados através da administração isolada de imunoterapia ou quimioterapia. O sistema imunitário é de facto essencial para a eficácia da quimioterapia da mesma forma que a modelação da resistência tumoral é fundamental para o planeamento de um protocolo de tratamento adequado.

Palavras-chave: Controlo ótimo, Resistência à quimioterapia, Imunoterapia, Terapêutica combinada, Princípio de Pontryagin.

Abstract

Besides being an inevitability, cancer is among the leading causes of death worldwide and its incidence is expected to increase due to population ageing. At the same time, chemotherapy resistance onset continues to be the major reason for chemotherapy failing. Moreover, the schedule design of anticancer treatments are not patient tailored but rather based on trial and error approaches. There is an evident need for *in silico* mathematical modelling and optimization of treatments protocols.

Given the important role of the immune system in chemotherapy efficacy, in this dissertation, for the first time an ODE model combining chemotherapy, chemotherapy resistance, immunotherapy and immunosurveillance is proposed. Chemotherapy resistance is modeled as being proportional to chemotherapy blood concentration. A modified version of Norton-Simon hypothesis is also suggested. An optimal control problem is then formulated and two proper performance indexes (linear and quadratic) are optimized using numerical methods based on the Pontryagin's principle. Iteratively, the state and adjoint equations are integrated forwards and backwards, respectively, and the Hamiltonian function is optimized with respect to the control variables in a grid of time points. Two gradient based numerical methods are adapted and improved for this purpose. Finally, numerical simulations are presented and the optimal treatment schedule for chemotherapy, immunotherapy and combined therapy are analyzed. Combination therapy is able to eradicate tumors impossible to be eliminated by immunotherapy or chemotherapy alone. The immune system prove to be essential in chemotherapy efficacy and the modeling of tumor resistance fundamental to the design of proper treatment schedules.

Keywords: Optimal control, Chemotherapy resistance, Immunotherapy, Combination therapy, Nonlinear control, Pontyagin's principle.

Contents

List of Tables

List of Figures

Glossary

T_C	Cytotoxic T cells
T_H	Helper T cells
T_{reg}	Regulatory T cells
ACT	Adoptive Cell Transfer
APCs	Antigen-Presenting cells
AUC	Area Under the Curve
BFS	Backward-Forward Sweep
CIS	Compromised Immune System
DNA	Deoxyribonucleic Acid
HIS	Healthy Immune System
IL-2	Interleukin-2
IS	Immune System
KIR	Killer Inhibitory Receptor
MHC	Major Histocompatibility complex
MTD	Maximal Tolerated Doses
NK cells	Natural Killer cells
NLP	Nonlinear Programming Problem
NaN	Not a Number
ODE	Ordinary Differential Equation
TCR	T-cell Receptor
TILs	Tumor-Infiltrating Lymphocytes

Chapter 1

Introduction

The main goal of this master thesis is to design an optimal therapy schedule for a combination of two anticancer treatments, chemotherapy and immunotherapy, using a mathematical model in the form of ordinary differential equations (ODE) that considers both the development of resistance to chemotherapy and a complete immune response. This optimal schedule will be obtained through optimal control methods.

1.1 Motivation

Tumor formation is a complex process that usually occurs over a period of decades and rarely goes far enough to origin a clinically detectable tumor mass [1]. In fact, as the human body ages, several populations of cells throughout the body evolve into cells with increasingly neoplastic phenotypes as they complete some, but fortunately not all, of the steps of tumor progression [1]. Considering that most of the individuals pass away from other diseases before the full schedule of requisite events has been completed, they never realize that any of these tumor progression had been initiated in their bodies and that they could have become victims of cancer in the near future [1]. Cancers are therefore an inevitability. Some individuals do develop a neoplastic disease during their lifetime. The probability of this event varies dramatically from one individual to another, being affected by several variables, including hereditary predisposition, aging, lifestyle and environmental exposition [1]. Under these circumstances and given the increasing life expectancy and the advances in medicine, especially in developed countries, it is not surprising that cancer is currently among the leading causes of death worldwide [2]. Indeed, in 2012, 14.1 million of new cancer cases were diagnosed and there were 8.2 million cancer deaths and 32.6 million cancer patients within 5 years of diagnosis, worldwide [3]. Moreover, it is estimated that there will be 23.6 million new cases of cancer each year by 2030 [3].

Despite the significant investment in cancer research and the concomitant advance in the knowledge of cancer biology, the anticancer treatments currently in widespread use (surgery, radiotherapy and chemotherapy) were developed prior to 1975 and little progress has been made since then [1]. The inevitable development of cancer resistance to chemotherapy drugs, manifested as the outgrowth of

drug-resistant variant cell populations, continues to be the major reason for chemotherapy failure [1, 4]. This stresses the importance and interest of designing new therapeutic approaches to treat cancer or overcome some of the current barriers associated with the traditional approaches. Cancer immunotherapy, whose first use dates back to 1893 [5], manipulates the immune system of the patient in ways that enables it to kill the neoplastic cells that have emerged throughout the body [1]. Although it has advantages over other cancer therapy strategies, it lacks clinical efficacy [5]. At the same time, recent evidence clearly suggests that the combination of immunotherapy and chemotherapy for the treatment of cancer may provide substantial clinical benefits for patients with advanced disease [6, 7].

All things considered, which is the best time–concentration profile for the chemo- and immunotherapy administration in order to led to the maximum therapeutic effect for a specific patient? Experimentally, this question is impossible to answer. It would be infeasible and both unethical to test all the possible dosing schedules in pre-clinical or clinical studies [8] using exhaustive, medically guided, expensive trial-and-error approaches [9]. Besides, even tumors of the same type that arise in different patients, behave differently [1]. Each cancer patient is thus a new case. This is even more complicated in the case of novel therapies, whose underlying biological mechanisms and schedule guidelines are not well defined [9]. This is where modern math and oncology came across, making the personalized cancer medicine and the optimization of a patient therapeutic care a realistic ambition. Mathematical modeling would not only challenge current paradigms, redefine the knowledge of mechanisms driving tumorigenesis and shape future research in cancer biology, but also enable the systematic search through these millions of possible dose administration strategies and drug combination schedules tailored for the patient [8]. By applying for instance, theory of optimal control to an anticancer therapy mathematical model, an optimal therapy for a given patient can be found.

1.2 Objectives

The present master thesis has two main objectives:

1. Expansion of an existing ODE mathematical model of tumor growth [10] incorporating innate and adaptive immune responses with combination of immuno- and chemotherapy as anticancer therapies, to include tumor heterogeneity and chemotherapy-drug-resistance onset.

2. Therapy design for the expanded model using optimal control techniques.

These two goals are strongly interconnected. Indeed, optimal control theory is used to minimize a linear and quadratic performance objective imposed on the dynamical system obtained in point 1 subjected to some constraints [9]. Figure 1.1 illustrates this problem. Controls (chemo- and immunotherapeuthic agents) are applied to this dynamical system inducing a system response [9]. The performance index, in other words a performance measure of the system related with the agents toxicity and the number of cancer cells during and at the end of treatment, is evaluated based on the system response [9]. This objective function is then minimized through the Pontryagin's minimum principle. The process is repeated iteratively until some criteria are met and the optimal therapy schedule is obtained.

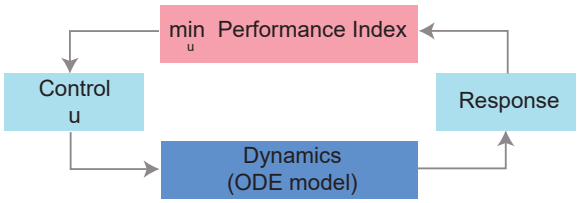

Figure 1.1: Structural elements involved in the optimal control problem approached in this master thesis. Adapted from [9].

1.3 Original contributions

In this master thesis, the development of an ODE mathematical model of tumor growth incorporating the immune response to the presence of tumor and both tumor heterogeneity and resistance to chemotherapeutic agents is proposed for the first time. Since the inevitable onset of chemotherapeutic-drug resistance is the major reason for the clinical failing of chemotherapy and the immune system response has a relevant role in the efficacy of this anticancer therapy, the model produced here has an important biological and clinical significance. Besides the development of this model, a modified version of the Norton-Simon hypothesis is also proposed. This version accounts for the process of cell division, according to which a pre-existent tumor cell gives rise to two new tumor cells.

For the sake of optimization of the performance objective, the linear Duda [11] algorithm is modified and improved. Moreover, a quadratic backpropagation algorithm for neural networks [12, 13] is also adapted and modified. Among these alterations are the consideration of initial weights based on the Hamiltonian gradient and some measures are taken in order to prevent the objective function from increasing between iterations.

1.4 Thesis outline

In chapter 2 some important key concepts underlying the biomedical background for the anticancer treatments and mathematical models of cancer development considered along this master thesis are discussed. A review of the tumor development, the immunosurveillance mechanism and three treatment modalities, chemotherapy, immunotherapy and the combination of both is made.

In chapter 3, a comprehensive review of the state of the art is made, regarding the models of cancer development which consider chemo- and immunotherapy. These models are reviewed by increasing complexity, both from a modeling and mathematical perspective. Finally, optimal control theory is revised.

In chapter 4, an expansion of the tumor growth models from de Pillis et al. [10] and Hahnfeldt et al. [14] is developed. The assumptions and behaviors inherent to the model developed are discussed and subsequently some numerical simulations are presented. These simulation are obtained using *Matlab*^{TM}.

In chapter 5, the linear and quadratic objectives used in optimal control are presented along with the numerical methods implemented in *Matlab*^{TM}. Afterwards, the importance of the modifications done to

these numerical methods are approached.

In chapter 6 the optimal schedule therapies obtained by applying the numerical algorithms from chapter 5 to the model developed in chapter 4 are presented and analyzed.

Finally in chapter 7, the conclusions are provided together with a discussion of the achievements and limitations of the work done and future work.

Chapter 2

Biomedical Background

This chapter presents a brief but indispensable overview concerning both cancer biology in primary tumors and medical treatments. Several key concepts for the comprehension of the biologic and medical motivation inherent to the cancer mathematical models exploited afterwards are addressed.

2.1 Cancer onset and heterogeneity

All somatic cells of the human body carry a complete and hypothetically identical genome (entire set of genetic information of an organism) and therefore far more information that they will ever need to perform their normal function [1, 15]. The epigenome (set of chemical modifications of the Deoxyribonucleic Acid (DNA) and DNA-associated proteins) dictates which is the genetic information available for the cell [1, 15]. Hence, when cells suffer accidental epigenetic modifications, they can either lose access to genetic information once available or gain access to information normally denied to them. As a result, they may assume roles that are inappropriate for normal tissue function and maintenance [1, 15]. Cells can also have their genome corrupted by several mechanisms. Curiously, endogenous biochemical processes contribute far more to genome mutation than exogenous mutagens and their metabolites do [1]. Even the process of DNA replication holds dangers for the genome.

Fortunately, cells have several strategies to ensure that the damage to DNA is unlikely to result in a heritable mutation. A complex DNA repair system is responsible for the continuously monitoring of the integrity of the genome, the removal of inappropriate bases or nucleotides created by both chemical or physical attacks, and the replacement of those bases/nucleotides for the ones existent prior to the attack [1]. This system can also join together double helices that have been broken by genotoxic agents or accidentally during replication [1]. Even when these intricate repair systems fail to detect and rectify these DNA lesions, there are other mechanisms that ensure the DNA integrity. During the cell cycle, cells undergo a programmed series of events that enables a cell to duplicate its contents and replicate [1]. At certain stages of these cycle there are checkpoint controls. When a genetic damage is detected, the cell cycle is arrested, providing not only time for repair but also inducing the transcription of genes that will facilitate it [16]. If DNA damage proves to be irreparable, cell initiates apoptosis (programmed

cell death) [9].

Nevertheless, these mechanism are not perfect and sometimes mutations do persist. However, a single point mutation cannot, on its own, originate a cancer cell from a preexisting normal cell. In fact, tumorigenesis is a complex, multi-step process that can even take some decades [1, 17]. Each consecutive step involves the disruption or deregulation of other key cellular signaling pathway and the mutations accumulated by the end of that step should cooperate with one another to program neoplastic growth [1]. As tumor progression advances, tumor genomes often become increasingly unstable. As a result, the rate at which mutations are acquired during each cell generation soars, thus helping themselves to accumulate the mutant genes and altered karyotypes driving their neoplastic growth [1]. Since these mutations and epigenetic alterations occur at a higher rate than the rate at which Darwinian selection can eliminate phenotypically less-fit clones, an increasing number of distinct populations develops in the tumor mass, each dominated by a genetically distinct subclone (figure 2.1) [1, 17]. There are still other sources of genetic diversity in primary tumors such as epigenetic plasticity and the re-seed of metastatic cells on the primary tumor [1]. On the other hand, multiple cells could have started the tumorigenesis process, becoming the ancestors of several, genetically distinct subpopulations of cells within a tumor mass [1]. As a consequence of this accumulated genetic and epigenetic heterogeneity, the same type of tumor can behave very differently in distinct patients [1, 17]. Once all the cellular key control circuits have been disrupted, the cells in these populations may be fully transformed and therefore capable of generating a vigorously growing tumor virtually immortal [1].

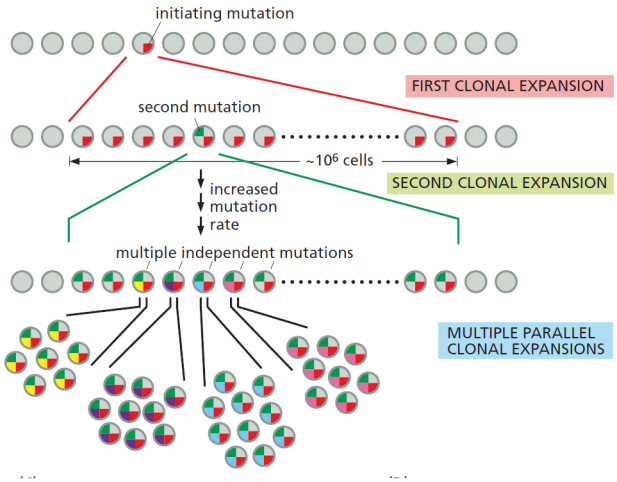

Figure 2.1: High mutation rates lead to tumor clonal diversification. Adapted from [1].

2.2 Anticancer immunosurveillance

Other line of defense against cancer exists beyond the cellular strategies mentioned before. The immune system is a highly specific and finely tuned system capable of recognize cancer cells and eliminate them, despite their great biochemical similarities to the other native cells [1]. Figure 2.2 provides an overview of the components of the innate and adaptive immune response discussed here.

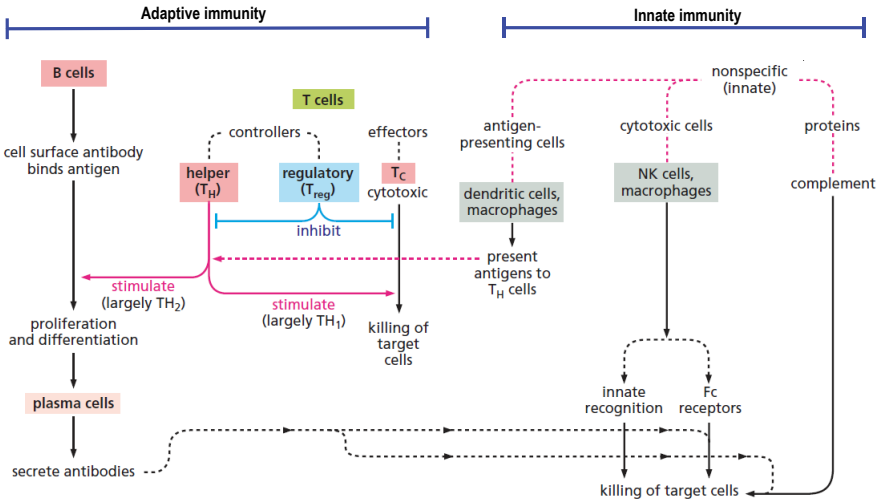

Figure 2.2: Overview of the innate and adaptive arms of the immune system. Adapted from [1].

The innate immune response is the first line of defense of the immune system. In fact, its cellular components do not depend on a prior exposure to a foreign agent or aberrant cell to recognize, attack and destroy them [1]. The first contact between cancer cells and the immune system is likely to be mediated by the Natural Killer (NK) cells [1]. These cells hold a variety of cell surface activating and inhibitory receptors, which regulate NK cell activities (see figure 2.3(a)) [18]. Some of these receptors recognize characteristic molecular patterns present on the surfaces of transformed cells that are not displayed by normal cells. Others recognize the absence of the proteins where antigens are displayed (Major Histocompatibility Complex class I - MHC class I) [1]. When both conditions are satisfied, the killing of cancer cells is far more efficient than when only one of these conditions is met [1]. After having been activated, NK cells kill the transformed cell either by inducing its perforin/granzyme-dependent necrosis or its apoptosis [19]. Thereafter, NK cells send out cytokine signals in order to recruit yet other innate immune cells, including macrophages and neutrophils, to the site of attack [1, 18]. As a result of this second wave of immunocytes, abnormal cells are engulfed by specialized phagocytic cells that after having ingested them act as Antigen-Presenting Cells (APCs) [1, 18].

The adaptive immune response is much more specific and ultimately more effective than the last one. In fact, the components of the adaptive response are educated through the initial encounter with the transformed cell to recognize certain antigens displayed by it and to mount a vigorous counterattack upon encountering this agent again - the so called immunological memory [1]. The adaptive immune response begins when APCs display the processed antigenic peptides to certain helper T (T_H) cells [1]. Consequently, the T_H cells that have a T-cell receptor (TCR) capable of recognizing and binding to the oligopeptide being presented by the APC are activated [1, 20]. The activated T_H cells activate B cells that also recognize the oligopeptide presented [1]. These cells, in turn, proliferate and differentiate into plasma cells that will manufacture soluble antibody molecules capable of specifically recognize and bind that particular antigen [1]. Once a cell or an infectious agent is coated (opsonized) by antibodies, it may be recognized, engulfed and destroyed by phagocytic cells, such as macrophages, or killed by cytotoxic cells such as NK cells [1]. In addition, a set of proteins of the plasma, termed complement,

also recognize and bind to these antibody molecules and proceed to punch roles in the adjacent plasma membrane, thereby killing the cell [1, 20]. At the same time, some of the T_H cells activate cytotoxic T (T_C) cells that also contain TCRs capable of recognizing the antigen that initially provoked an immune response (see figure 2.3(b)) [1, 20]. These cells are specialized to recognize and kill target cells displaying that particular antigen. T_C cells kill transformed cells through two separate mechanisms. Like NK cells, they can expose cancer cells to certain toxic proteins, for instance granzymes [1, 20]. The second killing mechanism involves the Fas death receptor displayed on many cell types throughout the body [1, 20]. T_C cells present the ligand of the Fas receptor - FasL - to their intended victims, activating their extrinsic apoptotic pathway [1, 20]. In contrast to antibodies, T_C cells are also capable of recognizing aberrant proteins synthesized within cells, since they are routinely cleaved into oligopeptides and then transported and displayed on the plasmatic membrane of the transformed cells [1]. Finally, accordingly to the cytokines released or to their TCR, regulatory T (T_{reg}) cells may suppress the proliferation and activation other types of T lymphocytes, such as T_H and T_C cells [1]. This may explain how many type of tumors can thrive even in the presence of large numbers of T_C cells that should, by all rights, be able to eliminate them [1].

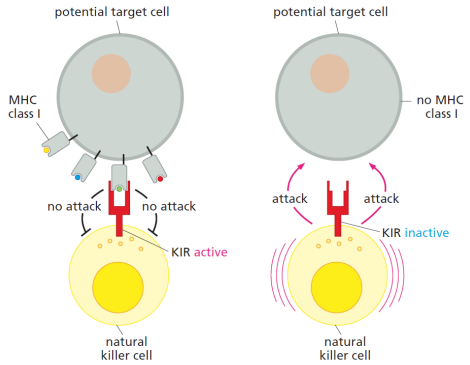

(a) Control of natural NK–mediated killing by positive and negative signals. Adapted from [1].

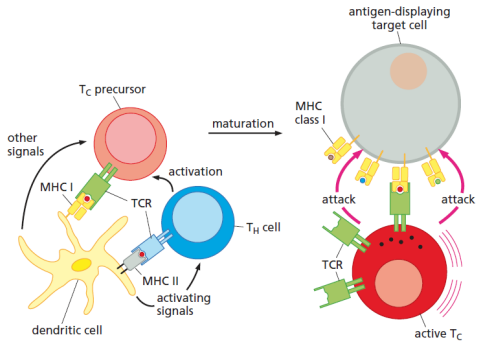

(b) Activation of T_C cells by dendritic cells and killing of antigen-expressing target cancer cells. Adapted from [1].

Figure 2.3: Cancer cells attack by the effector cells of the immune system.

At the same time, immune cells may play conflicting roles in foresting or suppressing tumor growth accordingly to the environment signals and physiologic signals released by tumors [1, 20]. The presence of certain subtypes of immune cells in some tumors may present a good prognosis, while in others their presence can even be a bad prognosis [1, 20]. It is still unclear how and when during tumor progression the immune system is first alerted to the presence of these cells. It may happen when cancer cells invade the stroma and directly confront immunocytes or during the inflammatory phases of tumor progression, when macrophages and other leukocytes are initially recruited into the tumor stroma [1].

2.2.1 Cancer immunoevasive strategies

Despite all efforts of the immune system, some cancers still thrive in the body by developing several immunoevasive strategies. In fact, immunoevasion is recognized as a hallmark of neoplasia [1].

Since most of the cancer cells are recognized by the antigens presented in their plasmatic mem-

brane, abnormal cells lower their immunological profiles [1, 21]. Cancer cells accomplish this by repressing tumor antigens and/or the expression of MHC I molecules. However, the immune system is able to anticipate this trick. Indeed, NK cells hold a receptor called Killer Inhibitory Receptor (KIR) on its surface that recognizes MHC I molecules displayed by target cells [1, 18]. When KIR binds to them, it release signals into the NK cell, preventing it from launching an attack on that cell [1, 18]. Henceforth, the total absence of MHC I molecules invites an attack by NK cells, since killing is allowed to proceed (see figure 2.3(a)) [1]. As a result, cancer cells block only part of the MHC I expression [1].

As a result of neoplastic transformation, some cancer cells display stress-associated proteins that are recognized by the NKG2D surface receptor of NK cells [1, 18]. The binding of these proteins to the NKG2D receptor results in strong activation of NK cells and consequently in cell death [1]. As a consequence, cancer cells down-regulate the expression of some of these ligands or disable this NKG2D signaling pathway [1]. Although they continue to synthesize significant amounts of an alarm protein, most of it is released into the medium around them. Then, this soluble protein binds to the NKG2D receptor of both NK cells and T_C cells, resulting in the endocytosis and degradation of these receptors and thus in the impairment of the cytotoxic action of these immunocytes [1].

Some cancer express proteins on their surface that work as an “eat-me” signal inviting phagocytosis by macrophages [1]. Accordingly, transformed cells can express high levels of another protein that work as a “do not eat-me” signal, protecting themselves from spontaneous attacks by roaming macrophages [1]. Furthermore, cancer cells may also express anti-complement proteins on their plasma membrane, avoiding being killed by the complement system [1]. In addition, they may also alter their own biochemistry to make themselves intrinsically less responsive to attacks launched by the immune system [1].

In the event that the latter strategies do not suffice, tumors may create localized microenvironments or even kill potential attackers [1]. Many cancer cells develop resistance to FasL-mediated killing, protecting themselves from the activation of the extrinsic apoptotic cascade and thus destruction by cytotoxic cells, such as T_C cells [1]. In a second step, they can even acquire the ability to produce and release soluble forms of FasL themselves that will cause the death of several types of lymphocytes and holding them at a safe distance [1, 21]. Cancer cells can also release potently immunosuppressive cytokines that have strong cytostatic effects on T lymphocytes, preventing the maturation of dendritic cells and the presentation of antigens. Under certain conditions, they may even induce the apoptosis of dendritic cells and macrophages, which are the two key APCs of the immune system [1, 21]. Cancer cells also try to modify the mix of immune cells around them [1]. This is the immunoevasive strategy that benefit them the most. T_{reg} cells can directly inhibit and even kill both T_H and T_C cells that recognize the same antigen as them [1, 21]. Tumors release a chemokine that recruits T_{reg} cells [1, 21]. Once present within a tumor mass, they suppress the action of T_H cells that are fundamental to the adaptive immune response, including T_C cells that are otherwise fully competent to attack and kill tumor cells [1, 21]. Cancer cells can also stimulate the transdifferentiation of other types of T cells into T_{reg} cells [1].

Table 2.1 provides a summary of the immunoevasive strategies aforementioned.

Table 2.1: Usual immunoevasive cancer strategies. Adapted from [1].

Strategy	Mechanism	Agent affected
Hide identity	Repress tumor antigens and/or MHC-I proteins.	T_C cells
Hide strategy	Repress NKG2D ligands.	NK cells
Inactivate immunocytes	Destroy immunocyte receptors.	NK cells, T_C cells
	Saturate immunocyte receptors.	NK cells; Variety of immunocytes
	Induce T_{reg} formation Saturate immunocyte receptors.	NK cells, variety of T lymphocytes
Avoid apoptosis	Inhibition of caspase cascade, acquisition of resistance to Fas-L mediated apoptosis.	
Induce immunocyte apoptosis	Release soluble Fas-L.	T_C cells
	Release cytokines.	T_C cells, dendritic cells, macrophages
Neutralize complement	Overexpression of anti-complement proteins.	Complement system
Avoid phagocytosis	Expression of “do not eat-me” signals on cell surface.	Phagocytic cells

2.3 Treatments

2.3.1 Anticancer chemotherapy

Although the term chemotherapy refers to the use of chemicals to treat any disease, this term is usually assigned to drug therapy for cancer [22]. There are several different types of antineoplastic agents, which kill cancer cells by distinct mechanisms [23]. They may disrupt the DNA or prevent its synthesis, interrupt mitosis, interfere with the normal functioning of specific metabolites or the enzymes that produce them, block critical signaling pathways for cancer cell growth and proliferation among other mechanisms [1, 23].

Nevertheless, these cytotoxic agents are not cancer-specific and therefore healthy cells are also undesirably affected, causing significant short- and long-term toxicity and side effects [24]. These side effects depend on the drug type, dose and schedule of administration [24]. Since chemotherapy agents preferentially target highly proliferative cells, they have a negative effect on proliferating hematopoietic and immune cells, leading to the depression of both natural and adaptive defense mechanisms [24]. As a result, T lymphocytes (mainly T_{reg} cells) and dendritic cells are depleted and some drugs also cause NK cells disfunction [25, 26, 27]. As a result, chemotherapy may interfere on antigen presentation processes [28] and reduce cell mobilization [29]. Conventional chemotherapy is administered at or close to the Maximal Tolerated Dose (MTD) in a cyclic fashion with interspersed drug-free periods to enable normal cells to allow hematopoiesis and restoration of peripheral leukocyte count [24, 30]. However, in this period cancer cells also grow [24, 30]. Besides being toxic, some of these agents are also carcinogenic. Hence cancer short-term remissions may be counterbalanced by the future appearance of a second-site tumor [1].

Despite the inherent chemotherapy toxicity, the major reason for chemotherapy failure is the inevitable acquisition of drug evasion mechanisms by cancer cells. Their unstable, mutable genomes constantly

generate new alleles, novel genetic configurations and occasionally new phenotypes [1]. Accordingly, much of the resistant variants already existed by chance within a tumor prior to the beginning of therapy and thus only suffered natural selection [1]. The acquisition of resistance during the treatment is a result of the adaptive genetic/epigenetic and subsequent phenotypic plasticity of cancer cell populations, which are always searching for combinations capable of improving their ability to survive and proliferate [1]. Under these circumstances, some populations of cancer cells may develop drug evasion mechanisms by increasing their anti-apoptotic defenses, inactivating certain parts of the apoptotic machinery or even acquiring an increased ability to repair the DNA molecules damaged by chemotherapy [1]. Others may lose checkpoint controls responsible for their sensitivity to certain types of drugs [1, 31]. They may even metabolize drug molecules, lose the ability to import drug molecules through their membrane or express drug efflux pumps and efficiently excrete several chemically unrelated drugs, thereby decreasing intracellular drug concentrations to subtoxic levels [1, 31]. Once the likelihood of pre-existing variants simultaneously resistant to several cytotoxic is expected to be astronomically low, multi-drug protocols were developed, often combining drugs with distinct and complementary modes of cell killing [1]. However cancer still manages to develop drug evasion mechanisms to all the drugs being used [1]. Moreover, multi-drug therapies are constrained by the realities of toxicity leading to unacceptable levels of systemic toxicity [1].

Recently, a revolutionary form of chemotherapy has emerged. Metronomic chemotherapy relies on a continuous dose administration of a minimum biologically effective dose of a chemotherapeutic agent (low toxicity) with no prolonged drug-free breaks [32]. This multi-targeted chemotherapy simultaneously affect cancer cells, the tumor vasculature and the immune system [30]. Indeed, metronomic chemotherapy is known to promote dendritic cell maturation, preferential depletion of T_{reg} cells and consequent enhancement of the cytotoxic activity of NK cells and T_C cells, thus promoting the elimination of cancer cells by the immune system [33, 34, 35, 36, 37, 38, 39, 40]. Furthermore, the low chemotherapy doses are expected to maintain a significant proportion of sensitive cells within the tumor, thus limiting the proliferation of the resistant population due to competition for space and resources between these populations [41]. Although, the development of resistance still occurs [42], resistance to conventional chemotherapy and metronomic chemotherapy are associated with distinct mechanisms [30, 43].

2.3.2 Immunotherapy

As discussed before, the immune system plays an important role in the fight against cancer. As a matter of fact, immunocompromised individuals do experience high levels of several cancers [1]. Biological therapies have emerged, which make use of living organisms, substances derived from them or their laboratory-produced versions to treat disease [44]. Immunotherapy is one of them. Immunotherapy does not target cancer cells directly [44]. Instead, it enhances/mobilizes this intrinsic capacity of the immune system of the patient to combat cancer [1].

Two types of immunotherapies will be addressed here. Cytokines are small proteins involved in cell signaling that can be used to boost the immune response, without targeting specifically the tumor [45]. The two main types of cytokines used to treat cancer are called interferons and interleukins [46]. In turn,

Adoptive Cell Transfer (ACT) involves the identification *ex vivo* of autologous or allogeneic lymphocytes with anti-tumor activity, which can or not be genetically engineered and then re-infused into cancer patients, often along with appropriate growth factors to stimulate their survival and expansion in vivo [47].

Almost all the immunotherapy treatments currently available do not reproducibly yield robust therapeutic responses in a significant proportion of treated patients [1]. Scientists are only now beginning to learn how to manipulate the immune system of cancer patients in order to cause tumor regression.

2.3.2.1 Cytokine: interleukin-2

Interleukin-2 (IL-2), discovered in 1975, was first described as a T cell growth factor [48]. This cytokine is mainly secreted by active T_H cells [49]. However, T_C cells, NK cells, and activated dendritic cells can also synthesize it [49]. Indeed, after have been activated, T_C secret IL-2 fueling their rapid and selective expansion [50]. Since tumors do not express IL-2 receptors, the anti-tumor activity of this cytokine is a result of its multiple effect on the cellular components of the immune system (see table 2.2) [49].

Table 2.2: Roles of IL-2 in several immune cells [49].

Cell type	**IL-2 activity**
T_H cells	Expansion and differentiation of antigen-specific clones.
	Enhanced production of other cytokines.
	Induced apoptosis of activated T cells.
T_C cells	Expansion of antigen-specific clones.
	Enhanced cytokine secretion and cytolytic activity.
	Differentiation into memory and more terminally differentiated lymphocytes.
T_{reg} cells	Involved on its development and maintenance.
B-cells	Enhanced antibody secretion.
	Proliferation promoter.
NK-cells	Proliferation promoter.
	Enhanced cytokine secretion and cytolytic activity.

IL-2 also promotes long-term survival of T cells [51]. Altogether, the administration of high-dose bolus regimen or a continuous infusion OF IL-2 results in the functional activation of endogenous tumor-reactive cells (mostly NK cells) *in vivo* [1, 47] with the consequent regression of some human solid cancers [52, 53, 54]. Important to realize that different doses of IL-2 have different effects in the immune system [55]. While at higher doses, IL-2 have an immunostimulatory and therefore an anticancer effect, at low doses it has instead a immunosuppressive effect (related with T_{reg} cells) [55].

The intravenous administration of IL-2 cause substantial toxicities owing to a capillary leak syndrome that leads to fluid extravasation into visceral organs, compromising their function [49, 56]. However, experience with the administration of this cytokine has resulted in treatment-related mortalities of $< 1\%$ [56].

2.3.2.2 ACT: Tumor infiltrating lymphocytes

The term Tumor-Infiltrating Lymphocytes (TILs) refers to lymphocytes found between the tumor cells, which are expected to be more reactive to cancer cells than the lymphocytes found at peripheral blood [51]. Although the bulk of populations of TILs are NK cells, a functionally critical subpopulation of cells consist of T_C cells that have acquired specific reactivity against the antigens displayed by the tumor from which they were isolated [1]. Nonetheless, the existence of T_{reg} cells between these TILs may drive tumor pathogenesis since these cells are responsible for the dysfunctional state of many tumor-associated T_C cells [1].

Figure 2.4 depicts the steps involved in the administration of this type of immunotherapy. First, tumor samples are surgically removed from the patient and the prepared TILs are cultured *ex-vivo* in IL-2 [47]. Then, high anti-tumor reactive cultures are expanded to large numbers ($> 10^{10}$) [47]. In order to obtain a long-lived TIL treatment, patients are treated with a conditioning lymphodepleting chemotherapy prior to injection of *ex vivo*-expanded TILs [1]. The objective is to reduce the populations of lymphocytes and lymphocyte precursors in the bone marrow of the patients, thereby "making room" for clones of subsequently introduced TILs [1]. The latter can then establish themselves in the marrows of patients, persist and even expand during the course of immunotherapy [1]. Moreover, this lymphodepletion also eliminates the immunosuppressive T_{reg} cells and the endogenous lymphocytes that otherwise would compete with the transferred cells for growth-promoting cytokines [47]. The patient is then treated with high-dose IL-2 to sustain the *in vivo* growth of T_C cells [1].

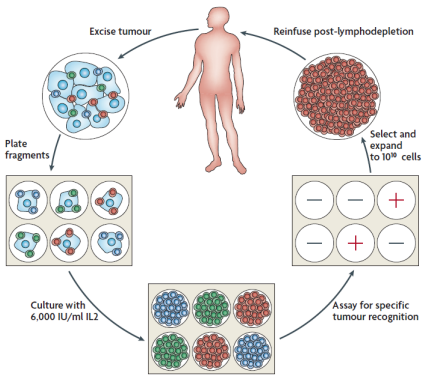

Figure 2.4: Administration of autologous TILs. Adapted from [47].

ACT using autologous TILs is currently the most effective treatment for patients with metastatic melanoma and can mediate objective tumor regressions in 50% of patients [47]. This was the first effective cancer immunotherapy and provided one of the first curative systemic therapies for any solid tumor [49]. Attempts at generating TILs having specific anti-tumor cytotoxic activity from other types of tumors have not met with comparable success to date [1].

2.3.3 Combination therapy

Although chemotherapy and immunotherapy may seem to be unrelated or even antagonistic due to the aforementioned immunosuppressive effect of chemotherapy, their combination can result in substantial

clinical benefits [7, 57]. As a matter of fact, the immune system is clearly implicated in the efficacy of several conventional chemotherapeutics [58]. Therefore, immunotherapy may be used either to subvert therapy-induced immunosuppression, improving the clinical profile of chemotherapy, or to maximize the immunostimulatory effects of some chemotherapeutic agents (table 2.3) [58].

Table 2.3: Potential systemic and local effects of chemotherapy on the capacity of immunotherapy to destroy tumors.

Possible systemic effects	**Possible local effects**
Non-specific activation of APCs [59, 60].	Delivery of a broader range of different tumor antigens (dead and dying cancer cells) [59].
Increased cross-presentation of tumor antigens [60, 61].	Increased tumor cells expression of tumor associated antigens [60, 61].
Tumor debulking: higher T_C cell to tumor-target ratio, less systemic suppression, smaller target, less chance for escape variants, among others [62].	Disruption of tumor stroma with consequent penetration and T cell accumulation within tumor [60, 63].
Reduction of cells with immunosuppressive activity, such as T_{reg} cells [60, 64, 65].	Decreased local suppressive activity of tumor cells, *i.e.* no tolerance induction by apoptotic tumor cells [60, 61].
Lymphopenia induction and resultant homeostatic T cell proliferation [7, 60].	Tumor-specific T-cell response increased by lymphopaenia-related proliferation [66].
	Partial sensitization of tumor cells for T_C cell lysis (increased permeability to its granzymes) [60, 67, 68].
	Up-regulation of *Fas* (and other death receptors) on tumor cells, or *FasL* on T_C cells [60].

Interestingly, the administration schedule of combinatorial immunochemotherapeutic regimens is a central determinant for its efficacy [69, 70]. Post-chemotherapy delivery of immunotherapy is in fact more effective than pre-treatment. Moreover, immunotherapy must be initiated shortly after chemotherapy so that the benefits listed in the table 2.3 are not lost [59]. Rather than the conventional 1 month between cessation of chemotherapy and commencement of immunotherapy, chemotherapy immediately followed by immunotherapy, conceivably in repeating cycles, might be more effective [59].

Chapter 3

State of the Art

This chapter provides a brief review of the literature regarding ODE tumor mathematical models that consider both chemotherapy and tumor-immune dynamics. These mathematical models are reviewed by crescent complexity. Finally, optimal control theory is also reviewed together with some numerical methods employed in the optimization of anticancer biomedical problems.

3.1 Tumor mathematical models

Due to the high tumor burden mortality, since early ages mathematical models were used to study the dynamics of cancer cell populations [71]. These earlier models can be written as

$$\dot{x} = xf(x), \tag{3.1}$$

where x is the cell population size at time t and $f(x)$ is the tumor growth model. This positive-valued, continuous, monotonically increasing function [71, 72], which can be written as $f(x) = p(x) - d(x)$, reflects the tumor density dependence on tumor cells death, $d(x)$, and proliferation, $p(x)$ [71].

3.1.1 Tumor growth models

The models used for the modulation of tumor growth can be phenomenological (descriptive models) or mechanistic (explicative models). The first ones are not based on biological processes and parameters [73]. In turn, the mechanistic models incorporate the influence of complex biological factors and processes, such as the effects of the immune system on cancer, therapy resistance, tumor heterogeneity, among others [73]. Although phenomenological models are simpler than the mechanistic ones, they proved to be able to forecast and describe experimental or clinical data [73], capturing many of the complex processes involved in tumor growth [74]. On the other hand, mechanistic models are based only on *in silico* testing. Consequently, they have limited preclinical and no clinical application until to date [73]. Several questions arise regarding their reliability and applicability in the development of drug regimens in patients [73].

Almost all tumor growth models study cancer at a single biological scale. However, multiscale models

do exist, which encompass at least two spatial scales and/or includes physical or biological processes that occur at two or more temporal scales [73]. These globally more-realistic models enable the translation of the complexity of cancer systems biology into clinical applications [73]. Nevertheless, they are far more difficult to develop than single scale models [73]. Additionally, the simulation of treatment approaches *in silico* remains an authentic challenge [73].

3.1.1.1 Phenomenological models

Overall, phenomenological models can be divided into exponential (*e.g.* Exponential growth law) and sigmoid shaped models (*e.g.* Gompertz, Logistic and von Bertalanffy growth laws). The model equations of the aforementioned growth laws are listed in table 3.1, as well as their maximum size and doubling time in the absence of an anticancer therapy.

Table 3.1: Tumor growth laws and their predictions in the absence of anticancer therapy. Adapted from [75].

Growth law	$f(x)$	**Maximum size**	**Doubling time**	**Growth condition**
Mendelsohn	rx^{b-1}	∞	$\frac{\ln(2)}{r}$	$r > 0$
Gompertz	$r \ln\left(\frac{x_{max}}{x}\right)$	x_{max}	$\frac{\ln(2)}{r \ln(x_{max})}$	$r \ln(x_{max}) > 0$
General logistic	$r\left(1 - \frac{x}{x_{max}}\right)^b$	x_{max}	$\frac{\ln(2)}{r}, b = 1$	$r > 0$
von Bertalanffy	$r_1 x^{b-1} - r_2$	$\left(\frac{r_1}{r_2}\right)^3, b = \frac{2}{3}$	$\frac{\ln(2)}{r_1 - r_2}$	$r_1 - r_2 > 0$

In a real system, the maximum possible tumor size x_{max}, also called carrying capacity or plateau population, depends on the tumor environment and its access to resources, such as nutrients [75, 76]. Therefore, it may change as the tumor grows, particularly when the tumor extends beyond the bounds of its primary location [75].

Figure 3.1 represents the tumor growth laws listed in table 3.1. While the exponential shaped models are unbounded, the sigmoid shaped ones are characterized by an increasing curve, which has one inflection point that asymptotically converges to the carrying capacity x_{max} [77]. The doubling time gives an indication of how quickly the tumor will reach its maximum size [75]. Experimentally, the tumor growth rate decreases with increasing tumor volume [72] as a result of the mutual competition between the cells for both nutrients and/or space, among others factors [77]. Hence, sigmoid shaped models are consistent with general patterns of organ and organismal growth, since they reproduce this experimentally observed growth slowdown [77].

Mendelsohn Growth Law The Mendelsohn growth law assumes that all cells proliferate with a constant cell cycle duration T_C, *i.e.* $r = \frac{ln(2)}{T_c}$ [77, 78]. Therefore, tumor growth is proportional to the power b of the population, with the proportionality constant r being the tumor growth rate [75]. The exponential growth law, which is a special case $(b = 1)$ of the Mendelsohn equation, is the simplest tumor growth model [78]. It is valid when a constant fraction of the volume proliferates [77]. However, the fraction of

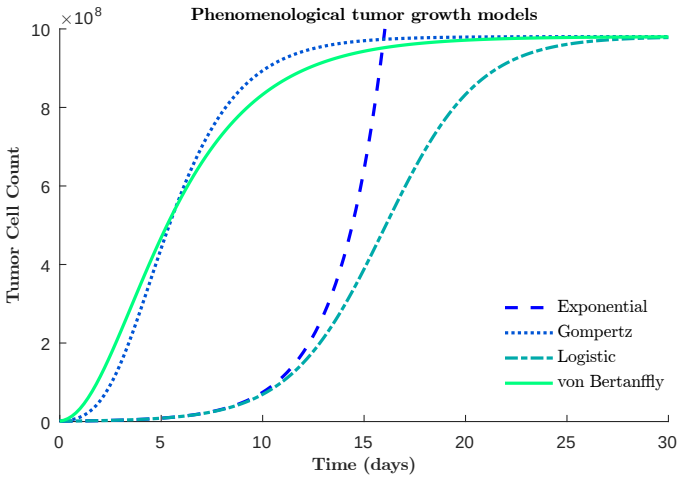

Figure 3.1: Tumor growth curves for four different models of tumor growth. The Gompertz (dotted), Bertalanffy (solid), and Logistic (dash-dotted) tend to a asymptotic value, whereas the Mendelsohn model (dashed) gives rise to unconstrained growth. For all the growth laws, $x_0 = 10^6$ tumor cells. Parameters: $r = 0.431$, $r_1 = 844.41$, $r_2 = 0.85$, $x_{max} = 0.9804 \times 10^9$, $\delta = 0.9$, $b = 1$ for Mendelsohn and General logistic, $b = \frac{2}{3}$ for von Bertalanffy.

cells that become quiescent increases as tumor growth progresses [72, 78]. Although the exponential growth match the early stages of tumor growth, it is unable to explain tumor growth dynamics in the longer term, resulting in a unrealistic unrestricted growth [77, 78]. In addition, the tumor doubling time is often variable over time, which cannot be reproduced using an exponential shaped model [78].

Gompertz Growth Law The growth pattern of the Gompertz law is similar to that of exponential growth law in the early stages, but plateaus as tumor size increases. The carrying capacity x_{max} can vary with time [78]. When $x(t) = x_{max}(t) \Rightarrow \ln\left(\frac{x_{max}(t)}{x(t)}\right) = 0$. In other words, the growth rate is equal to zero. Several equations for $x_{max}(t)$ can be found in the literature [78].

General Logistic Growth Law The well-known logistic growth law is a particular case ($\nu = 1$) of the generalized logistic growth law. Whereas the Gompertz equation assumes an exponentially decreasing growth rate, the logistic model is characterized by a linear decrease of the relative growth rate proportional to the tumor volume x, until it becomes equal to zero when it reaches $x(t) = x_{max}$ [78]. Therefore, the instantaneous probability for a cell to proliferate is proportional to $1 - \left(\frac{x}{x_{max}}\right)$ [77]. Initially ($x \ll x_{max}$) the exponential and logistic growth functions are close in value until $x \approx x_{max}$ [77]. However, this derivation ignores several important factors, such as limited nutrients.[78]

von Bertalanffy Growth Law This model derives general laws of organic growth from basic energetics principles [77]. It assumes that growth (r_1) is proportional to tumor surface area and that the loss of tumor mass due to cell death (r_2) occurs proportionately to the volume of the tumor. Usually, $b = \frac{2}{3}$. As a sigmoid shaped model, it converges to a fixed tumor volume in which the growth and loss term balance each other out [78]. Besides matching well experimental tumor growth curves, this model has a derivation with biologically meaningful parameters [78]. However, it has received considerably less

attention than the aforementioned growth models [78].

3.1.1.2 Description and prediction of experimental tumor growth

Usually the choice of a tumor growth model is driven by the ease of mathematical analysis rather than whether it provides the best model for tumor growth or not [78]. However, there are not conclusive comparative studies regarding which is the best model to describe and predict different tumor growths. Table 3.2 resumes some of the existent studies related with this topic.

Table 3.2: Conclusion of articles that describe and/or predict the tumor growth of a given tumor, using some phenomenological tumor growth models.

Authors	Tumor	Models	Results
Hartung et al., 2014 [79]	Orthotopic human breast tumor xenograft in mice.	Exponential, Mendelsohn, Gompertz, Logistic, Von Bertalnffy.	Bertalanffy and Gompertz models described better primary tumor growth. Doubling times estimated below the experimentally determined *in vitro*. Bertalanffy models missed the doubling time and the initial size x_0 by several orders of magnitude. Creation of hybrid models (Berta-Ex and Gomp- Ex).
Benzekry et al., 2014 [77]	Lewis lung carcinoma, orthotopic xenografted human breast carcinoma.	Exponential, Exponential-linear, Gompertz, Logistic, Generalized logistic, von Bertalanffy.	**Breast:** Gompertz and exponential-linear models captured better the dynamics with prediction scores of 80%; **Lung:** Gompertz and Mendelsohn provided the most parsimonious and parametrically identifiable description. None achieved a substantial prediction rate (70%) beyond the next day data point. Adjunction of a priori information on the parameter distribution led to considerable improvement.
Vaidya and Alexandro, 1982 [80]	Primary human lung carcinoma, induced sarcoma in mice.	Exponential, Gompertz, Logistic, Von Bertalnffy.	**Lung:** Logistic equation gave the best fit (7 in 7 patients), followed by Gompertz (4 in 7 patients) and,Bertalanffy and Exponential (1 in 7 patients); **Mice:** Bertalanffy give the best fit (7 in 10 mice) followed by Gompertz and Logistic (2 in 10 mice) and Exponential (0 in 10 mice).
Simpson-Herren et al., 1970 [81]	Nine experimental tumors.	Gompertz.	Gompertz used to fit nine experimental tumors.[80] Article not available.
Dethlefsen et al., 1968 [82]	Mouse mammary tumors.	Mendelsohn.	Data fited by Mendelsohn with $b = \frac{2}{3}$.
Laird, 1964 and 1965 [83, 84]	19 examples of 12 different tumors in mice, rats and rabbits	Exponential, Gompertz.	The growth of a transplanted or primary tumor is well described by the Gompertz equation.

As seen in table 3.2, there is no single model that commands universal superiority over the others. In terms of matching actual growth curves, the Logistic and Gompertz equation are quite similar. However,

it is believed that the Gompertz equation does better when the complete history of the tumor growth is analyzed, comparing to the logistic or the Bertalanffy equation [80]. Nonetheless, Gompertz model is the most applied model to describe tumor growth curves [78]. First, growth curves are used to predict the future size of the tumor and therefore a biological ground is not crucial. Second, it is quite easy to fit the Gompertz model to data that follows a different growth law [78]. However, this latter reason must not determine the use of Gompertz model over other more accurate models that are grounded in biology, enabling not only predictions, but also insights into the underlying dynamical process of tumor growth [78]. In some sense the Bertalanffy model achieves this. It produces growth curves that are nearly indistinguishable from the well-known Gompertz model, is biologically motivated, has few arbitrary constants, can be verified experimentally and gives good results in predicting the tumor volume [78, 80].

3.1.2 Tumor-chemotherapy models

Chemotherapy is one of the major pillars on which current cancer therapies rest [1]. Several mathematical models of tumor growth and anticancer treatments have been developed along the years.

3.1.2.1 One equation models

The simplest tumor-chemotherapy models are one-equation models which assume that the treatment interferes with the tumor by adding a time-dependent treatment term $G(x, u(t))$ to (3.1), [85] resulting in

$$\dot{x} = xf(x) - G(x, u(t)). \tag{3.2}$$

The term $G(x, u(t))$ describes the pharmacokinetic and pharmacodynamic effects of the chemotherapy agent in the system [86]. The time dependent pharmacokinetics of the drug can be modeled as a second state variable. In the first mathematical models, $G(x, u(t))$ followed the log-kill hypothesis, also called Skipper–Schabel–Wilcox model. Later on, Norton and Simon revisited the Skipper–Schabel–Wilcox log-kill model, extending it to tumors with non-constant specific growth rate [87]. Both cell kill models are depicted in figure 3.2 as well the tumor growth in the absence of the term $G(x, u(t))$.

Skipper–Schabel–Wilcox log-kill model This hypothesis is based on an analogy with the law of mass action for kinetic reactions in chemistry [87]. According to it, a given dose of cytotoxic chemotherapy kills the same fraction of tumor cells regardless of the tumor size at the time of treatment [88], as depicted in figure 3.2. In other words

$$G(x, u(t)) = cu(t)x, \tag{3.3}$$

where c is the magnitude of the dose and $u(t)$ is the time dependent pharmacokinetics of the drug.[89]

The log-kill model states that any drug capable of improving survival by some period of time can, when administered at enough additional doses, delay death and lead to cure [88]. However, the log-kill model has several weaknesses. It assumes an exponential tumor growth between treatment doses (linear in log-scale), which does not vary as a function of tumor size. Also, the tumor is assumed to be

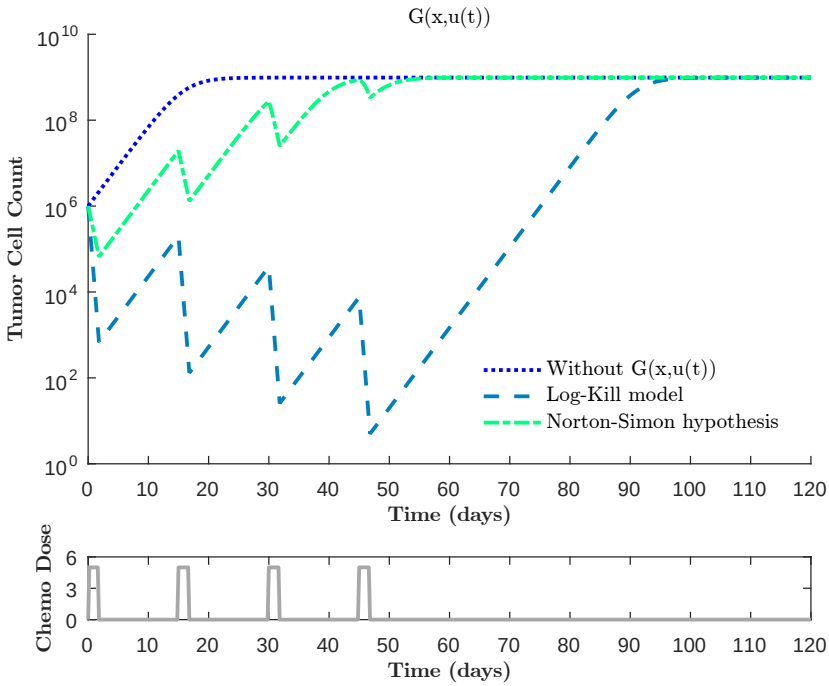

Figure 3.2: Tumor growth curves in the absence (equation (3.1)) and presence (equation (3.2)) of $G(x, u(t))$. Both Log-kill model (dashed) and Norton-Simon hypothesis (dash-dotted) tend to x_{max} (dotted) when four doses of chemotherapy are administered over 45 days in a 15 day cycle of strength $u_c(t) = 5$ to a $x_0 = 10^6$ cell tumor. $f(x)$ was considered to follow the logistic growth law. Parameters: $r = 0.431$, $x_{max} = 0.9804 \times 10^9$, $c = 0.9$.

a homogeneously sensitive population [88, 87]. Furthermore, it is not supported by clinical experience with several solid tumors and it does not completely predict or explain tumor cytokinetics [88].

Norton-Simon hypothesis As discussed in 2.3.1, the actively proliferating cells, which contribute the most to the size increase of the tumor, are expected to be the most affected by chemotherapy. Norton and Simon suggested a killing term proportional to the tumor growth rate at the time of treatment, instead of proportional to the tumor size at that time [90]

$$G(x, u(t)) = cu(t)f(x)x. \tag{3.4}$$

As represented in figure 3.2, Norton-Simon hypothesis considers that there is a kinetic advantage to treatment when the tumor volume is small (higher tumor relative growth and higher number of tumor cells actively proliferating) [88]. A denser chemotherapy administration protocol would then optimize the chemotherapy efficacy, favoring tumor eradication [87, 88]. In fact, when less inter-cycle time is allowed between chemotherapy administrations, the tumor regrows less and thus presents a larger growth rate and consequently the cumulative cell kill increases [90, 88]. Nonetheless, this increase in the cumulative cell kill may be compensated by the same high growth rates experienced by small tumors [87]. Consequently, a similar overall survival is obtained in both models, despite the significantly different times to relapse [87]. Besides being consistent with clinical observations, Norton-Simon hypothesis fits preclinical experiments and was demonstrated to be predictively superior than the log-kill model [90].

3.1.2.2 Two equation models

Overall, one-equation models are able to explain the macroscopic behavior of tumors, such as tumor growth and regression. However, they do not explain the mechanisms behind these behaviors and do not consider tumor heterogeneity [88]. In fact, controlling drug-resistant subpopulations within the tumor is essential to long-term patient survival [8].

The first non cell-cycle specific two-compartment models regarding tumor biochemical resistance viewed resistance as an absolute phenomenon. Goldie and Coldman [91] proposed the first stochastic model of drug resistance in which the resistance was developed due to (epi)genetic mutations [8]. Generally speaking, the heterogeneous population of cancer cells was considered to be composed of both resistant R and sensitive S cells [8] that could switch phenotypes between them [14], as represented in figure 3.3.

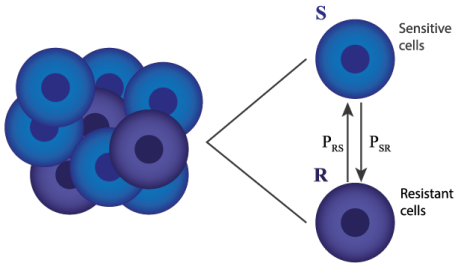

Figure 3.3: Schematic representation of an heterogeneous population of tumor cells, composed by tumor sensitive (S) and resistant (R) cells that can switch phenotypes between them with probability P_{SR} and P_{RS}.

Generally, these two-equation models can be written as

$$\dot{S} = Sf(S) - G(S, u(t)) - P_{SR}S + P_{RS}R, \tag{3.5}$$

$$\dot{R} = Rf(R) - G(R, u(t)) - P_{RS}R + P_{SR}S. \tag{3.6}$$

Table 3.3 summarizes the notation used in this section. If a logistic tumor growth law is considered for $f(j)$, thus $f(j) = r_j \left(1 - \frac{S+R}{x_{max}}\right)$.

Accordingly to the Norton–Simon hypothesis [90, 92], a tumor is composed by a population of faster-growing chemotherapeutically sensitive cells and a population of slower-growing increasingly more resistant cells. Since $f(j) = p(j) - d(j),\ p(S) \geq p(R)$. Furthermore, the mechanism by which sensitive

Table 3.3: Notation used in section 3.1.2.

State variables and rate functions	Description
x	Cancer cells,
S	Cancer cells sensitive to the treatment,
R	Cancer cells resistant to the treatment,
$f(j),\ j = \{x, R, S\}$	Tumor growth model,
$u(t)$	Time dependent drug concentration,
$G(j, u(t)),\ j = \{x, R, S\}$	Pharmacokinetic and pharmacodynamic effects of the chemotherapy agent in the state variable j,
$P_{ji},\ i, j = \{R, S\}$ and $i \neq j$	Probability of the state variable j become a state variable i.

cells acquire resistance to the cytotoxic agent and vice versa will determine the cell death rate $d(j)$ for each population. For instance, tumor cells that have developed resistance through acquired mutations will be more unstable than sensitive cells, *i.e.* $d(S) \leq d(R)$. The condition $G(S, u(t)) >> G(R, u(t))$, *i.e.* $c_S >> c_R$ is always verified. In the context of absolute resistance, $G(R, t) = 0$, i.e. $c_R = 0$, which means that the cytotoxic agent has no effect on the resistant population. Finally, the transitioning rates between the sensitive and resistant compartments and vice versa are given by the terms P_{SR} and P_{RS}, respectively. Usually $P_{SR} >> P_{RS}$. If $P_{RS} > 0$ then the model allows a re-sensitization effect. This two-equation model can be adjusted to fit several different mechanism of resistance development.

After the work of Goldie and Coldman [91], several mathematical models of drug resistance in cancer have been proposed. Some of these models view the development of resistance as single mutational event (*e.g.* Hahnfeldt et al. [14], Westman et al. [93]). Others (*e.g.* Harnevo and Agur [94], Kimmel and Axelrod [95]) describe the development of resistance (stable and unstable gene amplification) as a branching process. Some of the models developed also consider the development of multi-drug resistance during cancer chemotherapy with multiple killing agents.

An example: Hahnfeldt et al. [14] Considering the drug concentration seen by both sensitive and resistant tumor populations as an arbitrary function of time, $u(t)$, the model of Hahnfeldt is given by

$$\dot{S}(t) = r_S S(t) - c_S u(t) S(t) - P_{SR} S(t) + P_{RS} R(t), \tag{3.7}$$

$$\dot{R}(t) = r_R R(t) - c_R u(t) R(t) - P_{RS} R(t) + P_{SR} S(t), \tag{3.8}$$

where r_j is the net proliferation rate of the state variable j, c_j is the sensitivity of state variable j to the chemotherapeutic agent with concentration $u(t)$. Once each subpopulation is assumed to be large, the sensitivity terms also represent subpopulation survival fractions following drug exposure [14]. The Hahnfeldt two-equations model can be modified to consider a logistic tumor growth law and the Norton-Simon hypothesis. Figure 3.4 presents the simulation results of this modified Hahnfeldt model. As expected the total tumor burden is almost composed by resistant cells, the major reason behind the chemotherapy failure. Nevertheless, the chemotherapy was not enough to eradicate the sensitive tumor cells. As the total burden increases, the relative growth rate of the resistant and sensitive tumor cells population decreases, reason why the number of cells killed by chemotherapy decreases with time.

3.1.2.3 Three equation models

More equations representing various levels of chemotherapeutic sensitivity or drug resistance can be added to (3.5) and (3.6) by considering the transition rates between all the compartments, as illustrated in figure 3.5. Experimental data suggests that the values of these transition rates would be higher as the degree of resistance increases [96], which is in agreement with what was discussed in 2.1. As tumor progression advances, tumor genomes become increasingly unstable. The re-sensitization transitions follow the same rule. In other words, in figure 3.5(a), $P_{SM} < P_{MR}$ and $P_{MS} < P_{RM}$. Evidently, $P_{SR} << P_{SM}$. Figure 3.5(b), explores the concept of the pre-existence of stable intrinsically resistant

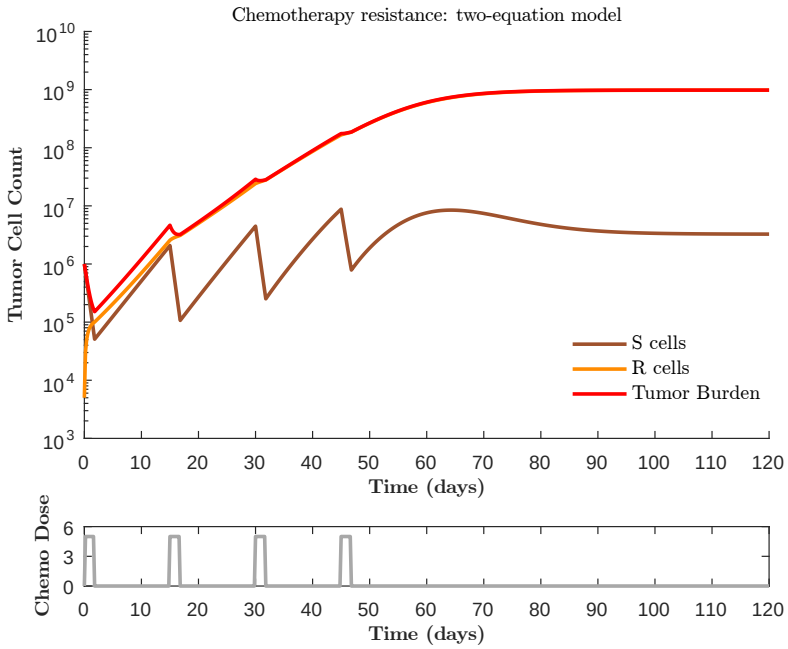

Figure 3.4: Tumor growth curves when a modified Hahnfeldt model for the tumor-chemotherapy resistance dynamics is considered. The total tumor burden tend to x_{max} (dotted) when four doses of chemotherapy are administered over 45 days in a 15 day cycle of strength $u_c(t) = 5$ to a $x_0 = 10^6$ cell tumor composed by $S_0 = 9.95 \times 10^5$ sensitive cells and $R_0 = 5 \times 10^3$ resistant cells. $f(j)$ was considered to follow the logistic growth law and $G(j, u(t))$, the Norton-Simon hypothesis. Parameters: $r_S = 0.431$, $r_R = 0.144$, $x_{max} = 0.9804 \times 10^9$, $c_S = 0.9$, $c_R = 0.1$, $P_{SR} = 0.15$, $P_{RS} = 5 \times 10^{-4}$.

tumor cells before chemotherapy administration, which was also reviewed in 2.1. Since I cells are more stable than R cells, $P_{RS} >> P_{IS}$. As before, the re-sensitizations transitions are far less probable than the respective resistance transition. Figure 3.6 presents an example of the simulation results of the two models outlined in figure 3.5. For both resistance schemes, the tumor burden is essentially composed by resistant tumor cells. The intrinsic resistant tumor cells (figure 3.4) ascend from 10 cells at the beginning of treatment to more than 10^7 cells at its end. Most of the tumor resistance can be, in fact, explained by the existence of resistant cells prior to the beginning of the treatment, as proposed in 2.3.1.

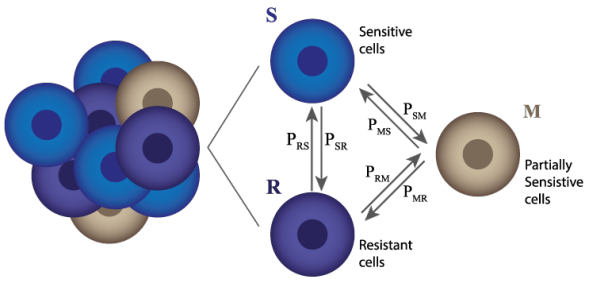

(a) Schematic representation of an heterogeneous population of tumor cells, composed by tumor sensitive (S), partially resistant (M) and resistant (R) cells. All the cells can switch phenotypes between them.

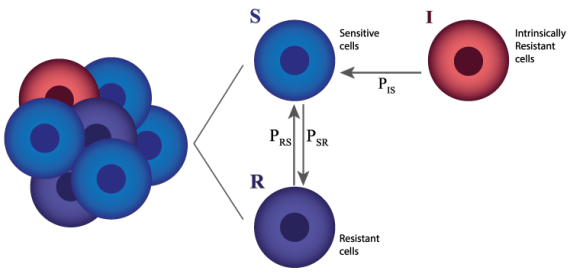

(b) Schematic representation of an heterogeneous population of tumor cells, composed by tumor sensitive (S), intrinsically resistant (M) and resistant (R) cells. R cells have acquired resistante due to chemotherapy administration. In turn, I cells were resistant to chemotherapy even before it was administered.

Figure 3.5: Examples of three equation models regarding chemotherapy resistance.

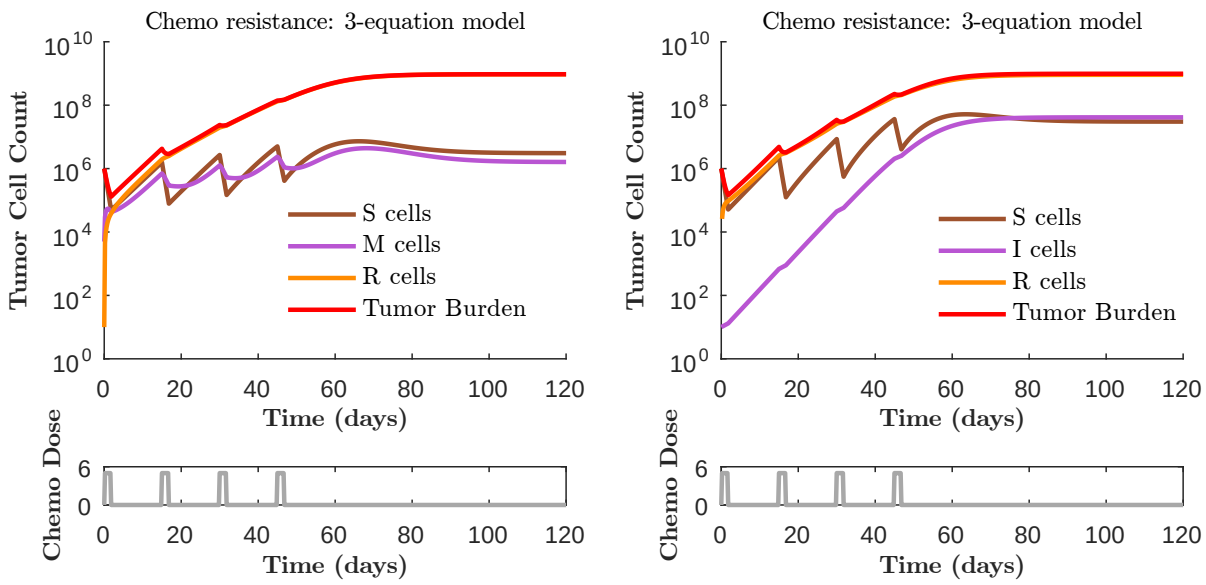

(a) Chemotherapy administered to a tumor composed by $S_0 = 9.95 \times 10^5$ sensitive cells, $M_0 = 4.99 \times 10^3$ partially sensitive cells and $R_0 = 10$ resistant cells. Parameters: $r_S = 0.431$, $r_M = 0.5 \times r_S$, $r_R = \frac{1}{3} \times r_S$, $c_S = 0.9$, $c_M = 0.5$, $c_R = 0.1$, $P_{SM} = 0.15$, $P_{MR} = 2 \times P_{SM}$, $P_{RM} = 5 \times 10^{-3}$, $P_{MS} = 0.5 \times P_{RM}$, $P_{SR} = 0.02$, $P_{RS} = 0.1 \times P_{RM}$.

(b) Chemotherapy administered to a tumor composed by $S_0 = 9.9999 \times 10^5$ sensitive cells, $I_0 = 10$ intrinsically resistant cells and $R_0 = 0$ resistant cells. Parameters: $r_S = 0.431$, $r_I = \times r_S$, $r_R = \frac{1}{3} \times r_S$, $c_S = 0.9$, $c_I = 0.07$, $c_R = 0.1$, $P_{SR} = 0.15$, $P_{RS} = 5 \times 10^{-3}$, $P_{IS} = 5 \times 10^{-3}$.

Figure 3.6: Examples of tumor growth curves when two different three-equation models for the tumor-chemotherapy resistance dynamics are considered. In both cases, four doses of chemotherapy are administered over 45 days in a 15 day cycle of strength $u_c(t) = 5$ to a $x_0 = 10^6$ cell tumor. $f(j)$ was considered to follow the logistic growth law and $G(j, u(t))$, the Norton-Simon hypothesis. $x_{max} = 0.9804 \times 10^9$.

In practice, tumor cells display a spectrum of ranging sensitivity to drug therapy [96]. There are already some models in the literature (Kimmel et al. [97], Swierniak and Smieja [98], Lorz et al. [99, 100] later expanded upon by Greene et al. [101], Lavi et al. [102]) that try to deal with this reality. However, due to their high dimensionality, these models only allow a limited analysis. This highlights the importance of finite-dimensional approximations which ,despite being approximations, are still illustrative [103].

3.1.3 Tumor-immune models

Over the years, several mechanistic mathematical models considering the interaction between the tumor cells and the immune system have been developed. The complexity of these models as well as their biological foundation have evolved progressively due to the inclusion of more features regarding the tumor micro-environment and the immune system [71].

3.1.3.1 Two equation models

The first two equation-models incorporate a poor caricature of the immunosurveillance mechanism described in 2.2. They only considered two cell types, the cancer cells and the immune cells able to kill them (effector immune cells) [104]. As competition models, they made use of the predator (effector cells)-prey (tumor cells) relationship represented in figure 3.7.

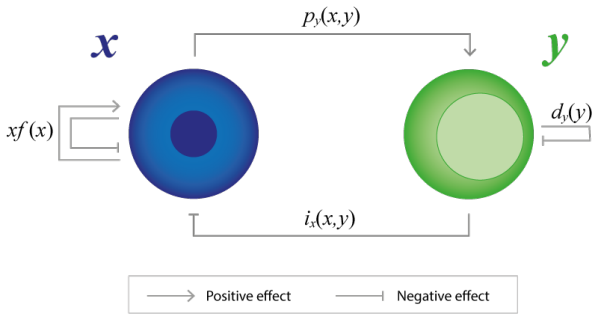

Figure 3.7: Schematic representation of the interactions between cancer cells (x) and effector immune cells (y) considered in the first competition models. The positive effects are associated with positive terms in this two-equation model and vice versa. Adapted from [71].

Mathematically, figure 3.7 can be translated into [71]

$$\dot{x} = xf(x) - i_x(x,y), \tag{3.9}$$

$$\dot{y} = p_y(x,y) - d_y(y). \tag{3.10}$$

Table 3.4 summarizes the notation used in this section. Examples of this type of models are the Lokta-Volterra predatory models [104]. Nevertheless, two of the assumptions of the predator-prey models are not valid in the context of tumor growth. Tumor cells do grow in the absence of the predators and the interactions between tumor cells and the effector cells are indeed simultaneously harmful to tumor $(i_x(x,y))$ and capable of recruiting effector cells $(p_y(x,y))$ [104]. Even in the absence of tumor cells, effector immune cells are still produced, namely the cells from the non-specific immunity (NK cells) [104]. Furthermore, the number of interactions between effector cells and tumor cells is not proportional to the product of these two populations, since immune cells do not have equal access to all the tumor cells [104].

The first predatory models (3.9) and (3.10) were then extended, incorporating more complex interactions between these two populations, as represented in figure 3.8 [71].

Table 3.4: Notation used in 3.1.3.

State variables and rate functions	**Description**
x	Cancer cells,
y	Effector Immune cells,
$z,\ w$	Other cells or cytokines,
$f(x)$	Tumor growth model,
$i_j, \quad j = \{x,y,z,w\}$	Inhibition of state variables (type j) by other state variables,
$p_j, \quad j = \{x,y,z,w\}$	Proliferation of state variables (type j) in the presence of x,
$d_j, \quad j = \{x,y,z,w\}$	Death (apoptosis)of state variables (type j),
$\phi_j, \quad j = \{x,y,z,w\}$	Time-(in)dependent treatment or influx of state variables (type j).

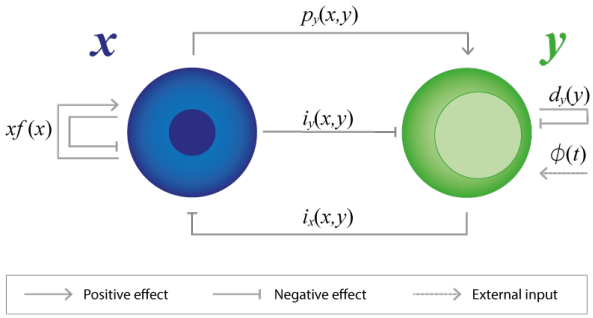

Figure 3.8: Schematic representation of the interactions between cancer cells (x) and effector immune cells (y) present in the improved predator-prey models. Tumor cells are considered to inhibit effector immune cells $(i_y(x,y))$. Effector immune cells grow even in the absence of tumor cells $(\phi(t))$. Adapted from [71].

Once again, figure 3.8 can be translated mathematically into [71]

$$\dot{x} = xf(x) - i_x(x,y), \tag{3.11}$$

$$\dot{y} = p_y(x,y) - i_y(x,y) - d_y(y) + \phi(t). \tag{3.12}$$

The term $p_y(x,y)$ should include a rate-limiting recruitment term. In fact, although the interaction between the cancer cells and immune cells stimulates the further production and recruitment of effector immune cells, there is a limit to the rate that the human body produce these cells [104]. The term $i_y(x,y)$ accounts for the immune cell death and inactivation resultant from the cancer immunoevasive strategies discussed in 2.2.1 [105]. It also accounts for the limit in the production of proteins such as FasL and perforin, which are used respectively by T_C cells and both NK cells and T_C cells to kill cancer cells (see 2.2). Each further interaction of these effector immune cells with cancer cells decreases their cytotoxic activity in the future [104]. Finally, the term $\phi(t)$ accounts for the direct source of immune cells through recruitment from the blood and bone marrow [105].

Examples of this family of models are the d'Onofrio model which has as particular cases the models from Stepanova [106], Michelson et al. [107], Michelson and Leith [108], de Vladar and González [109], Foryś et al. [110], Kuznetsov et al. [111], Gałach [112], Sotolongo-Costa et al. [113]. Figure 3.9 represents the tumor-effector immune cells dynamics of the Kuznetsov et al. [111] two-equation model. In this figure, the immune system is able to induce a spontaneous relapse and remission of the tumor. In fact, a decaying oscillation of the tumor burden to a dormant tumor state is shown. Simultaneously, a fluctuating number of effector immune cells increase as the tumor reach its dormant state. Even though these models explain some generic mechanisms observed in tumors (e.g. tumor regression and dormancy, oscillations in tumor size), they are too generic. Consequently, they cannot be used to understand the role of some immune cell types in tumor evolution or to develop therapies which will target specific components of the immune system, such as immunotherapy [71, 104].

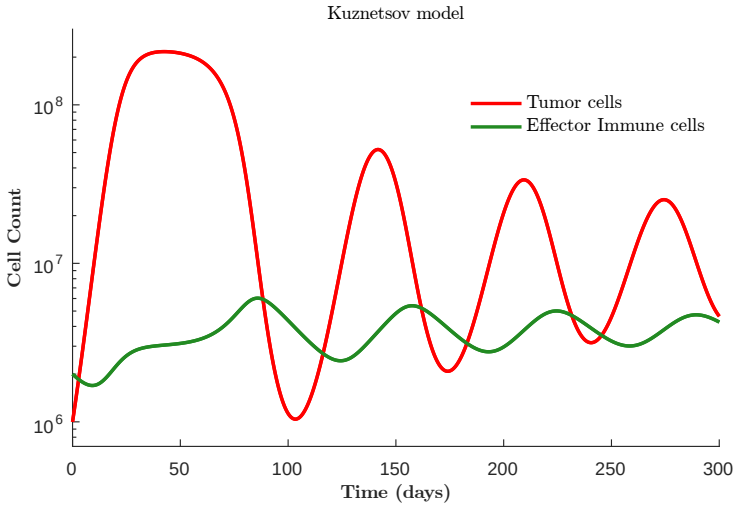

Figure 3.9: Behavior of tumor ($x_0 = 10^6$) and effector immune cells ($y_0 = 2 \times 10^6$) when a two-equation model for the tumor-immune system dynamics (Kuznetsov model [111]) is considered. $f(x)$ follow the logistic growth law. $i_x(x,y) = c_1xy$, $p_y(x,y) = \dfrac{pxy}{s+x}$, $i_y(x,y) = c_2xy$, $d_y(y) = dy$ and $\phi(t) = \phi$. Parameters: $r = 0.431$, $x_{max} = 0.9804 \times 10^9$, $c_1 = 1.101 \times 10^{-7}$, $p = 0.1245$, $c_2 = 3.422 \times 10^{-10}$, $d = 0.0412$, $s = 2.019 \times 10^7$, $\phi = 1.3 \times 10^4$.

3.1.3.2 Three and more equation models

The need to obtain more biologic accurate models has resulted in the introduction of more equations to the dynamics (3.11) and (3.12). These equations represent the behavior of certain cell types and/or molecules important in the immunosurveillance. Some models choose to model the immune system cells in just one equation, giving more importance to healthy cells (*e.g.* Pillis and Radunskaya [114], De Pillis and Radunskaya [115] and Owen and Sherratt [116] models) or signaling proteins, such as cytokines and chemokines (*e.g.* Kirschner and Panetta [117] and Arciero et al. [118]). Others distinguish the effector immune cells between two key cell types of the cellular immunity, NK cells and T_C cells (*e.g.* de Pillis and Radunskaya [119], de Pillis et al. [120] model), as represented in figure 3.10.

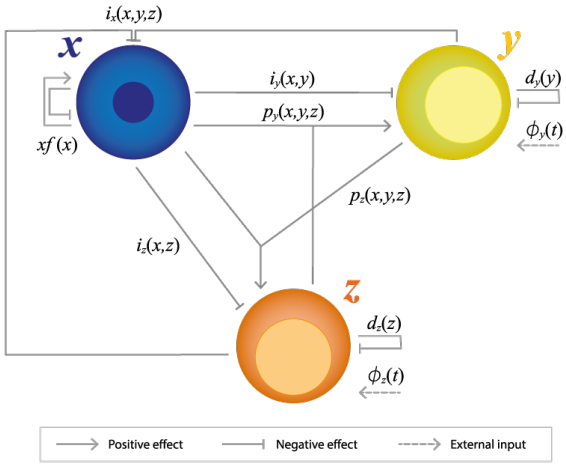

Figure 3.10: Schematic representation of the interactions between cancer cells (x) and two distinct immune cells, NK cells (y) and T_C cells (z). The positive effects are associated with positive terms in the respective three-equations model and vice versa. Adapted from [71].

Usually, the models consisting on two effector cell types have the following structure [71]

$$\dot{x} = xf(x) - i_x(x, y, z) \tag{3.13}$$

$$\dot{y} = \phi_y(t) + p_y(x, y, z) - d_y(y) - i_y(x, y), \tag{3.14}$$

$$\dot{z} = \phi_z(t) + p_z(x, y, z) - d_z(z) - i_z(x, z), \tag{3.15}$$

where y and z are the immune cell types, namely NK cells and T_C cells. The rate functions present in (3.13), (3.14) and (3.15) have the same meaning that the ones present on table 3.4, however they depend on one more state variable. Here, the term $i_x(x, y, z)$ represents the rate at which cancer cells are killed in interactions with NK cells ($i_x^y(x, y)$) and T_C cells ($i_x^z(x, z)$) [71]

$$i_x(x, y, z) = i_x^y(x, y) + i_x^z(x, z). \tag{3.16}$$

Special attention must be given to the fractional cell kill rates. $i_x^y(x, y)$ and $i_x^z(x, z)$ represent negative interactions (competition for space and nutrients, regulatory actions and direct cell population interactions) between immune and tumor cells [74]. In contrast to the fractional cell kill rate term considered in figure 3.9, this term should not be simply proportional to the number of effector cells [104]. First, immune cells are not equally likely to interact with any tumor cell. For instance, T_C cells are recruited to the tumor site by the presence of specific chemicals. Therefore, not all tumor cells are equally accessible to this type of attack [104]. Second, the number of predators per prey does affect the probability of a kill. Consequently, this term is expected to depend on the ratio of effector to tumor cells [104]. By performing data fitting experiments using cell lysis data from both mouse and human, de Pillis and Radunskaya [119] obtained the following expressions

$$\frac{i_x^y(x, y)}{x} = c_1 y^{\lambda}, \tag{3.17}$$

$$\frac{i_x^z(x, z)}{x} = c_5 \frac{\left(\frac{z}{x}\right)^{\lambda}}{s_3 + \left(\frac{z}{x}\right)^{\lambda}}, \tag{3.18}$$

where λ represents how the lysis rate depends on the effector cell and s_3 is the target ratio, which affects the steepness of the curve. Finally, c_5 is the maximum lysis rate. These expressions reflect the different nature of the interactions between NK/T_C cells and the tumor [104]. Equation (3.18) captures the observed *in vitro* and *in vivo* lysis dependence on the ratio of T_C cells to tumor cells and the saturation on the number of cells lysed. This saturation may result from T-cells antigen-specificity. Curiously, this effect was not observed for the NK cells [104].

Although the three-equation models produce the same behaviors as the two-equation models, they lead to substantial biological insights regarding the interactions among different types of cells, between cells and cytokines, and their influence on tumor size [71]. The same occur for the further introduction of equations. Some of the four equation models investigate the interactions among distinct cytokines and the major histocompatibility complex (*e.g.* Kronik et al. [121]). Others investigate the interactions among multiple immune cell populations (*e.g.* de Pillis et al. [10]), dendritic cells and cytokines (*e.g.* Cappuccio et al. [122], Castiglione and Piccoli [123], De Boer et al. [124]), cancer cells in different stages and

treatment drugs (*e.g.* Villasana and Radunskaya [125]). They can even include time delays (Villasana and Radunskaya [125]), which represents the time that the immune system takes to recognize the tumor cells. As more equations are included, the more realistic the model became but the more key costs it has and more difficult is to analyze.

An example: de Pillis et al. [10] This mathematical model describes the kinetics of tumor cells and three different immune cells, as well the bloodstream drug concentrations of two distinct drugs (see table 3.5).

Table 3.5: State variables of de Pillis et al. [10] model.

State variables	Description
$T(t)$	Tumor cell population,
$N(t)$	Total NK cell population,
$L(t)$	Total T_C cell population,
$W(t)$	Number of white blood cells (circulating lymphocytes),
$C(t)$	Chemotherapy drug concentration in the bloodstream,
$I(t)$	Immunotherapy drug concentration in the bloodstream.

The equations of the cell populations and the bloodstream drug concentrations can be written as (3.19) and (3.20), respectively

$$\dot{j} = G_j + R_j + K_j + In_j + \phi_j \tag{3.19}$$

$$\dot{i} = \kappa_i + \phi_i, \tag{3.20}$$

where j is one of the four cell populations (T, N, L, W) and i is one of the bloodstream drug concentrations (C, I). $G_j\,, R_j\,, K_j$, and In_j are respectively the growth term, cell recruitment rate, fractional cell kill rate and cell inactivation/inhibition rate. κ_i is the decay rate of the drug i and, finally, ϕ_j and ϕ_i are the time profile of the drug interventions. Tables 3.6 and 3.7 specify the mathematical form of $G_j\,, R_j\,, K_j\,, In_j\,, \phi_j$ and $\kappa_i\,, \phi_i$ for each cell population and each bloodstream drug concentration, along with its biological explanation.

Table 3.6: Specification of the terms used in (3.20) for each drug bloodstream concentration and their biological meaning.

Term	Drug (i)	Expression	Description
κ_i	$C(t)$	$-k_c C$	After the injection of chemotherapeutic agent or the $IL-2$ (immunotherapy), the drug is eliminated from the body over time proportionally to its concentration. Both drugs are assumed to decay exponentially.
	$I(t)$	$-k_i I$	
ϕ_i	$C(t)$	u_c	Amount of the chemotherapeutic agent given over time.
	$I(t)$	u_i	Amount of $IL-2$ given over time.

Table 3.7: Specification of the terms used in (3.19) for each cell population and their biological meaning.

Term	Cells (j)	Expression	Description
G_j	$T(t)$	$r\left(1-\frac{T}{T_{max}}\right)T$	Tumor growth considered to be logistic according to data from [126].
	$N(t)$	$a_1 W$	**Production rate:** Chemotherapy induced lymphopenia diminishes the white blood cells counts ($W(t)$) of the patient (see 2.3.1). A NK cell production rate proportional to the $W(t)$ takes into account the chemotherapy effect in the NK cells production rate.
		$-d_1 N$	**Death rate:** All immune cells are considered to have a natural lifespan. Therefore, all death terms are assumed to be proportional to the immune cells counts.
	$L(t)$	$-d_2 L$	**Death rate:** T_C cells are part of the adaptive immune response, i.e. they are not produced in the absence of tumor cells. There is no permanent source of T_C cells but only a natural death rate.
	$W(t)$	a_4	**Production rate:** White blood cells produced at a constant rate.
		$-d_3 W$	**Death rate.**
R_j	$N(t)$	$\rho_1 \frac{T^2}{s_1+T^2} N$	NK cells are recruited by the presence of tumor cells by a modified Michaelis–Menten dynamics.
	$L(t)$	$\rho_2 \frac{D^2T^2}{s_2+D^2T^2} L$	T_C cells can be recruited by tumor cells that have been lysed by other T_C cells (Michaelis–Menten dynamics).
		$a_2 NT$	T_C cells are also recruited by the debris from tumor cells lysed by NK cells. This recruitment term is proportional to the number of tumor cells killed.
		$a_3 WT$	The recognition of tumor cells by the immune cells will also recruit T_C cells proportionally to the average of encounters between white blood cells and tumor cells.
		$\rho_3 \frac{LI}{s_4+I}$	The $IL-2$ immunotherapy stimulates the production of T_C cells, which can be also described by a Michaelis–Menten dynamics.
K_j	$T(t)$	$-c_1 NT$	Tumor lysis due to the NK cells proportional to the number of NK cells.
		$-DT$	Tumor lysis by T_C cells is described by a rational functional response which captures the saturation on the number of tumor cells lysed.
	All	$-c_j\left(1-e^{-C}\right)j$	Chemotherapy drug kill term of population j. The effectiveness of chemotherapy is bounded since certain chemotherapeutic drugs only act at specific phases of the cell cycle.
In_j	$N(t)$	$-c_2 TN$	Reflects the immunoevasive strategies developed by tumor cells to escape elimination by either NK cells and T_C cells. Its cytotoxic activity decreases after some encounters with cancer cells. This inactivation term is then considered to be proportional to the number of encounters of these two populations.
	$L(t)$	$-c_3 TL$	
		$-c_4 NL^2$	When the levels of activated T_C cells not responsive to cytokines are too high, a regulation/suppression of the T_C cells activity occurs. The cytokine $IL-2$ increases the T_C cells resistance to this inactivation.
ϕ_j	$N(t)$	$u_L(t)$	Immunotherapy - TIL drug intervention term . T_C cells levels are boosted.

Finally, bringing together the terms presented for each cell population and bloodstream drug concentration, the following system of equations is obtained

$$\dot{T} = r\left(1 - \frac{T}{T_{max}}\right)T - c_1 NT - DT - c_T\left(1 - e^{-C}\right)T, \tag{3.21}$$

$$\dot{N} = a_1 W + \rho_1 \frac{T^2}{s_1 + T^2} N - d_1 N - c_2 TN - c_N\left(1 - e^{-C}\right)N, \tag{3.22}$$

$$\dot{L} = \rho_2 \frac{D^2 T^2}{s_2 + D^2 T^2} L + (a_2 N + a_3 W)T - d_2 L - c_3 TL - c_4 NL^2 - c_L\left(1 - e^{-C}\right)L \tag{3.23}$$

$$+ \rho_3 \frac{LI}{s_4 + I} + u_L(t), \tag{3.24}$$

$$\dot{W} = a_4 - d_3 W - c_w\left(1 - e^{-C}\right)W, \tag{3.25}$$

$$\dot{C} = -k_c C + u_c(t), \tag{3.26}$$

$$\dot{I} = -k_i I + u_i(t), \tag{3.27}$$

$$D = c_5 \frac{d\left(\frac{L}{T}\right)^{\lambda}}{s_3 + \left(\frac{L}{T}\right)^{\lambda}}. \tag{3.28}$$

Several simulations of this model can be found in [10].

3.2 Optimal control theory

Optimal control had its origins in the calculus of variations in the 17th century when Johann Bernoulli challenged other famous contemporary mathematicians (Newton, Leibniz, Jacob Bernoulli, L'Hôpital and von Tschirnhaus) with the brachystochrone problem [127]. The interest of Euler (student of Bernoulli) and Lagrange in this thematic led to the emergence of a general mathematical theory, opening the history of the calculus of variations [128]. Since then, several notable personalities (Legendre, Jacobi, Hamilton, Weierstrass, Bolza, Bliss, Bellman, McShane) have contributed to the further development of the calculus of variations [127]. In 1962, Lev S. Pontryagin expanded the classical calculus of variations to handle control variable inequality constraints, enunciating the Pontryagin maximum principle [128]. After the emergence of the digital computer, shooting algorithms and afterwards gradient algorithms were developed [127].

The first applications of optimal control methods to biomedical problems arising in cancer treatment concerned almost exclusively cancer chemotherapy and date back to the 80s [9]. Some decades later, optimal control methods were also applied to models concerning development of chemotherapeutic drug resistance, immunotherapy and other novel treatments [9].

In summary, optimal control aims to determine the inputs $u(t)$, which take values in the space of

admissible controls U (i.e. $u(t) \in U$) of a dynamical system with equations of motion

$$\dot{x} = f\left(x(t), u(t)\right), \tag{3.29}$$

where $x(t)$ is the trajectory in state space of the dynamic system. These optimal controls optimize (in other words, minimize or maximize) a specified performance index, which in its so-called Bolza form is given by

$$J(u(t)) = \varphi\left(x(T)\right) + \int_{t_0}^{T} L\left(x(t), u(t)\right)\, \mathrm{d}t, \tag{3.30}$$

while satisfying the design requirements. The variable $t \in [t_0, T]$, where t_0 is the initial time and T the terminal time. $\varphi\left(x(T)\right)$ is the penalty term on the final state and $L\left(x(t), u(t)\right)$ the Lagrangian or running cost. The Lagrangian measures the cost over the time interval considered [129, 130].

All in all, a minimization optimal control problem can be formulated in the following manner

[OC] For a free terminal T:

$$\begin{aligned} \min_{u(t)} \quad & J(u(t)), \\ s.t. \quad & \dot{x} = f\left(x(t), u(t)\right), \\ & x(t_0) = x_0, \\ & t \in [t_0, T], \\ & u(t) \in U. \end{aligned} \tag{3.31}$$

3.2.1 Pontryagin's maximum principle

According to the signs of the Hamiltonian, which is defined in this section, the maximum principle can be enunciated in four equivalent versions. Here, its minimum formulation is considered. The Pontryagin's principle gives the fundamental necessary conditions for the solution of (3.31) to be optimal in optimal control problems [130]. In order for this to happen and assuming that the optimal control $(x_*(t), u_*(t))$ is piecewise continuous, the Hamiltonian function given by

$$H(\lambda(t), x(t), u(t)) = \lambda_0' L(x(t), u(t)) + \lambda(t)' f(x(t), u(t)), \tag{3.32}$$

must be minimum $\left(\frac{\partial H}{\partial u} = 0\right)$ at every instant $t \in [t_0, T]$ when the optimal control $(x_*(t), u_*(t))$ is considered. $\lambda(t) \in \mathbb{R}^n$ is the co-state or adjoint variable. The control should not only satisfy the necessary conditions for minimality but also be a true minimizer over the control set U

$$H(\lambda(t), x_*(t), u_*(t)) = \min_{v \in U} H(\lambda(t), x_*(t), v(t)). \tag{3.33}$$

If the Lagrangian function $L(x(t), u(t))$ and the dynamics $f(x(t), u(t))$ are time-invariant, *i.e.* they do not depend on time t, the Hamiltonian function $H(\lambda(t), x(t), u(t))$ is constant over time [131].

The Hamiltonian partial derivatives hold the following expressions

$$H_\lambda(\lambda(t), x(t), u(t)) = \dot{x} \Leftrightarrow \dot{x} = f\left(x(t), u(t)\right), \tag{3.34}$$

$$H_x(\lambda(t), x(t), u(t)) = -\dot{\lambda}'(t) \Leftrightarrow \dot{\lambda}'(t) = -\lambda(t)' f_x(x(t), u(t)) - \lambda_0' L_x(x(t), u(t)). \tag{3.35}$$

Equation (3.35) is known as the adjoint equation. The adjoint variable at the terminal time T is given by

$$\lambda(T)' = \lambda_0 \varphi_x\left(x(T)\right). \tag{3.36}$$

For the sake of simplicity, the subscript applied to a function represents its partial derivative with respect to the variable in that subscript, i.e. $\xi_x \equiv \nabla_c \xi$. Moreover, to avoid confusions with the terminal time T, the transpose is represented by the prime superscript, i.e. $v' \equiv v^T$. The pair $((x(t), u(t)), (\lambda_0, \lambda(t))$ is called an extremal lift. The vector $(\lambda_0, \lambda(t))$ can be normalized given that the conditions are linear in the multipliers. Thereupon, when the extremal lift is normal $(\lambda_0 > 0)$, it is assumed that $\lambda_0 = 1$ without loss of generality.

3.2.2 Performance Index

The performance index (3.30), also known as cost function or objective, is artificially imposed from the outside and depending on its specific functional form and parameters, distinct trajectories and control laws are determined [132]. Generally, several forms of the objective are tested and the one which system response is the most satisfactory is chosen [132].

When the performance index dependence on the control $u(t)$ is linear, the norm of the objective is said to be L1. In contrast, when this dependence is quadratic, the norm of the cost functional is L2. Distinct norms lead to optimal solutions with different mathematical properties.

3.2.2.1 L1-norm

The L1-norm present some analytical challenges. The switching function is given by $\phi(t) = \frac{\partial}{\partial u} H(\lambda(t), x(t), u(t))$. Whenever $\phi(t_j) = 0$, all control values trivially satisfy the minimum condition and thus, in principle, all are candidates for optimality [132]. When $\phi(t) \neq 0$ or does not vanish on an open time interval $(\phi(t_j) = 0 \wedge \frac{\mathrm{d}\phi(t_j)}{\mathrm{d}t} \neq 0)$, the minimum of the Hamiltonian is obtained at the boundary points of H. The optimal control is thus a bang-bang control with discontinuities between the boundary values of the control interval when the switching function changes sign (at the bang-bang switch t^s)

$$u_*(t) = \begin{cases} u_{min}, & \phi(t) > 0, \\ u_{max}, & \phi(t) < 0. \end{cases} \tag{3.37}$$

However, when the switching function do vanishes during an open time interval $(\phi(x_*(t_j), \lambda(t_j)) = 0)$ as well as all its time derivatives, an extremal singular control arc is obtained. For more considerations about local optimal properties of singular control arcs see [133]. Singular control arcs are often the most natural candidates for optimality, while bang-bang controls only arise where singular controls are inadmissible or inexistent [132].

3.2.2.2 L2-norm

The L2-norm results in an Hamiltonian strictly convex in the control $u(t)$. Therefore, it has an unique minimizer, albeit only in the state-multiplier space, simplifying the mathematical analysis [132]. The equation $\frac{\partial H}{\partial u} = 0$ can be solved in order to $u(t)$, obtaining the indicator function $\psi(t)$ [132]. The optimal controls are thus continuous and can take any value inside the control set

$$u_*(t) = \begin{cases} u_{min}, & \psi(t) \leqslant u_{min}, \\ \psi(t), & u_{min} < \psi(t) < u_{max}, \\ u_{max}, & \psi(t) \geqslant u_{max}. \end{cases} \tag{3.38}$$

3.2.3 Numerical methods

Due to the high complexity of most applications, real-life optimal control problems are most often solved numerically [129]. These numeric methods can be classified into three main families: dynamic programming, and direct and indirect methods [133].

Dynamic Programming is based on the Hamilton-Jacobi-Bellman (HJB) equation. The principle of optimality considers that each sub-trajectory between an intermediate time and final time of an optimal trajectory is an optimal trajectory too. Therefore, the HJB equation is solved over a shorter horizon starting from the end and the complete solution is recursively find proceeding backwards [133].

Indirect Methods are based on the Pontryagin minimum principle. By using the Hamiltonian function, the problem is reduced to a two-point boundary value problem, which solutions are extremals, a necessary condition for optimality. Both adjoint equations and control equations are explicitly calculated [134]. This can be done using the backward-forward sweep (BFS) method, which numerical algorithm is as follow [134]:

1. Subdivide the interval $[t_0, T]$ into N_{int} equal subintervals;
2. Make an initial guess for the control $u(t)$. $u(t)$ must be piecewise-constant for each subinterval;
3. Integrate the state equation (3.29) from $[t_0, T]$ with initial value x_0 using the $u(t)$. Store the state trajectory $x(t)$;
4. Integrate the adjoint equation (3.35) backwards in time, i.e. $[T, t_0]$ with final condition $\lambda(T)$ using the $u(t)$ and the $x(t)$ obtained in step **3.**;. Store the costate trajectory $\lambda(t)$;
5. Update the value of $u(t)$ using the $x(t)$ and $\lambda(t)$ obtained in step **3.** and **4.**;
6. Verify convergence. Otherwise return to step **3.**.

The integration of steps **3.** and **4.** can be done using *ode45* numerical solver, at least as a first attempt [134]. Indirect shooting and multiple (time interval is divided in subintervals) shooting methods are also

used. Although they are similar to BFS, they take an initial value for the adjoint equation and solve it forward [134].

Some of the numerical methods are gradient-based and therefore the optimal solution is found upon a process of convergence [129]. In other words, the objective function is minimized through an iterative descent procedure for improving estimates of the control $u(t)$, so as to come closer to satisfying $\frac{\partial H}{\partial u} = 0$ [135]. An example is the steepest descent method, also known as the gradient descent, which is a first-order gradient method.[136] Steps (η) are taken in the opposite direction of the gradient of the Hamiltonian and proportionally to its magnitude. The steps 1, 2 and 3 of this algorithm are the same of the BFS method [136]

1.–3. See step **1.**, **2.**, **3.** and **4.** of the BFS algorithm;

5. Verify convergence and stopping criteria;

6. Update the value of $u(t)$, which will be used in the next iteration $(j+1)$ using the $x(t)$ and $\lambda(t)$ obtained in the previous steps

$$u^{(j+1)}(t) = u^{(j)}(t) - \eta \frac{\partial}{\partial u} H^{(j)}(x(t), \lambda(t), u(t)); \tag{3.39}$$

7. Return to step 2, until convergence is verified or the stopping criteria is met.

Direct Methods involve the discretization of the optimal control problem, which is then transcribed to a nonlinear programming problem (NLP). The control is parameterized with piecewise linear functions. Then, it can be numerically solved using direct shooting and multiple shooting methods [133, 134].

Chapter 4

Mathematical Model

As reviewed in 3.1, several ODE tumor mathematical models exist in the literature that consider the tumor-immune dynamics or the development of drug resistance. However, up to the present time there is not a single model that combines both. As discussed in 2.3.1, the development of drug resistance is the major reason behind chemotherapy failing. Moreover, the immune system is implicated in the efficacy of chemotherapy. Given these points, the development of tumor mathematical models that explore both realities is of utmost importance to develop effective anti-cancer therapies. With this in mind, in this chapter an ODE tumor mathematical model considering the immune system and the onset of drug resistance is developed and some numerical simulations are presented.

4.1 Model formulation

Herein, two ODE mathematical models reviewed in 3.1, de Pillis et al. [10] and Hahnfeldt et al. [14], are combined. Accordingly, a tumor-immune mathematical model consisting of cancer growth on a cell population level with combined immune and chemotherapy treatments and the concomitant development of drug resistance is obtained. This model has the state variables listed in table 4.1.

Table 4.1: State variables of the model developed.

State variables	Description
$S(t)$	Cancer cells sensitive to the chemotherapy treatment,
$R(t)$	Cancer cells resistant to the chemotherapy treatment,
$N(t)$	Total NK cell population,
$L(t)$	Total T_C cell population,
$W(t)$	Number of white blood cells (circulating lymphocytes),
$C(t)$	Chemotherapy drug concentration in the bloodstream,
$I(t)$	Immunotherapy drug concentration in the bloodstream.

As a consequence of the combination of the aforementioned models, the resulting model is able to generate the observed *in vivo* tumor behaviors exhibited by each individual model (see table 4.2).

Table 4.2: *In vivo* tumor behaviors generated by de Pillis et al. [10] and Hahnfeldt et al. [14] models.

de Pillis et al. [10]	**Hahnfeldt et al. [14]**
Uncontrolled growth of tumor cells.	Uncontrolled growth of tumor cells.
Tumor dormancy and outbreak.	Tumor heterogeneity.
Tumor injury due to the normal immune function.	Tumor injury due to chemotherapy.
Cytotoxic immune cells inactivation through interaction with tumor cells.	Onset of drug resistance due to (epi)genetic mutations.
Tumor stimulation on the immune response.	Tumor re-sensitization.
Innate and adaptive immune response to the presence of the tumor.	
System response to chemotherapy (direct cytotoxic effects on both tumor and immune cell populations).	
System response to immunotherapy (IL-2 and TIL injections).	

4.1.1 Model assumptions

Table 4.3 summarizes the assumptions underlining each one of the original models. Most of them are based on published statements or conjectures. For more details, see the original articles [10, 14].

As previously mentioned, the assumptions underlining the resulting model reflect the assumptions behind these two original models. Some of them have to be modified to enable a coherent combination of both models:

- Tumor cells are considered to follow a logistic growth law in the absence of an immune response and anticancer treatment.

For the reasons reviewed in 3.1.1.1, the exponential growth law is not appropriate to describe the tumor growth. For the sake of simplicity, it was decided to maintain the logistic growth law considered in the de Pillis et al. [10] model. However, the von Bertalanffy growth model would also have been a good option given its biological motivation.

Other assumptions are added or modified in order to improve the model:

- The initial tumor burden T_0 is considered to be composed mostly of sensitive cells and few intrinsically resistant cells.

Consequently, the tumor burden at every time instant is given by the sum of these two cell populations.

- Sensitive cells acquire drug resistance through (epi)genetic mutations. The higher the drug concentration, the more probable cancer cells are to develop chemotherapy resistance.

This assumption reflects the pressure of higher drug concentrations on the natural selection of cancer cells (see 2.3.1).

- Resistant tumor cells re-sensitization occur by chance through random (epi)genetic mutations.

The drug concentration is considered not to interfere with the re-sensitization effect experienced by resistant tumor cells. However, in the absence of the cytotoxic drug, the resistance phenotype does not confer any advantage to these cells. Therefore, the drug concentration may have a role in this effect.

- Resistant tumor cells are considered to be as sensitive to the immune response as the sensitive chemotherapeutic tumor cells.

In general, the strategies behind the acquisition of chemotherapy resistance are different from the cancer immunoevasive strategies (see 2.2.1 and 2.3.1). Therefore, it is reasonable to admit that drug resistance does not affect the immune response. It is important to realize that this conjecture may not be totally correct since the alteration of the apoptotic machinery as a strategy of drug resistance may prevent cancer cells from being killed by cytotoxic immune cells.

Table 4.3: Assumptions underlining the ODE mathematical models from de Pillis et al. [10] and Hahnfeldt et al. [14].

de Pillis et al. [10]	**Hahnfeldt et al. [14]**
Tumor cells follow a logistic growth law in the absence of an immune response and treatment.	Tumor cells follow an exponential growth law in the absence of treatment.
Cytotoxic immune cells (NK and T_C cells) kill tumor cells.	Tumor is composed by a population of faster growing chemotherapeutically sensitive cells and a population of slow-growing increasingly more resistant cells.
NK and T_C cells are stimulated by tumor cells, resulting in their expansion and enhancement of their cytolytic activity.	The probability of a resistant tumor cell undergo a mutation and became sensitive is less than the inverse phenomena.
Chemotherapy kills a fraction of tumor cells, NK cells, T_C cells and circulating lymphocytes dependent on the cytotoxic agent concentration and accordingly with the log-kill model.	Tumor cells are killed by the cytotoxic drug according to the log-kill model.
The fraction of tumor cells killed by the cytotoxic drug is higher than the fraction of immune cells killed by it. This fraction is always less than one.	Only a fraction of chemotherapeutically sensitive cells are killed by chemotherapy. A small percent of resistant cells are also killed. These fractions are always less than one.
NK cells (innate immunity) are present in the body even in the absence of tumor cells.	
T_C cells (adaptive immunity) are only present in great quantities in the presence of the tumor.	
NK and T_C cells became inactivated after some interactions with tumor cells.	
Circulating lymphocyte levels are used as a measure of patient health.	
NK and T_C cells are consider to stimulate or eliminate activated effector immune cells, reflecting the self-regulatory nature of the immune system.	

4.1.2 ODE model

The alteration of some assumptions mentioned in 4.1.1 and the inclusion of new ones has resulted in modifications at the mathematical level of both models. The time dependent pharmacokinetics on Hahnfeldt et al. [14] model was modeled as a third state variable, as in de Pillis et al. [10]. After the combination of both models, the first equation of the de Pillis et al. [10] model

$$\dot{T} = r\left(1 - \frac{T}{T_{max}}\right)T - c_1 NT - DT - c_T\left(1 - e^{-C}\right)T, \tag{3.21}$$

becomes

$$\dot{S} = r_S\left(1 - \frac{S+R}{T_{max}}\right)S - c_1 NS - DS - P_{SR}S + P_{RS}R - c_S\left(1 - e^{-C}\right)S, \tag{4.1}$$

$$\dot{R} = r_R\left(1 - \frac{S+R}{T_{max}}\right)R - c_1 NR - DR - P_{RS}R + P_{SR}S - c_R\left(1 - e^{-C}\right)R. \tag{4.2}$$

In order to privilege the administration of small drug concentrations, the transition rates between the sensitive and the resistant compartment were considered to be proportional to the concentration of the chemotherapeutic drug

$$\dot{S} = r_S\left(1 - \frac{S+R}{T_{max}}\right)S - c_1 NS - DS - \frac{C}{C_{max}}P_{SR}S + P_{RS}R - c_S\left(1 - e^{-C}\right)S, \tag{4.3}$$

$$\dot{R} = r_R\left(1 - \frac{S+R}{T_{max}}\right)R - c_1 NR - DR + \frac{C}{C_{max}}P_{SR}S - P_{RS}R - c_R\left(1 - e^{-C}\right)R, \tag{4.4}$$

where $C_{max} = \dfrac{max(u_c)}{k_c}$. The remaining equations of the de Pillis et al. [10] model have prevailed unchanged. However the tumor burden in now given by $T = R + S$.

All things considered, the final model, further referred as the dynamic $\dot{x} = F(x,t)$, is mathematically described by the following system of equations

Combination therapy model

$$\begin{aligned}
\dot{S} &= r_S\left(1 - \frac{S+R}{T_{max}}\right)S - c_1 NS - DS - \frac{C}{C_{max}}P_{SR}S + P_{RS}R - c_S\left(1 - e^{-C}\right)S,\\
\dot{R} &= r_R\left(1 - \frac{S+R}{T_{max}}\right)R - c_1 NR - DR + \frac{C}{C_{max}}P_{SR}S - P_{RS}R - c_R\left(1 - e^{-C}\right)R,\\
\dot{N} &= a_1 W + \rho_1\frac{T^2}{s_1 + T^2}N - d_1 N - c_2 TN - c_N\left(1 - e^{-C}\right)N,\\
\dot{L} &= \rho_2\frac{D^2T^2}{s_2 + D^2T^2}L + (a_2 N + a_3 W)T - d_2 L - c_3 TL - c_4 NL^2 - c_L\left(1 - e^{-C}\right)L\\
&\quad + \rho_3\frac{LI}{s_4 + I} + u_L(t),\\
\dot{W} &= a_4 - d_3 W - c_w\left(1 - e^{-C}\right)W,\\
\dot{C} &= -k_c C + u_c(t),\\
\dot{I} &= -k_i I + u_i(t),
\end{aligned} \tag{4.5}$$

where:

$$T = S + R, \tag{4.6}$$

$$D = c_5 \frac{d\left(\frac{L}{T}\right)^{\lambda}}{s_3 + \left(\frac{L}{T}\right)^{\lambda}}, \tag{4.7}$$

$$C_{max} = \frac{max(u_c)}{k_c}. \tag{4.8}$$

The terms considered here have the same biological meaning that the ones described in tables 3.7 and 3.6. The terms u_L, u_c, u_i concern the temporal administration of TILs, chemotherapy, and IL-2, respectively. 5×10^{11} TILs are administered as a bolus at day 7. In oder to study the model behavior in the absence of anti-cancer therapy or in the presence of only one type of therapy (chemo- or immunotherapy), three other models are used

Immunosurveillance model

$$\begin{aligned}
\dot{T} &= r_S \left(1 - \frac{T}{T_{max}}\right) T - c_1 NT - DT, \\
\dot{N} &= a_1 W + \rho_1 \frac{T^2}{s_1 + T^2} N - d_1 N - c_2 TN, \\
\dot{L} &= \rho_2 \frac{D^2 T^2}{s_2 + D^2 T^2} L + (a_2 N + a_3 W) T - d_2 L - c_3 TL - c_4 NL^2, \\
\dot{W} &= a_4 - d_3 W,
\end{aligned} \tag{4.9}$$

Immunotherapy model

$$\begin{aligned}
\dot{T} &= r_S \left(1 - \frac{T}{T_{max}}\right) T - c_1 NT - DT, \\
\dot{N} &= a_1 W + \rho_1 \frac{T^2}{s_1 + T^2} N - d_1 N - c_2 TN, \\
\dot{L} &= \rho_2 \frac{D^2 T^2}{s_2 + D^2 T^2} L + (a_2 N + a_3 W) T - d_2 L - c_3 TL - c_4 NL^2 + \rho_3 \frac{LI}{s_4 + I} + u_L(t), \\
\dot{W} &= a_4 - d_3 W, \\
\dot{I} &= -k_i I + u_i(t).
\end{aligned} \tag{4.10}$$

In both immunosurveillance and immunotherapy models, T is a state variable that represents the tumor burden. Since no cytotoxic drug is applied, the tumor burden is not partitionated in sensitive and resistant tumor cells.

Chemotherapy model

$$\dot{S} = r_S \left(1 - \frac{S+R}{T_{max}}\right) S - c_1 NS - DS - \frac{C}{C_{max}} P_{SR} S + P_{RS} R - c_S \left(1 - e^{-C}\right) S,$$

$$\dot{R} = r_R \left(1 - \frac{S+R}{T_{max}}\right) R - c_1 NR - DR + \frac{C}{C_{max}} P_{SR} S - P_{RS} R - c_R \left(1 - e^{-C}\right) R,$$

$$\dot{N} = a_1 W + \rho_1 \frac{T^2}{s_1 + T^2} N - d_1 N - c_2 TN - c_N \left(1 - e^{-C}\right) N, \tag{4.11}$$

$$\dot{L} = \rho_2 \frac{D^2 T^2}{s_2 + D^2 T^2} L + (a_2 N + a_3 W) T - d_2 L - c_3 TL - c_4 NL^2 - c_L \left(1 - e^{-C}\right) L,$$

$$\dot{W} = a_4 - d_3 W - c_w \left(1 - e^{-C}\right) W,$$

$$\dot{C} = -k_c C + u_c(t).$$

Table 4.4 presents a list of the parameters used in the models, their meaning, their estimated value and their source. The P_{RS} value was estimated below the value used in [103]. The number of TILs administered in the model (u_L) was not consistent with the clinical reality. Therefore, it was changed from 10^9 cells to 5×10^{11} cells [10].

These models are simulated for several T_0, where $S_0 = 0.995 T_0$ and $R_0 = 0.05 T_0$, in the case of a healthy immune system and a compromised one. Therefore, the two initial conditions used throughout this master thesis are

Initial conditions

$$\text{Healthy IS} \quad \longrightarrow \quad N_0 = 10^5, \quad L_0 = 10^2, \quad W_0 = 6 \times 10^{10}, \quad C_0 = 0, \quad I_0 = 0, \tag{4.12}$$

$$\text{Compromised IS} \quad \longrightarrow \quad N_0 = 10^3, \quad L_0 = 10, \quad W_0 = 6 \times 10^{8}, \quad C_0 = 0, \quad I_0 = 0. \tag{4.13}$$

Implementation notes To adjust these models to clinical reality, whenever the number of cells became lower than one, it is considered to be zero. It is only possible to have a rational cell number when the number of cells is above one. For instance, NK$= 1.5$ means that one NK cell is at half of its cellular division process. When T or $S + R$ are zero, D is also considered to be zero. In truth, T_C cells cannot kill inexistent tumor cells. Furthermore, the bloodstream concentration of chemo- and immunotherapy is always considered to be positive. Negative concentration values do not have a biological meaning and result in unrealistic behaviors of the models presented. Thereupon, in all the simulations presented throughout this master thesis, the cell count begins in 10^0 and the chemotherapy and $IL{-}2$ concentration in 0. Finally, contrary to the de Pillis et al. [10] model, u_L is administered as a bolus. This is accomplished by using two *ode45* to integrate the model, instead of just one. The first *ode45* integrate $\dot{x}$ from t_0 to the instant of the administration (t_a), and the second *ode45* from t_a until t_f. Therefore, the initial condition used in the second *ode45* is equal to $x(ta)$, with the exception of state L. In this case $L(ta) = L(ta) + TIL$, where TIL is the number of TILs administered at t_a (see Til in table 4.4).

Table 4.4: Description and value of the parameters used in the resulting model. Adapted from [10].

Param.	Value	Units	Description	Source
r_S	4.31×10^{-1}	day^{-1}	Growth rate of sensitive tumor cells.	M [126]
r_R	1.44×10^{-1}	day^{-1}	Growth rate of resistant tumor cells.	$\hbar$
T_{max}	9.80×10^{8}	day^{-1}	Carrying capacity.	M [126]
P_{SR}	0.15	$cell^{-1}$	Transitioning rate between the sensitive and resistant compartments.	[103]
P_{RS}	5.00×10^{-4}	$cell^{-1}$	Transitioning rate between the resistant and sensitive compartments.	$\hbar$
c_1	6.41×10^{-11}	$cell^{-1}$	Fractional tumor cell kill by NK cells.	H,M [7, 126]
c_2	3.42×10^{-6}	$cell^{-1}day^{-1}$	NK cell inactivation rate by tumor cells.	M [126]
c_3	1.42×10^{-6}	$cell^{-1}day^{-1}$	T_C cell inactivation rate by tumor cells.	M [111]
c_4	3.00×10^{-10}	$cell^{-2}day^{-1}$	Regulatory function by NK cells on T_C cells.	[10]
c_5	2.34	day^{-1}	Saturation level of fractional tumor cell kill by T_C cells.	H [7]
a_1	2.08×10^{-7}	day^{-1}	Fraction of circulating lymphocytes that become NK cells.	M [111]
a_2	1.10×10^{-7}	$cell^{-1}day^{-1}$	T_C cells production rate due to stimulation by tumor cells killed by NK cells.	M [137, 138]
a_3	6.50×10^{-11}	$cell^{-1}day^{-1}$	T_C cells production rate due to stimulation by tumor cells interacting with circulating lymphocytes.	[10]
a_4	7.5×10^{8}	$cellday^{-1}$	Constant source of circulating lymphocytes.	H**?**
d_1	4.12×10^{-2}	day^{-1}	Death rate of NK cells	M [111]
d_2	0.204	day^{-1}	Death rate of T_C cells.	M [137]
d_3	1.20×10^{-2}	day^{-1}	Natural death and differentiation of circulating lymphocytes.	H **?**
ρ_1	1.25×10^{-2}	day^{-1}	Maximum NK cell recruitment rate by tumor cells.	H,M [7, 126]
ρ_2	2.49×10^{-2}	day^{-1}	Maximum T_C cell recruitment rate.	H,M [7, 126]
ρ_3	0.125	day^{-1}	Maximum T_C cell recruitment rate by IL-2.	[117]
c_S	0.90	day^{-1}	Fractional sensitive tumor cell kill by chemotherapy.	[139]
c_R	0.10	day^{-1}	Fractional resistant tumor cell kill by chemotherapy.	$\hbar$
c_N,c_L, c_W	0.60	day^{-1}	Fractional immune cell kill by chemotherapy.	[139]
k_c	0.90	day^{-1}	Rate of chemotherapy drug decay.	[140]
k_i	1.00	day^{-1}	Rate of IL-2 decay.	[117]
s_1	2.02×10^{7}	$cell^2$	Steepness coefficient of the NK cell recruitment curve.	M [111]
s_2	3.66×10^{7}	$cell^2$	Steepness coefficient of the T_C cell recruitment.	H,M [7, 126]
s_3	8.39×10^{-2}	none		H [7]
s_4	2.00×10^{7}	$cell^2$	Steepness of T_C cell recruitment curve by IL-2.	[117]
λ	2.09	none		H [7]
Til	5×10^{11}	$cell$	Number of TIL administered.	H [47]

[M] Mouse data; [H] Human data; [$\hbar$] Estimated; [?] Data no longer available. See Bannock (2002); Hauser (2001) from [10].

4.2 Model Simulations

In this section, models (4.9), (4.10), (4.11) and (4.5) from 4.1.2 are simulated in order to analyse the contribution of the immune response, chemotherapy and immunotherapy alone in the combination therapy.

4.2.1 Immunosurveillance model

No alteration was made to the immune system terms present in the de Pillis et al. [10] model. Therefore, the results from figure 4.1 are only a reproduction of the ones that would be obtained using it. Several simulations are made considering various initial tumor burdens T_0. As in [10], the simulations outcome proved to be sensitive to the initial conditions used. Indeed, according with the simulations done, an healthy immune system (healthy IS) is capable of eradicating a tumor up to 10^7 cells, while an compromised (compromised IS) one only eradicates up to 3×10^5 tumor cells. Figure 4.1 present two cases in which the immunosurveillance mechanism succeeds to eliminate the tumor (left side) and other two cases where the tumor escapes immunosurveillance and reaches the carrying capacity (right side).

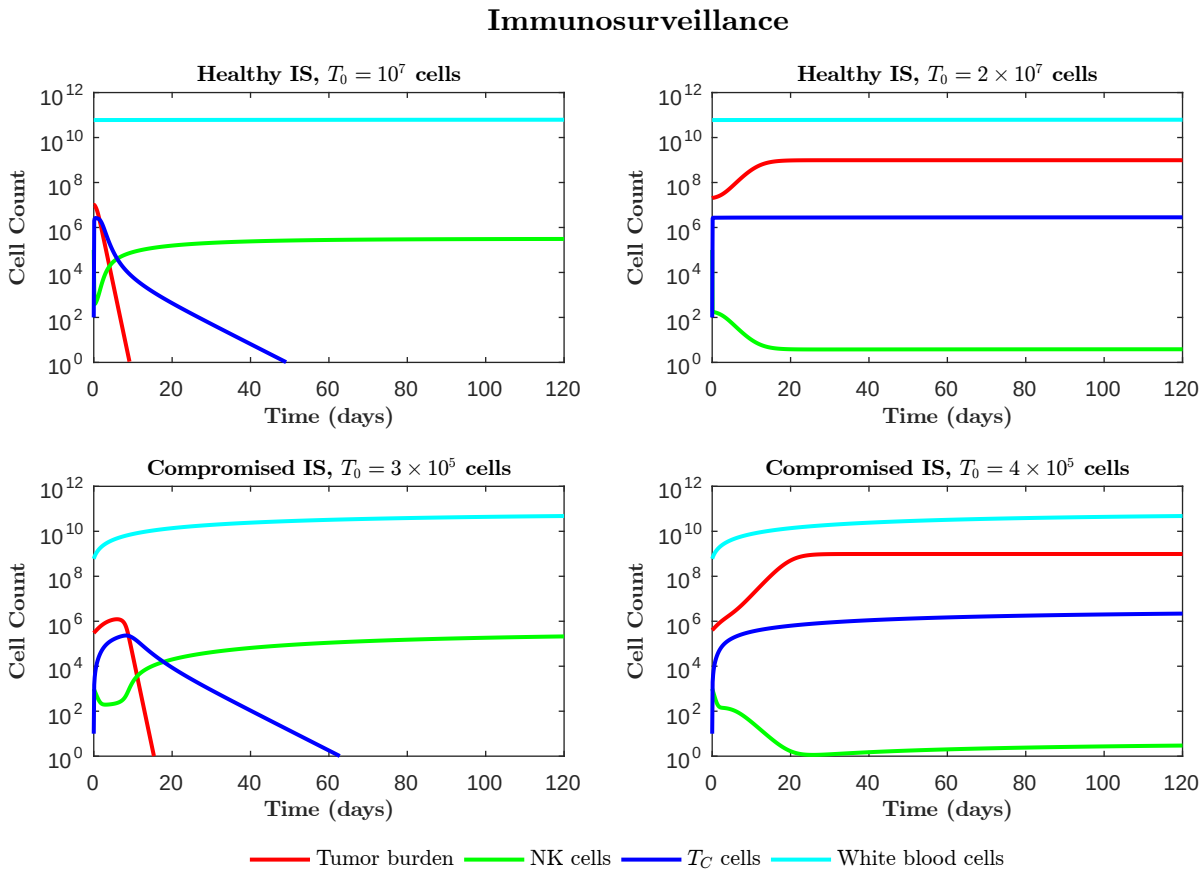

Figure 4.1: Healthy IS succeeds (see (4.12)) to eradicate a tumor with $T_0 = 10^7$ cells (top left) but fails to eliminate a tumor with $T_0 = 2 \times 10^7$ cells (top right). Compromised IS (see (4.13)) eradicates a tumor up to $T_0 = 3 \times 10^5$ cells (bottom left) but fails to eradicate $T_0 = 4 \times 10^5$ cells. Simulations obtained with the model (4.9).

The immune system is thus capable of eliminating tumors below the threshold of clinical detectability,

which accordingly to [141] is approximately 10^9 cells ($\approx 1g$ or $1cm^3$). As expected, the later the immune system became active against the tumor (higher T_0), the more difficult is to eliminate it. The results here obtained are consistent with Fig. 7. of the article de Pillis et al. [10].

When the tumor is successfully eradicated (figure 4.1, left side), the system asymptotically approaches the following steady state

$$F(N_0,t)=0 \quad \Leftrightarrow \quad \begin{cases} \dot{T}=0 \\ \dot{N}=0 \\ \dot{L}=0 \\ \dot{W}=0 \end{cases} \quad \Leftrightarrow \quad \begin{cases} T=0 \\ N=\dfrac{a_1}{d_1}W \\ L=0 \vee L=-\dfrac{d_2}{c_4 N} \\ W=\dfrac{a_4}{d_3} \end{cases} \quad \Leftrightarrow \quad \begin{cases} T=0 \\ N=3.16\times 10^5 \\ L=0 \vee L=-2.16\times 10^3 \\ W=6.25\times 10^{10} \end{cases} . \tag{4.14}$$

The number of white blood cells does not depend on tumor presence or its absence. In fact, this value is given by an equilibrium between the bone marrow constant source of white blood cells (a_4) and its natural death or differentiation into other cell type (d_3W). Henceforth, no matter the initial conditions, W will always tend to 6.25×10^{10} cells. Whenever the tumor is eradicated, T_c cells tend to zero. T_c cells belong to the adaptive immunity, being only produced in the presence of tumor cells. In their absence $\dot{L}=-d_2L-c_4NL^2$. T_c cells die due to both natural causes ($-d_2L$) and the self-regulatory effect of the immune system (c_4NL^2). It is not possible to have a negative number of cells of any type. Accordingly, whenever the cell number became less than one, it is considered to be zero. Conversely, NK cells belong to the innate immunity. Henceforth, they are always present in the body regardless the presence or absence of tumor cells. When tumor cells are eradicated $\dot{N}=a_1W-d_1N$. The NK cells steady state value is given by the equilibrium between its constant source, which is a fraction of the white blood cells (a_1W), and the cells that die due to its natural lifespan (d_1N).

On the other hand, when the tumor is not eradicated, the behavior of T_c and NK cells reverses. The constant source of NK cells and its recruitment rate by the tumor cells $\left(\rho_1\frac{T^2}{s_1+T^2}N\right)$ is not sufficient to compensate the number of cells that die naturally and mainly due to the tumor immunoevasive strategies (c_2TN). In contrast, T_c cells "production" is continuously stimulated by tumor cells that have been lysed by T_c cells $\left(\rho_2\frac{D^2T^2}{s_2+D^2T^2}L\right)$, NK cells (a_2NT) and recognized by white blood cells (a_3WT). This stimulation is so high that even the natural death of T_c cells, the immunoevasive strategies of the growing tumor (c_3TL) and the self regulatory effect of the immune system are not capable of compensate it.

When a compromised immune system is considered, the immune system takes more time to eradicate the tumor and to evolve to the steady-sate values (4.14), even for smaller values of T_0. The tumor negative effect in the immune cell types (immunoevasive strategies) is more visible in this case (initially, the number of NK cell decreases in the bottom left simulation). The behavior of compromised immune system when the tumor escapes immunosurveillance (bottom right simulation) is the same of the healthy immune system (top right simulation).

4.2.2 Immunotherapy

After some experiments, it is seen that a healthy immune system is capable of eradicating a tumor up to 10^7 cells as a healthy immune system by itself, without considering any sort of therapy. The same results are obtained either when a full dose of $IL-2$ is administered during 120 days or only from day 8 to 11. Figure 4.2 left simulation shows an healthy immune system incapable of eradicating a $T_0 = 2 \times 10^7$. Conversely, a compromised immune system is capable of eradicating up to 7×10^5 cells (see figure 4.2 right). By using immunotherapy it is possible to duplicate the number of cells eliminated by a compromised immune system by itself. Although immunotherapy directly strengths the immune system, its effectiveness appears to be limited to small tumors.

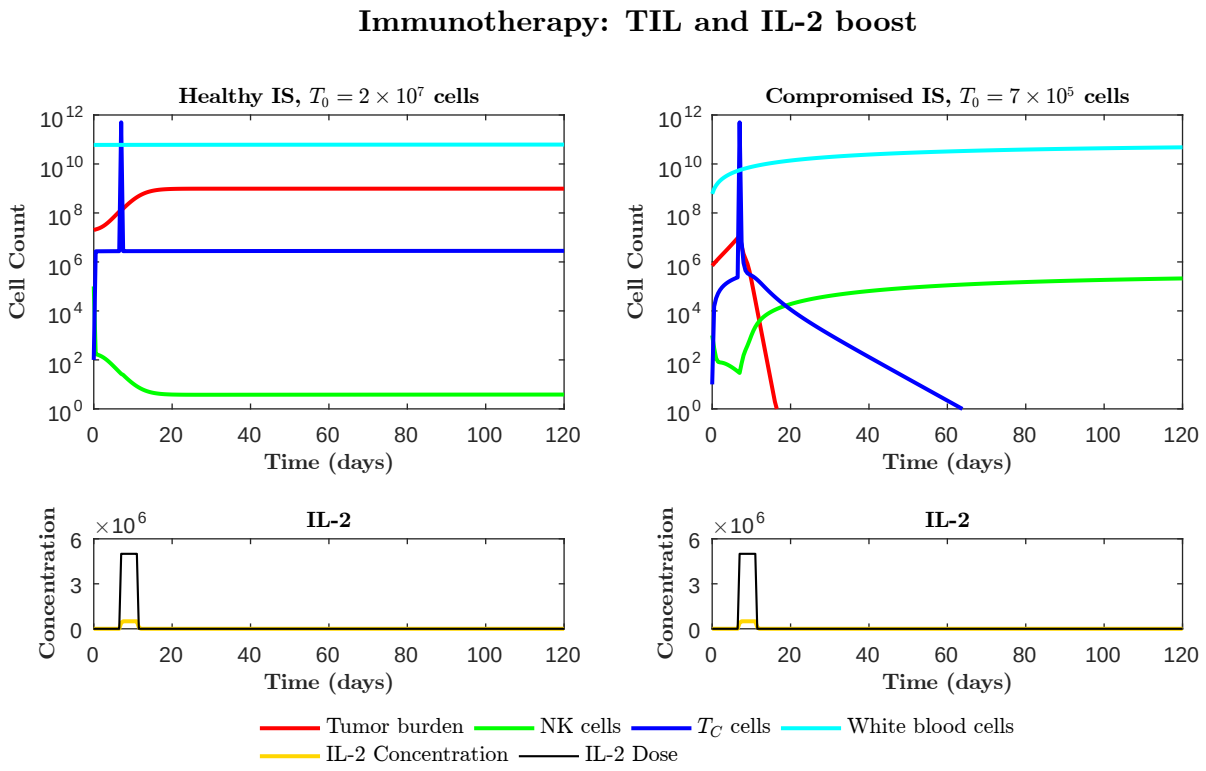

Figure 4.2: Healthy IS (see (4.12)) fails to eradicate a tumor with $T_0 = 2 \times 10^7$ cells (left). Compromised IS (see (4.13)) is capable of eradicating a tumor up to $T_0 = 7 \times 10^5$ cells. Simulations obtained with model (4.10) when 5×10^{11} TILs are administered at day 7 and IL-2 is administered from day 7 to 11 at a dose of 5×10^6.

The peak observed for the T_c cells curve corresponds to the administration of 5×10^{11} TILs at day 7. The results from de Pillis et al. [10] (see Fig. 9) shows that a compromised immune system can in fact eliminate an initial tumor burden of 10^6 cells. This inconsistency is explained by the different number of TILs administered and distinct methods of administration. While de Pillis et al. [10] have administrated 10^9 TILs during a whole day (from day 7 to 8), here they are administered as a single injection. Furthermore, in the results of de Pillis et al. [10] Fig. 9., IL-2 is only administered after the TIL administration (from day 8 to 11). As discussed in 2.3.2, the patients should be immediately treated with IL-2 after TILs infusion, in order to sustain the *in vivo* growth of T_c cells. Therefore, in this

simulation the administration of IL-2 is considered to start at day 7, the day when TILs are administered. Nevertheless, the number of TILs decays quickly. Although IL-2 increases the T_C cells resistance to inactivation $\left(\rho_3 \frac{LI}{s_4+I}\right)$, the number of T_C cells suppressed for not being responsive to cytokines, namely IL-2, was much higher $(c_4 N L^2)$.

4.2.3 Chemotherapy

The alterations made to the de Pillis et al. [10] model comprised only the tumor cells response to chemotherapy.

Modified Norton-Simon hypothesis First of all, rather than considering a log-kill model for the chemotherapy cell kill term, an adaptation of the Norton-Simon model is considered.
Imagine that at a certain instant t_0 there are $T(t) = 12$ cells. Of these 12 cell, 10 undergo cell division (see figure 4.3 top). During cell division, each one of the 10 cells dividing give rise to 2 cells, $\left(\text{i.e. } r_S \left(1 - \frac{T}{T_{max}}\right) T = 10\right)$. Accordingly, at $t + \Delta t$ there are $T(t + \Delta t) = 2 + 2 \times 10 = 22$ cells. Considering that chemotherapy kills for instance 90% (i.e. $c_S = 0.9$) of the cells in active division (figure 4.3 bottom), 9 of the 10 cells dividing are killed. Therefore, at $T(t + \Delta t) = 2 + 2 \times 10(1 - 0.9) = 4$.

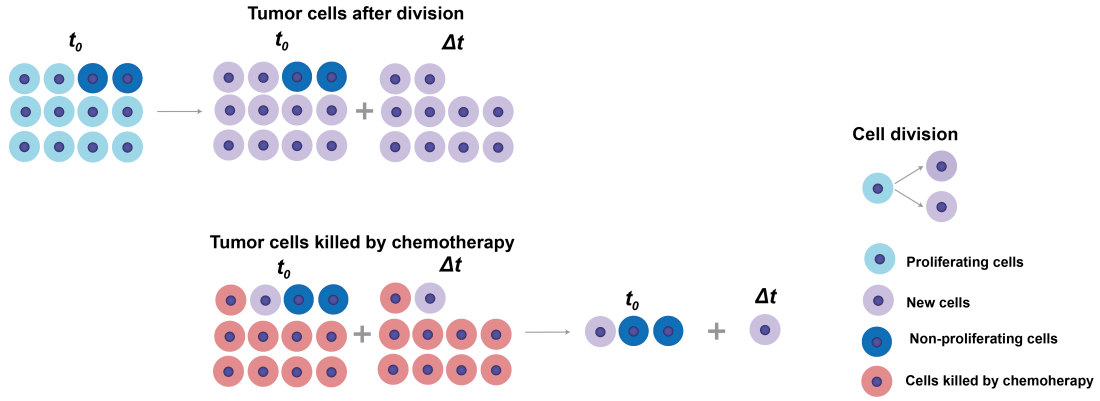

Figure 4.3: Motivation underlining the modified Norton-Simon hypothesis proposed.

Mathematically, the Norton-Simon hypothesis considers that 90% of the 10 cells are killed and therefore, $T(t + \Delta t) = 12 + 10 \times (1 - 0.9) = 13$ cells. The hypothesis proposed here $(G(T, t) = 2 c_T C f(T) T)$ considers that chemotherapy kills the double of the tumor cells that would be killed using the Norton-Simon model, according with figure 4.3. Therefore, $T(t + \Delta t) = 12 + 10 \times (1 - 2 \times 0.9) = 4$ cells.
After considering this modification of the Norton-Simon hypothesis, the first equation of the chemotherapy model (without considering resistance), becomes

$$\dot{T} = r_S \left(1 - \frac{T}{T_{max}}\right) T \left(1 - 2 c_S \left(1 - e^{-C}\right)\right) - c_1 N T - D T. \tag{4.15}$$

Although immune cells are also affected by chemotherapy, the log kill hypothesis was maintained for these cells for the sake of simplicity. Figure 4.4 presents the simulations when a log-kill term is considered (left) and when the modified Norton-Simon hypothesis is taken into account (right). Assuming that

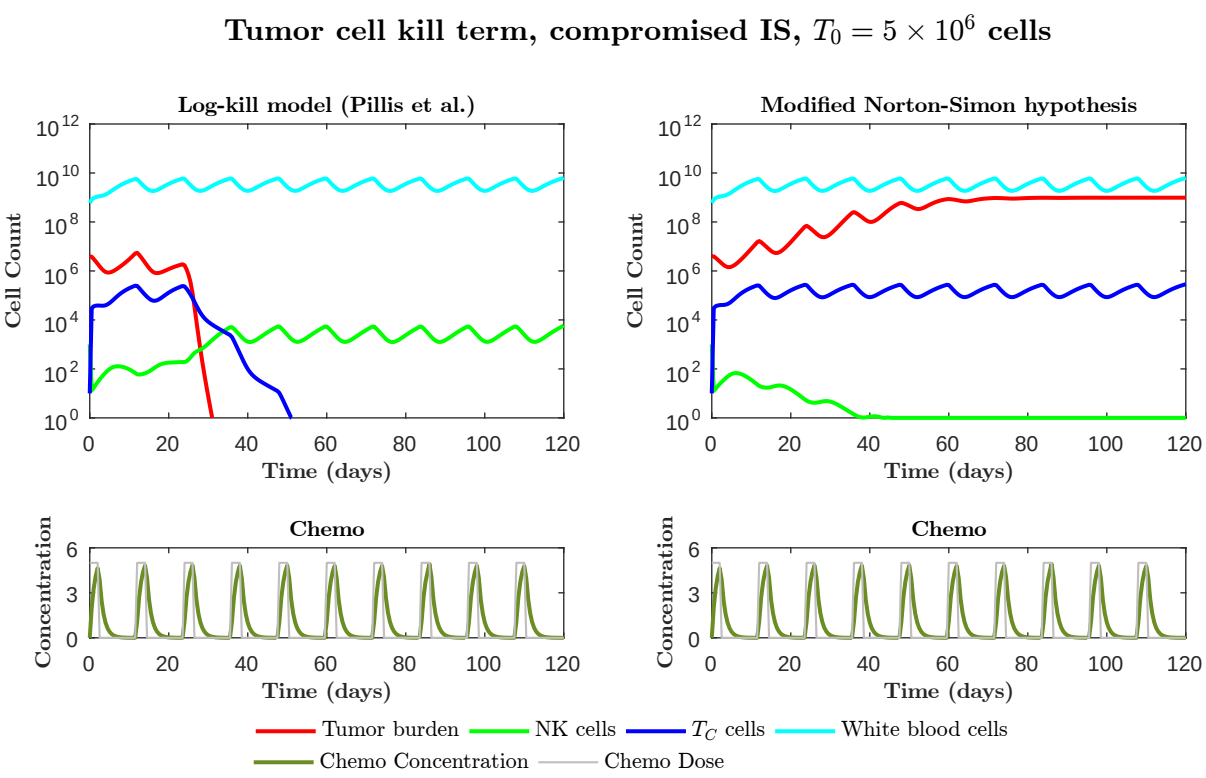

Figure 4.4: Compromised IS (see (4.12)) succeeds to eradicate a tumor with $T_0 = 5 \times 10^6$ cells when the log-kill model is considered (left) but fails to do it when the modified Norton-Simon is used (right).

only the actively proliferating tumor cells are susceptible to chemotherapy has indeed a huge impact in the simulations outcome. A tumor $T_0 = 5 \times 10^6$ cells before eradicated with the log-kill hypothesis is impossible to eliminate using this modified Norton-Simon hypothesis. Although interesting, this alteration has a high computational cost. Figure 4.4 right simulation has taken about 6 hours to run. For this reason it was decided to maintain the Log-kill hypothesis.

Resistance Rather than considering a homogeneous tumor population, the tumor is considered to be comprised by both sensitive (S) and resistant (R) tumor cells. $R_0 \neq 0$ reflects the existence of intrinsically resistant tumor cells before the treatment has started.

To begin with, the tumor resistance development was considered to be independent of the bloodstream chemotherapy concentration. In other words,

$$\dot{S} = r_S \left(1 - \frac{S+R}{T_{max}}\right) S - c_1 N S - D S - P_{SR} S + P_{RS} R - c_S \left(1 - e^{-C}\right) S, \tag{4.16}$$

$$\dot{R} = r_R \left(1 - \frac{S+R}{T_{max}}\right) R - c_1 N R - D R + P_{SR} S - P_{RS} R - c_R \left(1 - e^{-C}\right) R. \tag{4.17}$$

Therefore, a constant fraction of sensitive cells ($P_{SR}S$) would become resistant to the cytotoxic agent even when it was not being administered. As a result, a tumor previously eradicated (figure 4.5 *No resistance*) was now impossible to be eliminated (figure 4.5 *Resistance - Case 1)*.

In the second place, the tumor resistance development was assumed to be directly proportional to

bloodstream chemotherapy concentration

$$\dot{S} = r_S \left(1 - \frac{S+R}{T_{max}}\right) S - c_1 NS - DS - \frac{C}{C_{max}} P_{SR} S + P_{RS} R - c_S \left(1 - e^{-C}\right) S,$$

$$\dot{R} = r_R \left(1 - \frac{S+R}{T_{max}}\right) R - c_1 NR - DR + \frac{C}{C_{max}} P_{SR} S - P_{RS} R - c_R \left(1 - e^{-C}\right) R.$$

This modification takes into account the natural selective pressure of the drug concentration in the development of resistance by sensitive tumor cells. Under these circumstances, the model is in fact capable of eradicating a tumor burden of 3.2×10^6 cells (figure 4.5 *Resistance - Case 2*). However it takes more

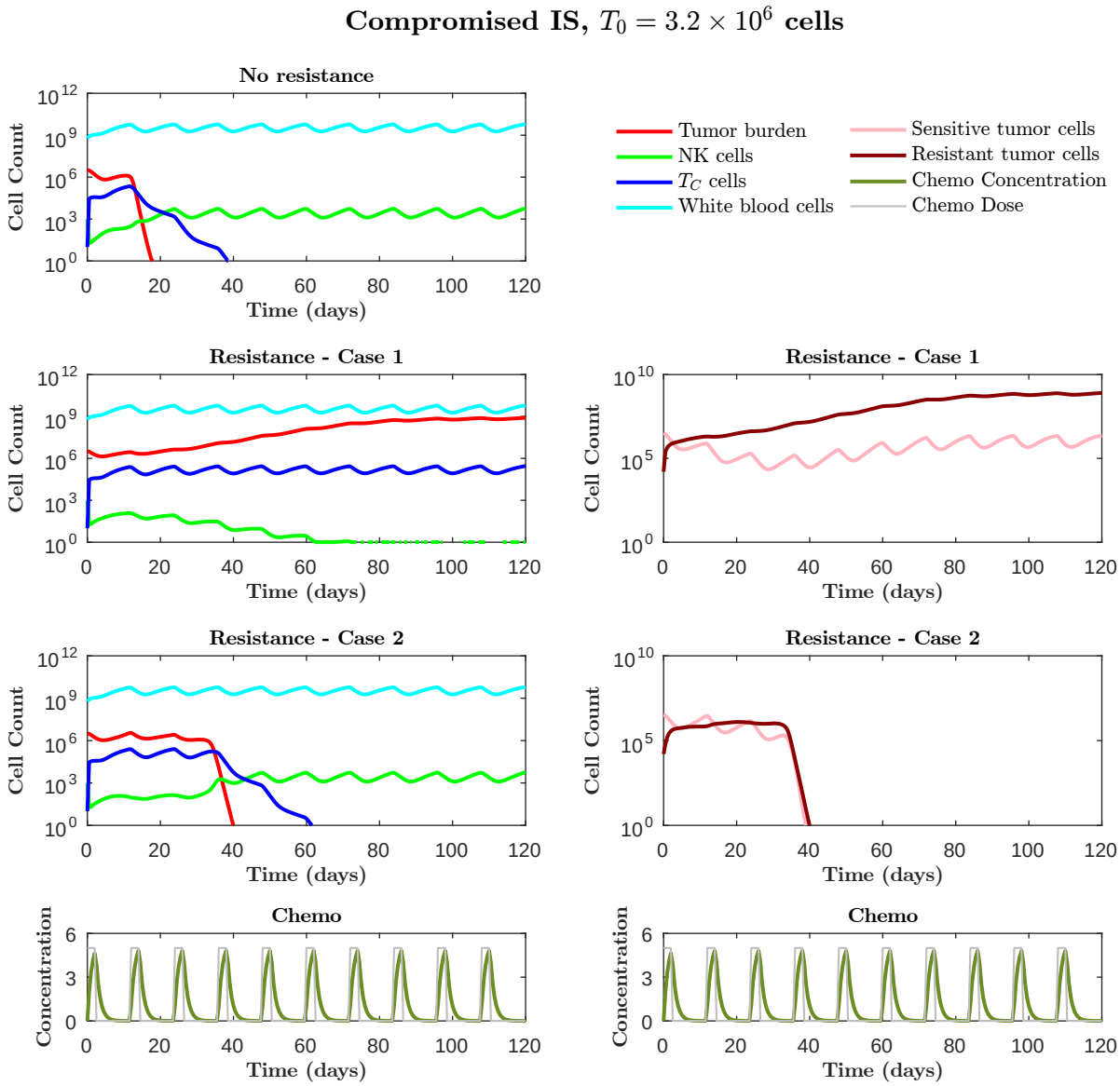

Figure 4.5: Simulation of the chemotherapy model response to a compromised IS (see (4.12)) and tumor burden of $T_0 = 3.2 \times 10^6$ when the development of chemotherapy resistance is ignored (No resistance), considered independent of drug concentration (Resistance - Case 1) and proportional to drug concentration (Resistance - Case 2). Bottom simulations (Chemo) represent the chemotherapy profile.

time to do it comparatively with figure 4.5 - *No resistance*, where the development of chemotherapeutic resistance was discarded.

After some experiences, it was seen that a full dose of chemotherapy during 120 days was only capable of eradicating a tumor up to $T_0 = 2.4 \times 10^7$ and $T_0 = 3.0 \times 10^6$ (see figure 4.6 left) cells on a healthy and compromised immune systems, respectively. Notably, several cycles of chemotherapy on the same circumstances were capable of eliminating up to $T_0 = 2.5 \times 10^7$ and $T_0 = 3.2 \times 10^6$ (see 4.6 right) cells, respectively. Hence, a full dose of chemotherapy results on a higher development of drug resistance. Henceforth, the consideration of chemotherapy resistance by chemotherapy models is essential to design a correct chemotherapy time-concentration profile.

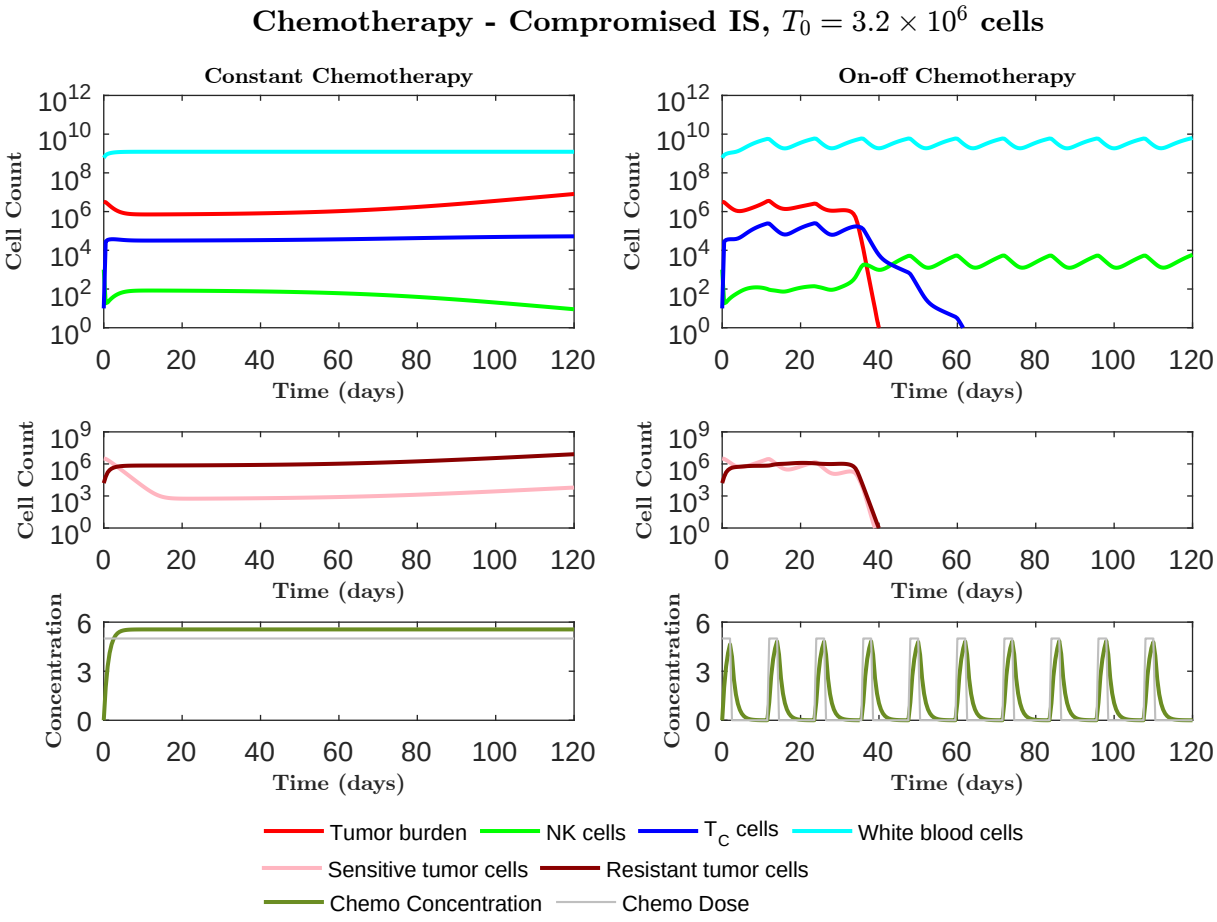

Figure 4.6: Compromised IS (see (4.12)) fails to eradicate a tumor with $T_0 = 3.2 \times 10^6$ cells when a full dose of chemotherapy is administered (left) but succeeds to do it when chemotherapy is a bang-bang process (right). Simulations performed with model (4.11).

4.2.4 Combination therapy

After some experiences it is seen that a combination therapy succeeds to eliminate a tumor whenever one of the therapies alone is capable of doing so but also when neither chemotherapy or immunotherapy had that power (see table 4.5). A compromised immune system eliminates tumor burdens up to $T_0 = 2.5 \times 10^7$, while healthy immune systems eradicate tumor burdens up to $T_0 = 3.5 \times 10^7$.

Table 4.5: Tumor burdens T_0 eradicated or not when chemotherapy and immunotherapy are administered alone or combined in a compromised immune system (CIS) and healthy immune system (HIS).

T_0	Combination therapy		Chemotherapy		Immunotherapy	
	CIS	HIS	CIS	HIS	CIS	HIS
4.0×10^7	✘		✘		✘	
3.5×10^7	✘	✔	✘		✘	
2.5×10^7	✔		✘	✔	✘	
3.2×10^6	✔		✔		✘	

✔ Tumor eradicated; ✘ Tumor not eradicated.

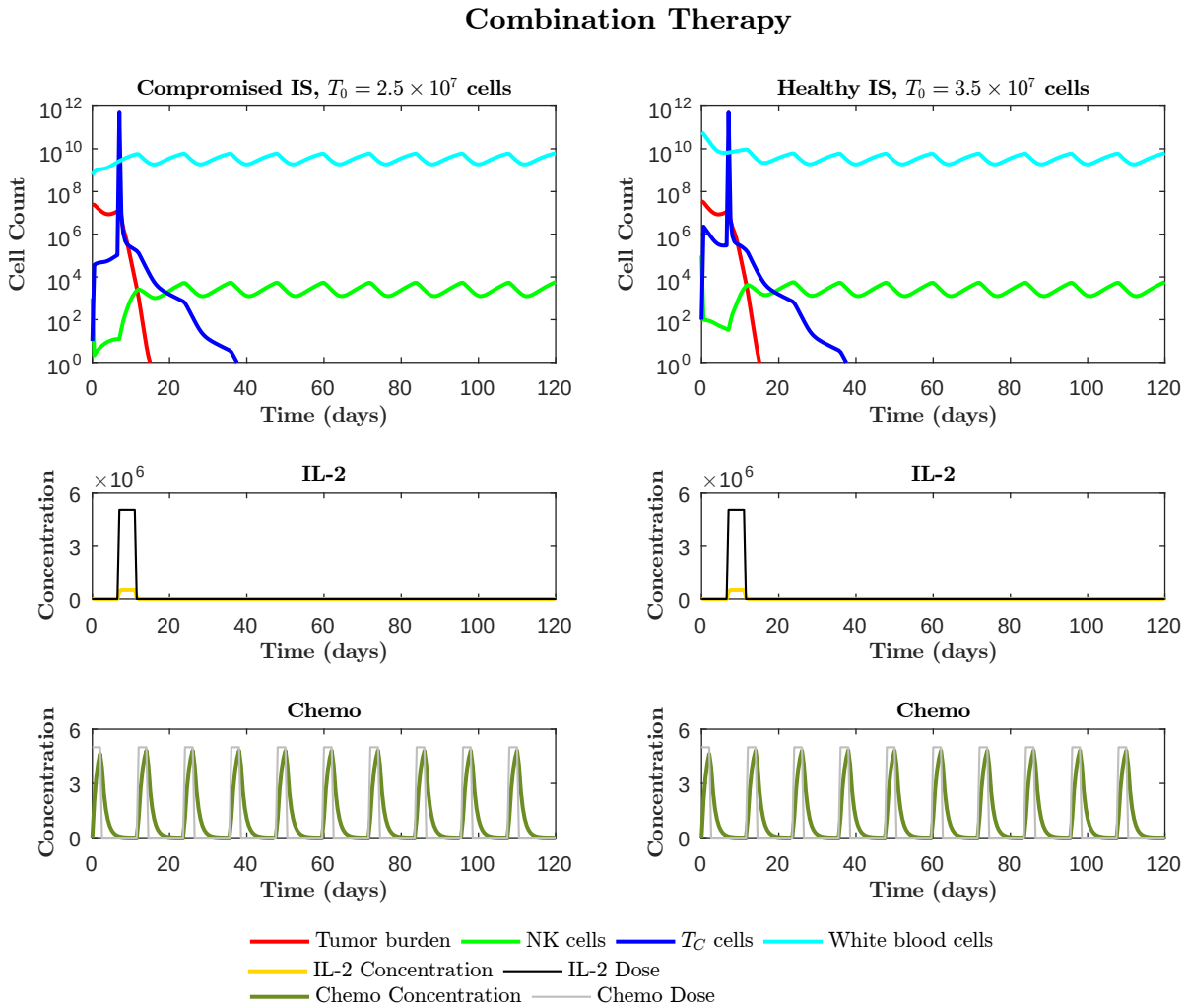

Figure 4.7: Compromised (left) and healthy IS (right) when subjected to combination therapy succeed to eradicate a tumor burden that neither chemotherapy or immunotherapy were capable of eliminating alone. Simulations performed with model (4.5).

Given these points, the combination of these two anti-cancer therapies has unequivocal advantages. Probably, the resistant tumor cells that chemotherapy was not able to kill alone (see $T_0 = 2.5 \times 10^7$ and

$T_0 = 3.5 \times 10^7$ in table 4.5) were effectively killed with the help of a strengthened immune system as consequence of immunotherapy. Moreover, the enhancement of the immune system might compensate the number of immune cells that were lost due to chemotherapy. Figure 4.7 illustrates the two cases were both chemotherapy and immunotherapy alone failed to eradicate the tumor burden in a compromised and healthy immune system, but the combination therapy has succeed.

Chapter 5

Optimal Control

The present chapter resumes the discussion initiated in 3.2. In the first place, the L1- and L2-norm performance indexes employed to formulate the optimal control problems associated to cancer therapy are defined for all the three models (4.10)*,* (4.11)*, and* (4.5)*. Subsequently, these optimal control problems are formulated. Afterwards, the numerical optimization methods adopted are described and finally the changes made to them are discussed.*

5.1 Performance index

The main objective of this master thesis is to design a drug schedule that eliminates the tumor level at the end of treatment, while infusing the least drug dosage (to avoid toxicity), and maintaining low tumor levels along the treatment [142]. Let $b = (b_1, ..., b_7)$, $e = (e_1, ..., e_7)$, $m = (m_1, m_2)$ be row vectors of non-negative weights and T an a priori specified therapy horizon. The state is denoted by $x = (R, S, N, L, W, C, I)$ and the control by $u = (u_c, u_i)'$. The terms u_c, u_i concern the temporal administration chemotherapy and Interleukin-2 (IL-2), respectively. The administration of TILs (u_L) is not optimized. The aforementioned goals can be translated to the cost function

$$J(u(t)) = \varphi\left(x(T)\right) + \int_{t_0}^{T} L\left(x(t), u(t)\right)\, \mathrm{d}t, \tag{3.30}$$

introduced in 3.2 in the following manner:

- *Minimize the number of cancer cells at the end of the treatment:* $\varphi\left(x(T)\right) = bx(T)$.
- *Minimize the number of cells during the treatment:* Penalty term $e\,x(t)$ in the Lagrangian function $L\left(x(t), u(t)\right)$.
- *Minimize the treatment side effects/toxicity:* Measure of side effects as a penalty term $m\,u(t)$ in the Lagrangian function $L\left(x(t), u(t)\right)$.

Including both measures of the number of tumor cells and the total amount of drugs given, the objective forces an equilibrium between these two conflicting terms [9]. Both L1 and L2 formulations are considered.

5.1.1 L1-norm

The cost function chosen for the linear optimization is given by

$$J(u(t)) = b\,x(T) + \int_{t_0}^{T} e\,x(t) + m\,u(t)\,\mathrm{d}t. \tag{5.1}$$

The L1-objective has an intuitive biological meaning since, for $u(t) \geq 0$, $\int_{t_0}^{T} u(t)\,\mathrm{d}t$ in (5.1) represents the AUC (area under the concentration time curve), *i.e.* the body exposition to drugs [143].

5.1.2 L2-norm

The performance index chosen for the quadratic optimization is given by

$$J(u(t)) = b\,x(T) + \int_{t_0}^{T} e\,x(t) + \frac{1}{2}m\,[u(t)]^2\,\mathrm{d}t. \tag{5.2}$$

In contrast to (5.1), the L2-objective is rather difficult to justify biomedically since $\int_{t_0}^{T}[u(t)]^2\,\mathrm{d}t$ does not have a biological meaning [9, 132]. Furthermore, it is important to realize that a quadratic objective favours lower drug concentrations. Consequently, such feature in solutions do not result from the properties of the dynamics, but is rather artificially imposed from the outside through the choice of the performance index [132].

For both L1- and L2-norm performance indexes, the influence of four different sets of weights will be discussed. These weights define the relative importance attributed to each element of the cost function (see table 5.1).

Table 5.1: Goals privileged by the four distinct performance indexes considered.

J_1	Do not privilege any measure.
J_2	Minimization of the tumor burden along the treatment.
J_3	Minimization of the tumor burden at the treatment end.
J_4	Minimization of treatment toxicity.

The m weights were computed taken into account that $u_{i_{max}} = 5 \times 10^6$, and $u_{c_{max}} = 5$. Furthermore, chemotherapy was considered to be 2.5 times more toxic than immunotherapy (IL-2). For instance, when $m_2 = 2$, $m_1 = \dfrac{2 \times 5}{2.5}\dfrac{1}{5 \times 10^6} = 8 \times 10^{-7}$. For more considerations regarding the toxicity of chemotherapy and IL-2, see 2.3.1 and 2.3.2.1, respectively. In summary, the weights b, e, and m for the three models are as follow.

Immunotherapy model (4.10) **performance index weights**

$$J_1: \quad b = \{1,\,0,\,0,\,0,\,0\}, \quad e = \{1,\,0,\,0,\,0,\,0\}, \quad m = \left\{2 \times 10^{-7}\right\}. \tag{5.3}$$

$$J_2: \quad b = \{1,\,0,\,0,\,0,\,0\}, \quad e = \{2,\,0,\,0,\,0,\,0\}, \quad m = \left\{2 \times 10^{-7}\right\}. \tag{5.4}$$

$$J_3: \quad b = \{2,\,0,\,0,\,0,\,0\}, \quad e = \{1,\,0,\,0,\,0,\,0\}, \quad m = \left\{2 \times 10^{-7}\right\}. \tag{5.5}$$

$$J_4: \quad b = \{1,\,0,\,0,\,0,\,0\}, \quad e = \{1,\,0,\,0,\,0,\,0\}, \quad m = \left\{8 \times 10^{-7}\right\}. \tag{5.6}$$

Chemotherapy model (4.11) **performance index weights**

$$J_1: \quad b = \{1,\,1,\,0,\,0,\,0,\,0\}, \quad e = \{1,\,1,\,0,\,0,\,0,\,0\}, \quad m = \left\{\frac{1}{5}\right\}. \tag{5.7}$$

$$J_2: \quad b = \{1,\,1,\,0,\,0,\,0,\,0\}, \quad e = \{2,\,2,\,0,\,0,\,0,\,0\}, \quad m = \left\{\frac{1}{5}\right\}. \tag{5.8}$$

$$J_3: \quad b = \{2,\,2,\,0,\,0,\,0,\,0\}, \quad e = \{1,\,1,\,0,\,0,\,0,\,0\}, \quad m = \left\{\frac{1}{5}\right\}. \tag{5.9}$$

$$J_4: \quad b = \{1,\,1,\,0,\,0,\,0,\,0\}, \quad e = \{1,\,1,\,0,\,0,\,0,\,0\}, \quad m = \{2\}. \tag{5.10}$$

Combination therapy model (4.5) **performance index weights**

$$J_1: \quad b = \{1,\,1,\,0,\,0,\,0,\,0,\,0\}, \quad e = \{1,\,1,\,0,\,0,\,0,\,0,\,0\}, \quad m = \left\{\frac{1}{5},\,2 \times 10^{-7}\right\}. \tag{5.11}$$

$$J_2: \quad b = \{1,\,1,\,0,\,0,\,0,\,0,\,0\}, \quad e = \{2,\,2,\,0,\,0,\,0,\,0,\,0\}, \quad m = \left\{\frac{1}{5},\,2 \times 10^{-7}\right\}. \tag{5.12}$$

$$J_3: \quad b = \{2,\,2,\,0,\,0,\,0,\,0,\,0\}, \quad e = \{1,\,1,\,0,\,0,\,0,\,0,\,0\}, \quad m = \left\{\frac{1}{5},\,2 \times 10^{-7}\right\}. \tag{5.13}$$

$$J_4: \quad b = \{1,\,1,\,0,\,0,\,0,\,0,\,0\}, \quad e = \{1,\,1,\,0,\,0,\,0,\,0,\,0\}, \quad m = \left\{2,\,8 \times 10^{-7}\right\}. \tag{5.14}$$

5.2 Optimal Control problem formulation

As referred in 1.2, the optimal therapy schedules for the chemotherapy (model (4.11)), immunotherapy (model (4.10)), and combination of both (model (4.5)), are obtained by applying optimal control theory to minimize the performance objectives (5.1) and (5.2), with distinct set of weights, imposed on the dynamical systems (4.10), (4.11), and (4.5), subjected to some constraints [9].

In this section, the optimal control problems to be considered in the present master thesis are formulated for all the three models (4.10), (4.11) and (4.5). The Pontryagin's minimum principle necessary conditions for a controlled trajectory (x, u) to be optimal were already enunciated in 3.2.1. For this reason, in this section, the adjoint equations, the tranversality conditions and the Hamiltonians are simply presented for all the three optimal control problems.

Regarding the constraints considered for the optimal problems, several initial tumor burdens T_0 are tested along with three distinct time horizons, $T = 60$ days, $T = 120$ days and $T = 240$ days. A

compromised immune system is always considered (see (4.13)). In summary, regardless of the control problem,

$$\begin{aligned} &S_0 = 0.995T_0, \quad R_0 = 0.05T_0, \quad N_0 = 10^3, \quad L_0 = 10, \quad W_0 = 6 \times 10^8, \quad C_0 = 0, \quad I_0 = 0; \\ &t_0 = 0, \quad T \in \{60,\, 120,\, 240\} \text{ days}; \\ &u_{c_{min}} = 0, \quad u_{c_{max}} = 5; \\ &u_{i_{min}} = 0, \quad u_{i_{max}} = 5 \times 10^6. \end{aligned} \tag{5.15}$$

Note that, although $u_{c_{max}} > 1$, $\left(1 - e^{-C}\right)$ is always smaller than 1. Moreover, 5×10^{11} TILs are administered as a bolus at day 7.0.

Independently of the model and the norm of the objective function considered, the adjoint equation and transversality condition read

$$\dot{\lambda}'(t) = -\lambda(t)' f_x(x(t), u(t)) - e, \tag{5.16}$$

$$\lambda(T) = b. \tag{5.17}$$

In order to decrease the complexity of the optimal control problems, singular control arcs are not considered as optimal candidates. However, as mentioned in 3.2.2, in the case of linear objectives, singular control arc are usually the most natural candidates for optimality [132].

5.2.1 Immunotherapy

For the immunotherapy model (4.10), states are given by $x(t) = (T(t),\, N(t),\, L(t),\, W(t),\, I(t))$. Furthermore, the set of weights of the four L1- and L2-norm cost functions are given by (5.3), (5.4), (5.5), and (5.6). All in all, these two optimization problems sum up to [OC1] and [OC2] described below. Note that [OC1] comprises the minimization of the linear objective (5.1), and [OC2] considers the minimization of the quadratic objective (5.2).

[OC1, OC2] For a specified terminal time T:

$$\begin{aligned} \min_{u(t)} \quad & J_k(u(t)) \quad \text{given by (5.1) or (5.2), with } \; k \in \mathbb{N} : k = \{1,\, 2,\, 3,\, 4\} \\ s.t. \quad & \dot{x}(t) = F\left(x(t), u_i(t)\right) \quad \text{given by (4.10)}, \\ & x(0) = (T_0,\, N_0,\, L_0,\, W_0,\, I_0)\,, \\ & t \in [0,\, T]\,, \\ & u(t) \in U = [u_{i_{min}}, u_{i_{max}}] \subset \mathbb{R}. \end{aligned} \tag{5.18}$$

The initial tumor burdens considered are $T_0 \in \mathbb{N} : T_0 = \left\{7.0 \times 10^5,\, 8.0 \times 10^5\right\}$.

5.2.1.1 Necessary conditions for optimality

The necessary conditions for the optimality (see 3.2.1) of problem [OC1], which comprises the linear objective (5.1), and for the problem [OC2], that encompasses the L2- objective (5.2), are given below.

L1-norm For the linear objective function, the Hamiltonian is given by

$$H(\lambda(t), x(t), u_i(t)) = e\, x(t) + m_2\, u_i(t) + \lambda(t)' F(x(t), u_i(t)). \tag{5.19}$$

The switching function, which was defined in 3.2.2.1, takes the form

$$\phi(u_i(t)) = \frac{\partial}{\partial u_i(t)} H(\lambda(t), x(t), u_i(t)) = m_2 + \lambda_5(t). \tag{5.20}$$

Consequently, the optimal control $u_i^*(t)$ satisfies

$$u_i^*(t) = \begin{cases} u_{i_{min}}, & \lambda_5(t) < -m_2, \\ u_{i_{max}}, & \lambda_5(t) > -m_2. \end{cases} \tag{5.21}$$

L2-norm When the quadratic objective is considered, the Hamiltonian is also quadratic in the control

$$H(u_i(t)) = e\, x(t) + \frac{1}{2} m_2\, [u_i(t)]^2 + \lambda(t)'\, F(x(t), u_i(t)). \tag{5.22}$$

The indicator function defined in 3.2.2.2, can be obtained by solving the Hamiltonian in order to $u(t)$

$$\frac{\partial}{\partial u_i(t)} H(\lambda(t), x(t), u_i(t)) = m_2 u_i(t) + \lambda_5(t) = 0 \ \rightarrow \psi(u_i(t)) = -\frac{\lambda_5(t)}{m_2}. \tag{5.23}$$

Finally, the optimal control $u_i^*(t)$ satisfies

$$u_i^*(t) = \begin{cases} u_{i_{min}}, & \lambda_5(t) \geq -m_2\, u_{i_{min}}, \\ -\dfrac{\lambda_5(t)}{m_2}, & -m_2\, u_{i_{max}} < \lambda_5(t) < -m_2\, u_{i_{min}}, \\ u_{i_{max}}, & \lambda_5(t) \leq -m_2\, u_{i_{max}}. \end{cases} \tag{5.24}$$

5.2.2 Chemotherapy

For the chemotherapy model (4.11), states are given by $x(t) = (S(t),\, R(t),\, N(t),\, L(t),\, W(t),\, C(t))$. As before, a quadratic and linear objective with four distinct set of weights (5.7), (5.8), (5.9), and (5.10), are minimized, while complying with some necessary constraints. These two optimization problems can be formulated as [OC3] and [OC4].

[OC3, OC4] For a specified terminal time T:

$$\begin{aligned} \min_{u(t)} \quad & J_k(u(t)) \quad \text{given by (5.1) or (5.2), with } \ k \in \mathbb{N} : k = \{1,\, 2,\, 3,\, 4\} \\ s.t. \quad & \dot{x}(t) = F\left(x(t), u_c(t)\right) \quad \text{given by (4.11),} \\ & x(0) = (S_0,\, R_0,\, N_0,\, L_0,\, W_0,\, C_0)\,, \\ & t \in [0,\, T]\,, \\ & u(t) \in U = [u_{c_{min}}, u_{c_{max}}] \subset \mathbb{R}. \end{aligned} \tag{5.25}$$

The initial tumor burdens considered are $T_0 \in \mathbb{N} : T_0 = \{7 \times 10^5,\ 3.2 \times 10^6,\ 2.5 \times 10^7\}$.

5.2.2.1 Necessary conditions for optimality

Once again, the necessary conditions for the optimality of the optimal problems [OC3] and [OC4] (see 3.2.1), which comprise the linear (5.1) and quadratic objective (5.2), respectively, are given below.

L1-norm In the case of the linear objective, the Hamiltonian is given by

$$H(\lambda(t), x(t), u_c(t)) = e\,x(t) + m_1\,u_c(t) + \lambda(t)' F(x(t), u_c(t)), \tag{5.26}$$

and its gradient, *i.e.* the switching function, takes the form

$$\phi(u_c(t)) = \frac{\partial}{\partial u_c(t)} H(\lambda(t), x(t), u_c(t)) = m_1 + \lambda_6(t). \tag{5.27}$$

Finally, the optimal control $u_c^*(t)$ satisfies

$$u_c^*(t) = \begin{cases} u_{c_{min}}, & \lambda_6(t) < -m_1, \\ u_{c_{max}}, & \lambda_6(t) > -m_1. \end{cases} \tag{5.28}$$

L2-norm For the quadratic objective, the Hamiltonian takes the form

$$H(u_c(t)) = e\,x(t) + \frac{1}{2} m_1\,[u_c(t)]^2 + \lambda(t)' F(x(t), u_c(t)). \tag{5.29}$$

The indicator function $\psi(u_c(t))$ is now given by

$$\frac{\partial}{\partial u_c(t)} H(\lambda(t), x(t), u_c(t)) = m_1 u_c(t) + \lambda_6(t) = 0 \ \rightarrow \psi(u_c(t)) = -\frac{\lambda_6(t)}{m_1}. \tag{5.30}$$

The optimal control $u_c^*(t)$ thus satisfies

$$u_c^*(t) = \begin{cases} u_{c_{min}}, & \lambda_6(t) \geq -m_1\,u_{c_{min}}, \\ -\dfrac{\lambda_6(t)}{m_1}, & -m_1\,u_{c_{max}} < \lambda_6(t) < -m_1\,u_{c_{min}}, \\ u_{c_{max}}, & \lambda_6(t) \leq -m_1\,u_{c_{max}}. \end{cases} \tag{5.31}$$

5.2.3 Combination therapy

In what regards the combination therapy (4.5), the states are given by $x(t) = (S(t),\ R(t),\ N(t),\ L(t),\ W(t),\ C(t),\ I(t))$. Once again, a quadratic and linear objective with four distinct set of weights (5.11), (5.12), (5.13), and (5.14), are minimized, while complying with some necessary constraints. These two optimization problems are then formulated as [OC5] and [OC6].

[OC5, OC6] For a specified terminal time T:

$$\begin{aligned}
\min_{u(t)} \quad & J_k(u(t)) \quad \text{given by (5.1) or (5.2), with } \; k \in \mathbb{N} : k = \{1,\, 2,\, 3,\, 4\}\,, \\
s.t. \quad & \dot{x}(t) = F\left(x(t), u(t)\right) \quad \text{given by (4.5)}, \\
& x(t_0) = (S_0,\, R_0,\, N_0,\, L_0,\, W_0,\, C_0,\, I_0)\,, \\
& t \in [t_0, T]\,, \\
& u(t) \in U = [u_{c_{min}}, u_{c_{max}}] \times [u_{i_{min}}, u_{i_{max}}] \subset \mathbb{R}^2.
\end{aligned} \tag{5.32}$$

The initial tumor burdens considered are $T_0 \in \mathbb{N} : T_0 = \left\{3.2 \times 10^6,\, 4.0 \times 10^7\right\}$.

5.2.3.1 Necessary conditions for optimality

Finally, the necessary conditions (see 3.2.1) for the optimality of the optimal control problems [OC5] (linear objective (5.1)) and [OC6] (quadratic objective (5.2)), are stated below.

L1-norm Regarding the linear objective, the Hamiltonian takes the form

$$H(\lambda(t), x(t), u_c(t), u_i(t)) = e\, x(t) + m_1\, u_c(t) + m_2\, u_i(t) + \lambda(t)' F(x(t), u_c(t),\, u_i(t)). \tag{5.33}$$

The switching functions for the two controls are given by

$$\phi(u_c(t)) = \frac{\partial}{\partial u_c(t)} H(\lambda(t), x(t), u_c(t), u_i(t)) = m_1 + \lambda_6(t), \tag{5.34}$$

$$\phi(u_i(t)) = \frac{\partial}{\partial u_i(t)} H(\lambda(t), x(t), u_c(t), u_i(t)) = m_2 + \lambda_7(t). \tag{5.35}$$

Finally, the controls satisfy

$$u_c^*(t) = \begin{cases} u_{c_{min}}, & \lambda_6(t) < -m_1, \\ u_{c_{max}}, & \lambda_6(t) > -m_1, \end{cases} \tag{5.36}$$

$$u_i^*(t) = \begin{cases} u_{i_{min}}, & \lambda_5(t) < -m_2, \\ u_{i_{max}}, & \lambda_5(t) > -m_2. \end{cases} \tag{5.37}$$

L2-norm When a quadratic objective is considered, the Hamiltonian is given by

$$H(\lambda(t), x(t), u_c(t), u_i(t)) = e\, x(t) + \frac{1}{2} m_1 \left[u_c(t)\right]^2 + \frac{1}{2} m_2 \left[u_i(t)\right]^2 + \lambda(t)' F(x(t), u_c(t),\, u_i(t)). \tag{5.38}$$

The indicator functions take the form

$$\frac{\partial}{\partial u_c(t)} H(\lambda(t), x(t), u_c(t), u_i(t)) = m_1 u_c(t) + \lambda_6(t) = 0 \;\rightarrow \psi(u_c(t)) = -\frac{\lambda_6(t)}{m_1}, \tag{5.39}$$

$$\frac{\partial}{\partial u_i(t)} H(\lambda(t), x(t), u_c(t), u_i(t)) = m_2 u_i(t) + \lambda_7(t) = 0 \;\rightarrow \psi(u_i(t)) = -\frac{\lambda_7(t)}{m_2}, \tag{5.40}$$

and finally, the optimal controls satisfy

$$u_c^*(t) = \begin{cases} u_{c_{min}}, & \lambda_6(t) \geq -m_1\, u_{c_{min}}, \\ -\dfrac{\lambda_6(t)}{m_1}, & -m_1\, u_{c_{max}} < \lambda_6(t) < -m_1\, u_{c_{min}}, \\ u_{c_{max}}, & \lambda_6(t) \leq -m_1\, u_{c_{max}}, \end{cases} \tag{5.41}$$

$$u_i^*(t) = \begin{cases} u_{i_{min}}, & \lambda_7(t) \geq -m_2\, u_{i_{min}}, \\ -\dfrac{\lambda_7(t)}{m_2}, & -m_2\, u_{i_{max}} < \lambda_7(t) < -m_2\, u_{i_{min}}, \\ u_{i_{max}}, & \lambda_7(t) \leq -m_2\, u_{i_{max}}. \end{cases} \tag{5.42}$$

5.3 Numerical Methods

Four distinct indirect numerical methods are implemented in order to find the optimal therapy for the dynamics (4.10), (4.11) and (4.5). While algorithms A and B are used to minimize the linear objective (5.1), algorithms C and D minimize the quadratic cost function (5.2). Both algorithms B and D are gradient-based. For all the algorithms, the first four steps are identical to those of the BFS method reviewed in 3.2.3. Henceforth, with the exception of algorithm B, only the subsequent steps are presented for the algorithms. Index j represents the iteration number, N_{it} the maximum number of iterations pre-established and N_{int} the number of time subintervals accordingly with the time discretization considered. For the sake of simplicity, the temporal dependency of some functions is omitted.

1. Subdivide the interval $[t_0, T]$ into N_{int} equal subintervals;
2. Make an initial guess for the control $u(t)$, which must be piecewise-constant for each subinterval;
3. Integrate the state equation $\dot{x}(t) = F\left(x(t), u(t)\right)$ from $[t_0, T]$ with initial value x_0 using the $u(t)$. Store the state trajectory $x(t)$;
4. Integrate the adjoint equation (5.16) backwards in time, i.e. $[T, t_0]$ with final condition $\lambda(T)$ (see (5.17)) using the $u(t)$ and the $x(t)$ obtained previously. Store the costate trajectory $\lambda(t)$;

5.3.1 Algorithm A - L1 objective

This numerical method is essentially the BFS method resumed in 3.2.3. Since the minimum of the Hamiltonian is obtained at the its boundary points, the optimal solution is computed accordingly with the signal of the Hamiltonian gradient. In summary, the subsequent steps of this algorithm can be described in the following way:

5. Compute the performance index $J^{(j)}(u)$;

6. Evaluate the stopping criteria

$$\left|J^{(j)}(u) - J^{(j-1)}(u)\right| \leq \varepsilon_1 \vee j \geq N_{it}; \tag{5.43}$$

7. Compute the switching function(s) $\phi(u)$;

8. Update the optimal control(s) $u(t)$

$$u_*(t) = \begin{cases} u_{min}, & \phi(t) > 0, \\ u_{max}, & \phi(t) < 0; \end{cases} \tag{5.44}$$

9. Repeat from **3.** until the stopping criteria are met.

5.3.2 Algorithm B - L1 objective

This algorithm is an adaptation of the gradient method from Duda [11]. The optimal solution is considered to be a bang-bang process, excluding the hypothesis of singular control arcs. Accordingly, the initial guess of $u(t)$ is an alternate function that switches from u_{max} to u_{min} and so on at the N_s switching times $(t_1^s, ..., t_{N_s}^s)$, starting in u_{max} as represented in figure 5.1.

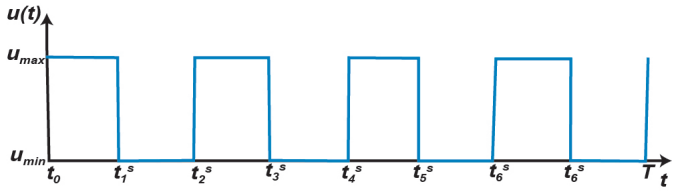

Figure 5.1: The initial guess of algorithm B is a bang-bang process.

Mathematically, $u(t)$ is given by

$$u(t) = \sum_{n=1}^{N_s} g(n) \left[\theta\left(t - t_n^s\right) - \theta\left(t - t_{n+1}^s\right)\right], \tag{5.45}$$

where θ is the heaviside step function, $t_0^s = t_0$ and $t_{N_s+1}^s = T$. If n is even then $g(n) = u_{max}$, otherwise $g(n) = u_{min}$. The number of switching times (N_s) is specified at the beginning. Although the switching times can collapse and thus disappear, N_s determines the maximum number of transitions. An upper limit can be assumed to N_s based on the clinical reality and the properties of the drug being used [11].

In the long run, the steps of this algorithm are described as:

1. Subdivide the interval $[t_0, T]$ into Ni_{int} equal subintervals;

2. Choose N_s, compute t_n^s and store them in vector vts. Compute the subinterval index referent to those t_n^s and store those indexes in vector $vtsi$;

3. Admitting that the control is a bang-bang process given by expression (5.45), compute $u(t)$ using $vtsi$;

4. Integrate the state equation $\dot{x}(t) = F\left(x(t), u(t)\right)$ from $[t_0, T]$ with initial value x_0 using $u(t)$. Store the state trajectory $x(t)$;

5. Integrate the adjoint equation (5.16) backwards in time, i.e. $[T, t_0]$ with final condition $\lambda(T)$ using the $u(t)$ and $x(t)$ obtained in step **3.** and **4.**. Store the costate trajectory $\lambda(t)$;

6. Compute the performance index $J^{(j)}(u)$;

6.1. If $J^{(j)}(u) > J^{(j-1)}(u)$:

6.1.1. Stop if $\kappa_1 \leq \varepsilon_1$, where κ_1 is given by

$$\kappa_1 = \sum_{n=1}^{N_s} [\,\delta(t_n^s)\,]^2; \tag{5.46}$$

6.1.2. Return to the initial values of the previous iteration saved in **8.** and reduce the step size ($w_1 < 1$) according to

$$\eta(t_n^s)^{j-1} = w_1 \times \eta(t_n^s)^{j-1}; \tag{5.47}$$

6.1.3. Decrease the iteration number $j = j - 1$ and jump to step **10.**;

7. Evaluate the stopping criteria

$$\left(\left|J^{(j)}(u) - J^{(j-1)}(u)\right| \leq \varepsilon_2 \ \wedge \ \sum_{n=1}^{N_s} [\,\delta(t_n^s)\,]^2 \leq \varepsilon_1\right) \ \vee \ \text{Number of } t^s = 0 \ \vee \ j \geq N_{it}; \tag{5.48}$$

Note: Initialize $J^{(0)} = -\infty$ and $\delta(t_n^s)$ as a vector of $-\infty$.

8. Save $u(t)$, vts, vts, $\phi(t_n^s)$, $J^{(j-1)}(u)$ and $J^{(j)}(u)$ in a matrix;

9. Compute the step size η for each t_n^s (w_2 is a weight)

$$\eta(t_n^s) = \begin{cases} 0, & \phi(t_n^s) = 0, \\ w_2 \times 10^{-floor(\log_{10}|\phi(t_n^s)|)-1}, & \phi(t_n^s) \neq 0; \end{cases} \tag{5.49}$$

10. Compute $\delta(t_n^s)$

$$\delta(t_n^s) = -\eta(t_n^s)\, ind_n\, \phi(t_n^s), \quad \text{where} \quad ind_n = \begin{cases} 1, & u(t_n^s) = u_{max} \text{ on } [t_{n-1}^s, t_n^s[, \\ -1, & u(t_n^s) = u_{min} \text{ on } [t_{n-1}^s, t_n^s[; \end{cases} \tag{5.50}$$

11. Compute the new switching times one by one

$$t_n^s = t_n^s + \delta(t_n^s), \tag{5.51}$$

and update vts, and $vtsi$ accordingly.

11.1. If $t_1^s - t_0 \leq \varepsilon_3$ eliminate t_1^s;

11.2. If $T - t_N^s \leq \varepsilon_4$ eliminate t_N^s;

11.3. If $t_n^s - t_{n-1}^s \leq \varepsilon_3$ eliminate both t_n^s and t_{n+1}^s;

11.4. Update vts, and $vtsi$;

12. Update $u(t)$ using $vtsi$;

13. Repeat from **4.** until the stopping criteria are met. If the result is unexpected, increase the number of N_s and repeat all steps.

Multiple controls In the presence of multiple control variables $u = (u_1, u_2, ..., u_n)$, step **6.** of algorithm B suffers some changes.

6. Compute the performance index $J^{(j)}(u)$, switching function $\phi(t_n^s)$, κ_1 and κ_2 for all the controls

$$\kappa_2 = \sum_{n=1}^{N_s} \left(\phi(t_n^s)^{(j)} - \phi(t_n^s)^{(j-1)} \right)^2 . \tag{5.52}$$

6.1. If $J^{(j)}(u) > J^{(j-1)}(u)$:

6.1.1. Considering that $u(t) = (u_c, u_i)$, stop if

$$(\kappa_1(u_i) \leq \varepsilon_1 \wedge \kappa_1(u_c) \leq \varepsilon_1) \vee [(\kappa_1(u_c) \leq \varepsilon_1 \vee \kappa_2(u_c) \leq \varepsilon_1) \wedge (\kappa_1(u_i) \leq \varepsilon_1 \vee \kappa_2(u_i) \leq \varepsilon_1)]\,; \tag{5.53}$$

6.1.2. If $\kappa_1 > \varepsilon_1 \ \wedge \ \kappa_2 > \varepsilon_1$ perform steps **6.1.2.** and **6.1.3.** for each control;

Note that each control has its own initial guess, N_s, vts, $vtsi$, $\kappa 1$, $\kappa 2$, η, δ, w_1, w_2, ϕ. Accordingly, the steps of algorithm B have to be performed for all the controls. By the same token the stopping criteria have to be met by all the controls. Nevertheless, steps **8.**, **9.**, **10.**, **11.** and **12.** are only performed for the controls whose $\kappa_1 > \varepsilon_1 \vee \kappa_2 > \varepsilon_1$.

5.3.3 Algorithm C - L2 objective

This numerical method is essentially the BFS method adapted to a L2-objective. In this case the Hamiltonian is strictly convex in the control $u(t)$. Therefore, the optimal control is computed by solving $\frac{\partial H}{\partial u} = 0$ in order to $u(t)$. Briefly, the remaining steps of this algorithm can be described as:

5. Compute the performance index $J^{(j)}(u)$;

6. Evaluate the stopping criteria

$$\left| J^{(j)}(u) - J^{(j-1)}(u) \right| \leq \varepsilon_1 \vee j \geq N_{it}; \tag{5.54}$$

7. Compute the indicator function(s) ψ;

8. Update the optimal control(s) $u(t)$

$$u_*(t) = \begin{cases} u_{min}, & \psi \leqslant u_{min}, \\ \psi(t), & u_{min} < \psi < u_{max}, \\ u_{max}, & \psi \geqslant u_{max}; \end{cases} \tag{5.55}$$

9. Repeat from **3.** until the stopping criteria are met.

5.3.4 Algorithm D - L2 objective

This gradient method is a modified version of the steepest descent method reviewed in 3.2.3. In this algorithm, two acceleration techniques proposed in [12, 13] are used, namely iterative step sizes and a momentum technique. Furthermore, some measures are taken for the purpose of preventing the cost function from increasing between iterations. Generally speaking, the numerical algorithm is as follows:

5. Compute the performance index $J^{(j)}(u)$;

5.1. If $J^{(j)}(u) > J^{(j-1)}(u)$:

5.1.1. Return to the initial values of the previous iteration saved in **7.** and reduce the step size parameters ($w_3 < 1$) according to

$$w_1 = w_3 \times w_1, \tag{5.56}$$

$$w_2 = w_3 \times w_2; \tag{5.57}$$

5.1.2. Set the momentum memories to zero, i.e. $g(t) = 0$ for each time subinterval;

5.1.3. Decrease the iteration number $j = j - 1$ and jump to step **8.**;

6. Evaluate the stopping criteria

$$\left(\left| J^{(j)}(u) - J^{(j-1)}(u) \right| \leq \varepsilon_2 \ \wedge \ \sum_{t=1}^{N_{int}+1} \left(\left[\frac{\partial H(t)}{\partial u} \right]^{(j)} - \left[\frac{\partial H(t)}{\partial u} \right]^{(j-1)} \right)^2 \leq \varepsilon_1 \right) \vee \ j \geq N_{it}; \tag{5.58}$$

Note: Initialize $J^{(0)} = -\infty$ and $\left[\frac{\partial H}{\partial u}\right]^{(j=0)}$ as a vector of $-\infty$.

7. Save $u(t)$, $\frac{\partial H}{\partial u}$, $J^{(j-1)}(u)$ and $J^{(j)}(u)$ in a matrix;

8. Compute the weights $\eta^{(j)}$ for each subinterval

8.1. If $j = 1$:

$$\eta^{(j=1)}(t) = \begin{cases} 0, & \frac{\partial H(t)}{\partial u} = 0, \\ w_4 \times 10^{-floor\left(\log_{10}\left|\frac{\partial H}{\partial u}\right|\right)-1}, & \frac{\partial H(t)}{\partial u} \neq 0; \end{cases} \tag{5.59}$$

8.2. If $j \neq 1$:

$$\eta^{(j)}(t) = \begin{cases} w_1\, \eta^{(j-1)}(t), & \left[\frac{\partial H}{\partial u}\right]^{(j)} \left[\frac{\partial H}{\partial u}\right]^{(j-1)} > 0, \\ w_2\, \eta^{(j-1)}(t), & \left[\frac{\partial H}{\partial u}\right]^{(j)} \left[\frac{\partial H}{\partial u}\right]^{(j-1)} < 0, \end{cases} \tag{5.60}$$

where $w_1 > 1$ and $w_2 < 1$.

9. Compute $g^{(j)}$ according to

$$g^{(j)}(t) = \left[\frac{\partial H}{\partial u}\right]^{(j)} + w_5\, g^{(j-1)}(t), \tag{5.61}$$

where $0 \leq w_5 < 1$.

10. Update the optimal control(s) $u(t)$

$$u^{(j+1)}(t) = u^{(j)}(t) - \eta^{(j)}(t) g^{(j)}(t); \tag{5.62}$$

11. Repeat from **3.** until the stopping criteria are met.

Multiple controls In the presence of multiple control variables, algorithm D step **5.1.** suffers some alterations.

5. Compute the performance index $J^{(j)}(u)$, $\frac{\partial H}{\partial u}$ and κ_2 for all the controls

$$\kappa_2 = \sum_{t=1}^{N_{int}+1} \left(\left[\frac{\partial H(t)}{\partial u}\right]^{(j)} - \left[\frac{\partial H(t)}{\partial u}\right]^{(j-1)} \right)^2; \tag{5.63}$$

5.**1.** If $J^{(j)}(u) > J^{(j-1)}(u)$:

5.**1.1.** Compute κ_1

$$\kappa_1 = \sum_{t=1}^{N_{int}+1} \left[\eta(t)^{(j)} g(t)^{(j)} \right]^2, \tag{5.64}$$

5.**1.2.** Considering that $u(t) = (u_c, u_i)$, stop if

$$(\kappa_1(u_i) \leq \varepsilon_1 \wedge \kappa_1(u_c) \leq \varepsilon_1) \vee [(\kappa_1(u_c) \leq \varepsilon_1 \vee \kappa_2(u_c) \leq \varepsilon_1) \wedge (\kappa_1(u_i) \leq \varepsilon_1 \vee \kappa_2(u_i) \leq \varepsilon_1)]; \tag{5.65}$$

5.**1.3.** If $\kappa_1 > \varepsilon_1 \ \wedge \ \kappa_2 > \varepsilon_1$ perform steps **5.1.1.**, **5.1.2.** and **5.1.3.** for each control;

Note that each control has its own initial guess, g, $\frac{\partial H}{\partial u}$, η, $\kappa 1$, $\kappa 2$, w_1, w_2, w_3, w_4, w_5. Accordingly, the steps of algorithm D are performed for all the controls. However, steps **7.**, **8.**, **9.**, and **10.** are only performed for the controls whose $\kappa_2 > \varepsilon_1$. Finally, the stopping criteria have to be met by all the controls.

5.3.5 Control parameters

The choice of the control parameters for the gradient based algorithms, *i.e.* algorithm B and D, has a direct impact on the optimal solution found. Consequently, an exhaustive search for the optimal combination of the control parameters is made for each numerical simulation present in 6. Several combinations of the control parameters were tested. The parameters set that has resulted in the lowest objective was chosen.

5.4 Algorithm optimization

Several alterations have been made to the algorithms proposed until their final versions were achieved. In this section these alterations are discussed and its importance is emphasized. All the figures used to illustrate the importance of these modifications were obtained using the chemotherapy model (4.11) with $T_0 = 3.2 \times 10^6$ cells and the compromised immune system initial conditions (4.13). The cost function parameters were $b = e = (1, 1, 0, 0, 0, 0)$ and $m_1 = 2$. Finally, the algorithms presented are validated.

In all the algorithms, the stopping criteria is evaluated immediately after the cost function computation for the new solution, which was found in the previous iteration. As a result, the execution of unnecessary steps is avoided.

5.4.1 Algorithm A

The first algorithm proposed, algorithm A, has not converged to an optimal solution. For instance, when it is applied to (4.11), the algorithm keep jumping between four solutions with different costs. Figure 5.2 represents the value of the cost function over the iterations.

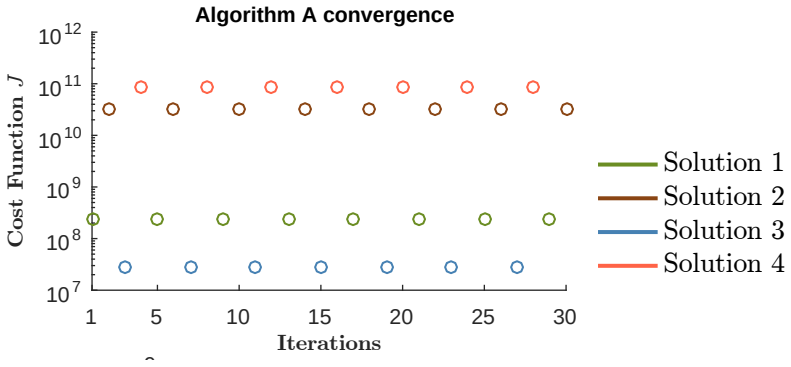

Figure 5.2: Left: Algorithm A jumps between four different solutions. Control parameters: $\varepsilon_1 = 10^{-10}$, $u_{guess} = C_{max}\, ones(1, N_{int} + 1)$, $N_{int} = 240$.

Only one solution (blue), which is the one with lowest cost is possibly the true optimal solution. Possibly, the other three solutions result from the roughness of the cost function. In chapter 6, the solution with the lowest cost is presented and analyzed.

5.4.2 Algorithm B

Several alterations were made to the Dudda algorithm in Duda [11].

5.4.2.1 Improvements

Algorithm B.1: Unique fixed step sizes Initially, an unique fixed step $\eta(t_n^s)$ was considered to all the switching times. In order to enable a correct convergence to the optimal solution, the step was chosen to be of an order of magnitude above the maximum value of the $\frac{\partial H}{\partial u}$ times -1. However, when $\frac{\partial H}{\partial u}$ takes values with different orders of magnitude, the process of convergence may be too slow for some switching times. In the example below $\eta(t_n^s) = 10^{-7}$

$$\frac{\partial H(t_n^s)}{\partial u} = \left[-2\times10^{6},\, 4\times10^{5}, (...),\, 6,\, 2\right] \quad \rightarrow \quad |\delta(t_n^s)| = \left[2\times10^{-1},\, 4\times10^{-2}, (...),\, 6\times10^{-7},\, 2\times10^{-7}\right].$$

In fact, during the simulations performed, this algorithm could not converge to the optimal solution (see figure 5.3 left). This is explained by the tiny value of $|\delta(t_n^s)|$ obtained for some switching times. For this reason the control found at iteration 25 is essentially the initial guess.

Algorithm B.2: Distinct fixed step sizes for each switching time With this in mind, a different step size was chosen for each t_n^s. This step was considered to be of an order of magnitude above the value of the $\frac{\partial H(t_n^s)}{\partial u}$ times -1 (see (5.49)). Whenever $\frac{\partial H(t_n^s)}{\partial u} = 0$, $\eta(t_n^s)$ is also considered to be zero. Considering $w_2 = 2$, the example above becomes

$$|\delta(t_n^s)| = \left[2\times10^{-1},\, 2\times10^{-1}, (...),\, 2\times10^{-1},\, 2\times10^{-1}\right].$$

This modification has resulted in a notable improvement of the algorithm convergence (see figure 5.3 middle). At iteration 25, the control found is completely different from the one found with the algorithm B.1. However, after some iterations this algorithm started to diverge and jumping between different solutions. As in Algorithm B.1, the stopping criteria was never met. This algorithm only stopped when the maximum number of iterations established was reached.

Algorithm B.3: Robustness To correct the previous problem, at the end of each iteration, the cost, the switching time positions, the control and $\eta(t_n^s)$ were saved on a matrix. In other words, a matrix with the old values of some important variables were actualized at each iteration. Whenever the objective of the present iteration became larger than the previous one, the algorithm returned to the previous iteration and the $\eta(t_n^s)$ of that iteration was re-calculated, *i.e.* reduced, accordingly with (5.47), where $w_1 < 1$. As a result, the algorithm smoothly converged to the optimal solution (see figure 5.3 right).

5.4.2.2 Final algorithm

After all these modifications have been done, the final algorithm was tested with different control guesses (for instance 5, 10 and 12 switching times), as represented in figure 5.4 top. The optimal solution found was exactly the same regardless of the control guess considered. The optimal solution as well as the hamiltonian and $\frac{\partial H}{\partial u}$ for the three control guesses are represented in figure 5.4 bottom and are perfect overlaps.

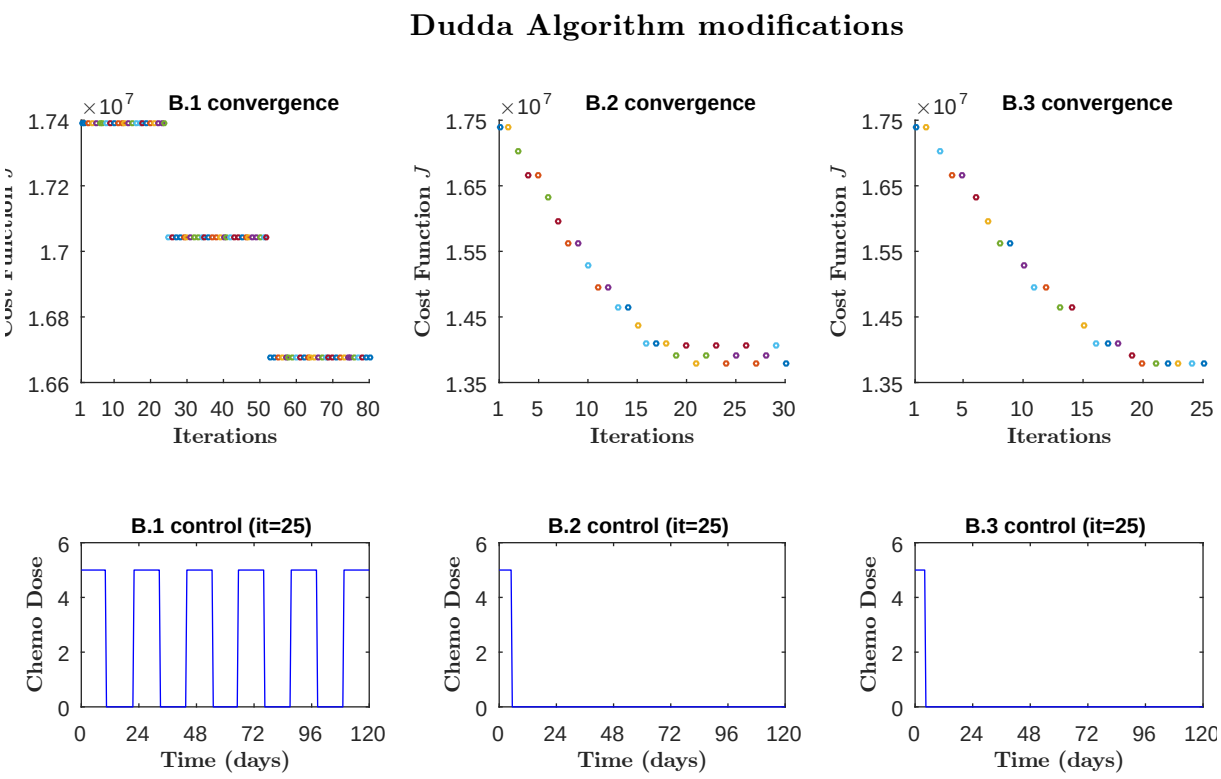

Figure 5.3: Top: Consequences of the algorithm alterations in the convergence to the optimal solution. Bottom: Iteration 25 of algorithm B.1, B.2 and B.3. Parameters: $N_s = 10$, $w_2 = 2$, $w_1 = 0.8$, $\varepsilon_1 = \varepsilon_2 = 10^{-10}$, $\varepsilon_3 = 1$, $\varepsilon_4 = 3$, $N_{int} = 240$.

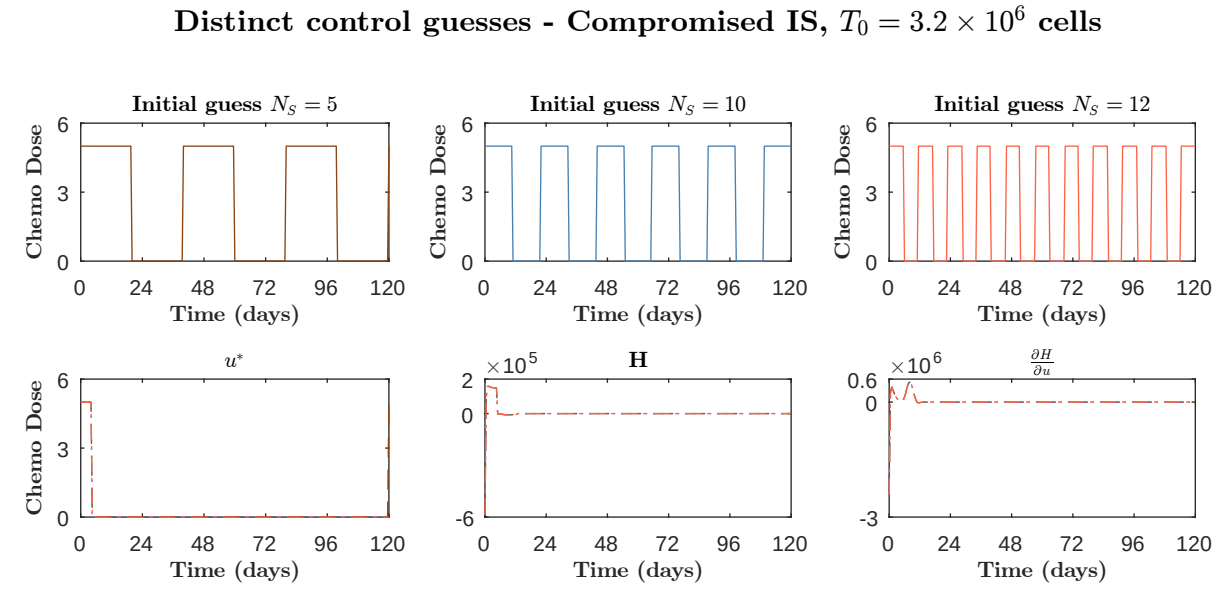

Figure 5.4: Top: Initial control guesses. Bottom: Optimal solution, hamiltonian, $\frac{\partial H}{\partial u}$ for the three initial guesses. Parameters: $w_2 = 2$, $w_1 = 0.8$, $\varepsilon_1 = \varepsilon_2 = 10^{-10}$, $\varepsilon_3 = 1$, $\varepsilon_4 = 3$, $N_{int} = 240$.

Finally, algorithm B was applied to a problem with a known solution (Schättler and Ledzewicz [144, p.48–65]). As a matter of convenience, both the results found with algorithm B and the solution given in Schättler and Ledzewicz [144, p.65] are presented in the appendix (see A). The solutions found with this algorithm (see figure A.1) are extremely similar to those of Fig.24 in Schättler and Ledzewicz [144, p.65]

(see figure A.2). The algorithm implemented is thus capable of converging to the optimal solutions.

5.4.3 Algorithm C

Similarly to Algorithm A, algorithm C has not converged to the optimal solution. In fact, it also keeps jumping between the same four distinct solutions of figure 5.2. As before, figure 5.5 shows the value of the cost function during thirty iterations. Figure 5.2 and figure 5.5 are exactly alike. As before, the solution with the lowest cost function is presented and analyzed in chapter 6.

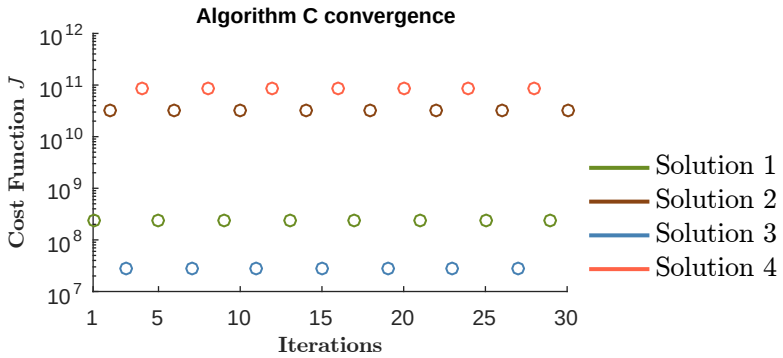

Figure 5.5: Algorithm C jumps between four different solutions. Control parameters: $\varepsilon_1 = 10^{-10}$, $u_{guess} = C_{max}\, ones(1, N_{int}+1)$, $N_{int} = 240$.

5.4.4 Algorithm D

Algorithm D is inspired in a backpropagation algorithm for Neural Networks studied in the course Machine Learning at Instituto Superior Técnico.

5.4.4.1 Improvements

Algorithm D.1: Unique fixed step sizes Similarly to algorithm B, first an unique fixed step η was considered to all time subintervals. The control u was simply uploaded at each iteration according with

$$u^{(j+1)}(t) = u^{(j)}(t) - \eta \left[\frac{\partial H(t)}{\partial u}\right]^{(j)}. \tag{5.66}$$

For $\eta = 10^{-6}$, the algorithm minimum cost was found in iteration 1197 (see table 5.2). Figure 5.6 *D.1 convergence* shows the first 500 iterations performed with this algorithm and a zoom in of the region where the minimum of the cost function was obtained. Besides presenting a slow convergence, which is explained by the tiny value of u increments obtained for some time subintervals, algorithm D.1 was not able to stop at the iteration of interest.

Algorithm D.2: Distinct fixed step sizes In order to deal with this slow convergence, a different step size $\eta(t)$ was chosen to each time subinterval according with (5.59). This alteration has resulted in a faster convergence (see figure 5.6 *D.2 convergence*). The minimum of the cost function was found at $j = 123$ (see table 5.2) and its value was smaller than the one found for algorithm D.1. Similarly to algorithm D.1, this algorithm was not able to stop at the iteration of interest.

Algorithm D.3: Iterative step sizes Iterative step sizes are useful when the convergence process reaches ravines that are parallel, or almost parallel, to some axis [13, 145]. Instead of considering a fixed step size $\eta(t)$, $\eta^{(j)}(t)$ is adapted at every time subinterval, for each iteration, depending on the successive signs of $\frac{\partial H}{\partial u}$ between the iterations [12, 13, 145]. If $\frac{\partial H}{\partial u}$ has the same signal in two subsequent iterations, *i.e.* two subsequent updates of $u(t)$ have been performed in the same direction, the step size should be increased [13, 145]. At the first sight, it is possible to move faster without passing beyond the minimum [145]. If the opposite occurs, the step size should be decreased since probably the solution may have jumped over a minimum [13, 145]. Therefore, the step size and control were uploaded according with (5.60) and (5.67), respectively

$$u^{(j+1)}(t) = u^{(j)}(t) - \eta^{(j)}(t) \left[\frac{\partial H(t)}{\partial u} \right]^{(j)}. \tag{5.67}$$

The initial step sizes were computed as in algorithm D.1. The minimum of J was found at $j = 339$ (see 5.6 *D.3 convergence*) but this alteration has resulted in an increase of the cost function (see table 5.2).

Algorithm D.4: Momentum technique The momentum term is a recursive linear low pass filtering of $\frac{\partial H}{\partial u}$ since it attenuates high frequency oscillation that might occur across ravines [13, 145]. When successive $u(t)$ updates are made in the same direction, the moment term g, given by (5.61), has an accumulation effect, which increases the movement speed along the ravine, helping to prevent oscillations across it [13, 145]. Its combination with iterative step sizes makes this algorithm effective even in the case of ravines oblique to all axes [12, 13, 145]. The control $u(t)$ is then updated according with (5.62). The effects of the momentum term are more pronounced as w_3 becomes closer to 1 [145]. However, ravines are usually curved. Therefore, in a bend, if too much momentum has been previously acquired, the procedure may be driven far from the valley bottom, *i.e.* up a ravine wall [12, 13, 145]. Accordingly, $0.5 \leq w_3 < 0.95$. Values below 0.5 may introduce little improvement. In turn, values above 0.95 often tend to cause divergence at bends since a small deviation in the gradient direction may require many iterations to be corrected, and sometimes may drive the process far away from the bottom of the ravine [12]. With this alteration the minimum of the cost function was found at $j = 164$ (see 5.6 D.4 convergence) and its value, although smaller than the one found with algorithm D.3, is still higher than the one obtained for algorithm D.2 (see table 5.2).

Robustness When the current step size parameters are too large and/or too much momentum has been acquired, the cost function increases [145]. To prevent this from happening, whenever the cost function becomes higher than its value in the previous iteration, the algorithm returns to the previous iteration, it reduces the step size parameters and set the momentum memory to zero (see Algorithm D step 5.**1.**) [145]. Usually the step size parameters are reduced by $w_3 = 0.5$ [145].This alteration has resulted in a fast convergence (see figure 5.6 *D.5 convergence*) and algorithm D.5 was in fact able to stop at the desired iteration. The minimum of the cost function was found at $j = 58$ (see table 5.2) and it was the best value obtained until now.

Table 5.2: Minimum value of the cost function found using algorithm D.1, D.2, D.3, D.4 and D.5.

	D.1	**D.2**	**D.3**	**D.4**	**D.5**
Cost function J $\left(\times 10^7\right)$	1.270783	1.270578	1.271226	1.270593	1.270574
Iteration j	1197	123	339	164	58

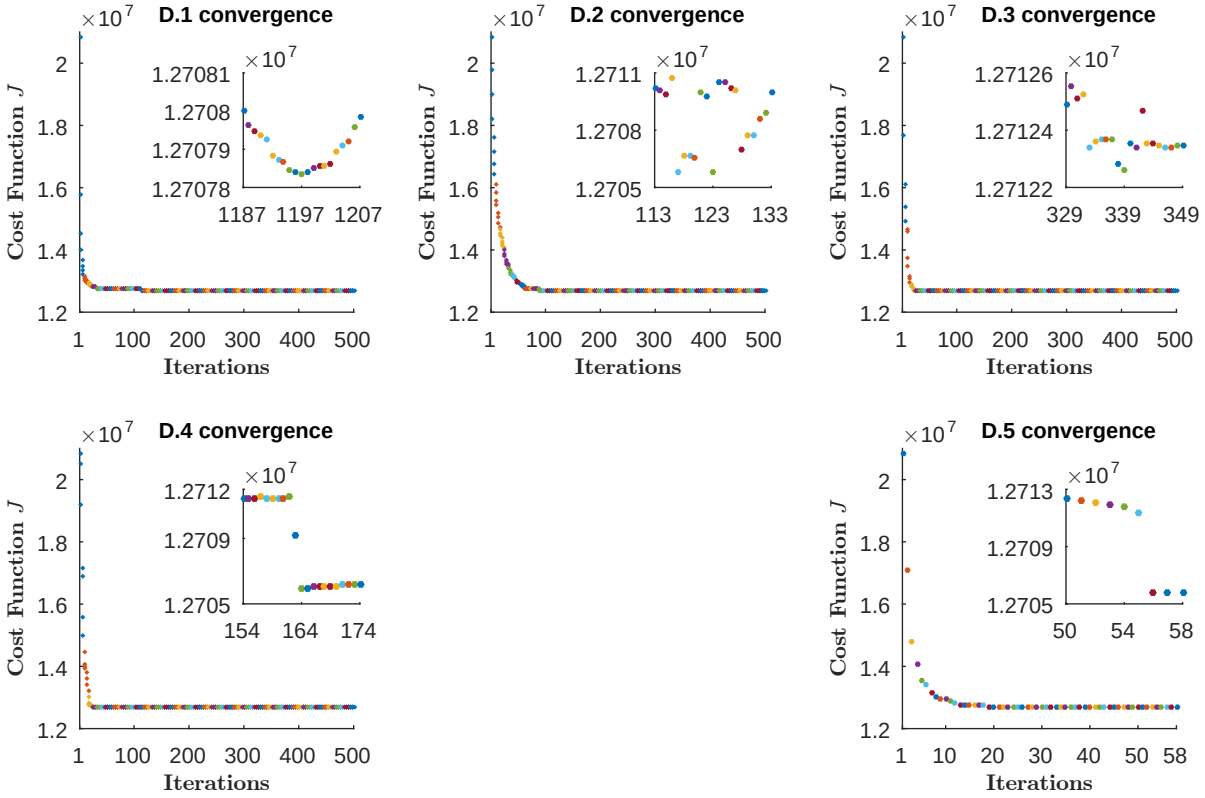

Figure 5.6: Consequences of the algorithm alterations in the convergence to the optimal solution. Although the minimum objective of algorithm D1 was found at iteration 1997, the the x-axis of the main figure is only represented until iteration 500 in order to enable a easier comparison with the remaining figures. Control parameters: $\varepsilon_1 = \varepsilon_2 = 10^{-10}$, $N_{int} = 240$, $u_{guess} = zeros(1, N_{int} + 1)$; $u_{guess}(1, 1 : 15) = 1.5$;. D.1 convergence - $\eta = 10^{-6}$. D.2 convergence - $w_4 = 0.15$. D.3 convergence - $w_4 = 72$, $w_1 = 1.20$, $w_2 = 0.99$, D.4 convergence - $w_4 = 72$, $w_1 = 1.20$, $w_2 = 0.99$, $w_5 = 0.61$ D.5 convergence - $w_4 = 0.94$, $w_1 = 2.83$, $w_2 = 0.99$, $w_5 = 0.61$, $w_3 = 0.41$.

5.4.4.2 Final algorithm

Finally, algorithm D was applied to a problem with a known solution ([132, p.158–160]). Once again, as a matter of convenience, both the results found with algorithm D and the solution given in the literature are presented in the appendix (see A). The solutions found with this algorithm (see figure A.1) are similar to those of Fig.4.1 in [132, p.159] and Fig.4.2 in [132, p.160] (see figures A.4 and A.5). The algorithm implemented is thus capable of converging to the optimal solutions. Note: in Fig.4.2 [132, p.160] the initial conditions used were wrong. Figure A.3 used the initial conditions mentioned in [132, p.159].

5.4.5 Multiple controls

Only algorithms B and D were modified to enable the optimization of multiple controls simultaneously (algorithms A and C could not converge to the optimal solution).

Some controls may converge faster to u^* than others. With this in mind, before computing the new controls, their $\frac{\partial H}{\partial u}$ error between the actual and past iteration, κ_2, are computed using (5.52) or (5.63). When κ_2 is smaller than a given value, for a specific control, it is considered that u^* has been reached and its optimization is stopped.

Whenever the cost function is higher than its value in the previous iteration, among the controls that have not reached its optimum value, only the ones which κ_1 (see (5.46) and (5.64)) is higher than a given value are computed again. This prevents the algorithm from entering in an infinite loop, since the optimization of a given control stops when its increments are too tiny.

Chapter 6

Results and discussion

In this chapter the optimal treatment schedules for chemotherapy, immunotherapy, and combination therapy obtained with the algorithms discussed in 5.4 are presented. Several performance indexes, initial tumor burdens, and distinct time horizons are tested and analyzed.

6.1 Chemotherapy

The results from the optimal control problems [OC3] (algorithms A and B) and [OC4] (algorithms C and D) are presented respectively in the subsections 6.1.1 and 6.1.2, and subsections 6.1.4 and 6.1.3.

6.1.1 Algorithm A: L1 norm

As suspected in 5.4.1, algorithm A is indeed incapable of converging to the optimal solution. Figure 6.1 presents the model dynamic response to the supposed optimal control (solution 3 of figure 5.2), the development of resistance and the Hamiltonian.

The control presented in figure 6.1 is not optimal. First, the performance index J_4 tries to minimize the treatment toxicity (see table 5.1). Accordingly, the administration of chemotherapy after the eradication of the tumor cells would never be privileged. Moreover, the resulting Hamiltonian is not constant along time, which is a sign of non-optimality. Given the obvious limitations of this algorithm, it will not be applied to the remaining models.

6.1.2 Algorithm B: L1 norm

In contrast to algorithm A, algorithm B has in fact converged to the optimal solutions.

6.1.2.1 Performance index

Since optimal control theory aims at minimizing a given performance index, distinct objectives yield different optimal solutions. Figure 6.2 presents the optimal controls u_c^* (left) and the respective Hamiltonians (right) for a initial tumor burden of 3.2×10^6 in a case of a compromised immune system, when the

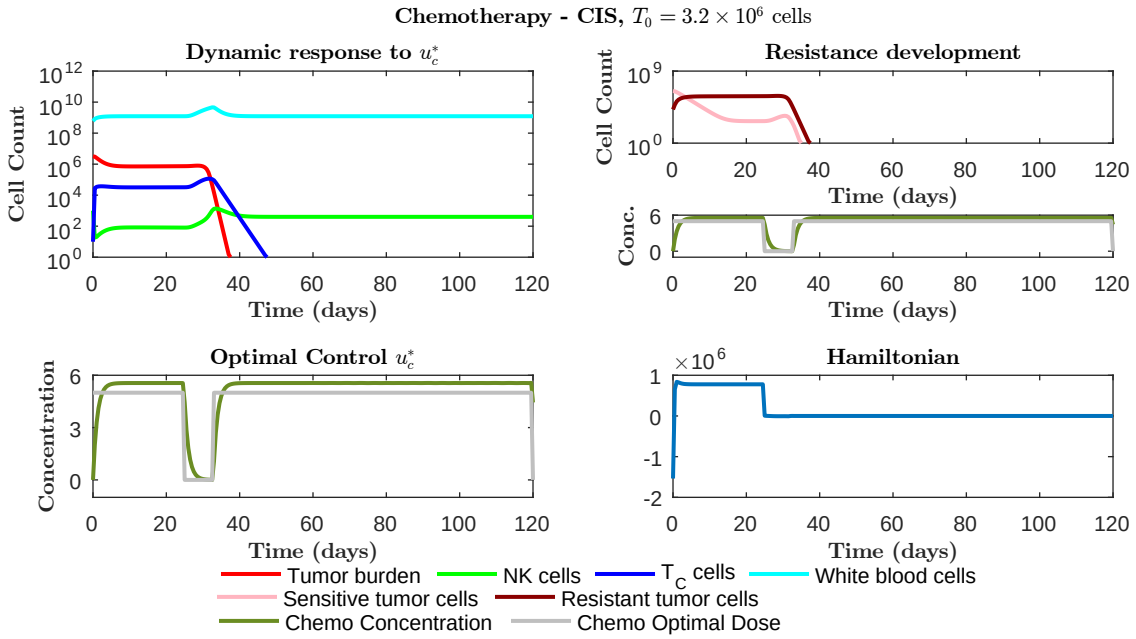

Figure 6.1: Dynamic response of model (4.11) (top left) to the supposed optimal control (bottom left), development of resistance (top right) and the Hamiltonian (bottom right). Simulation parameters: $\varepsilon_1 = 10^{-10}$, $u_{guess} = C_{max}\, ones(1, N_{int}+1)$, $N_{int} = 240$, $T = 120$, $T_0 = 3.2 \times 10^6$ considering a compromised IS (see (4.13)).

four distinct objective functions J_1, J_2, J_3, and J_4 are considered. Figure 6.2 bottom is simply a zoom in of figure 6.2 top. Tumor burden is eradicated in all cases.

Unexpectedly, the four optimal solutions do not differ from each other (figure 6.2 left). These results may be due to the high discretization time (0.5 days) considered when the time subintervals were created in Algorithm B, step **1.**. Possibly, the last day of therapy of these solutions differs in less than 0.5 days between them, and therefore the administration period obtained is the same for all of them. Despite their similarity, the values of their cost functions differ among the optimal solutions as a result of the different set of weights considered in their respective performance index. In summary, $J_2 > J_4 > J_3 > J_1$, where $J_4 - J_3 = 41.54$, and $J_3 - J_1 = 2.00$. Accordingly, favouring the minimization of the tumor burden along the treatment has a higher cost than privilege the minimization of the chemotherapy toxicity or favouring the minimization of the tumor burden at the end of the treatment, respectively. However, the added cost of privilege the minimization of the tumor burden at the terminus of the therapy, comparing to not favouring anything, is almost insignificant.

As discussed in 3.2.1, whenever the Lagrangian function $L(x(t), u(t))$ and the dynamics $F(x(t), u(t))$ are time-invariant, *i.e.* they do not depend on time t, the Hamiltonian function $H(\lambda(t), x(t), u(t))$ is constant over time [131]. However, the Hamiltonian functions obtained for every performance index minimized (see figure 6.2 right) are not constant over time. Moreover, the initial bad behavior of the Hamiltonian is more pronounced for the cost function with the highest cost value - J_2. Possibly, the optimal solution that would give rise to a constant Hamiltonian is not a solution of the dynamics or it does not comply with the constraints imposed. Furthermore, a high time discretization and a poor selection of the control parameters may result in a solution distinct of the optimal one.

In the following sections, the solutions obtained result from the minimization of the J_4 cost function.

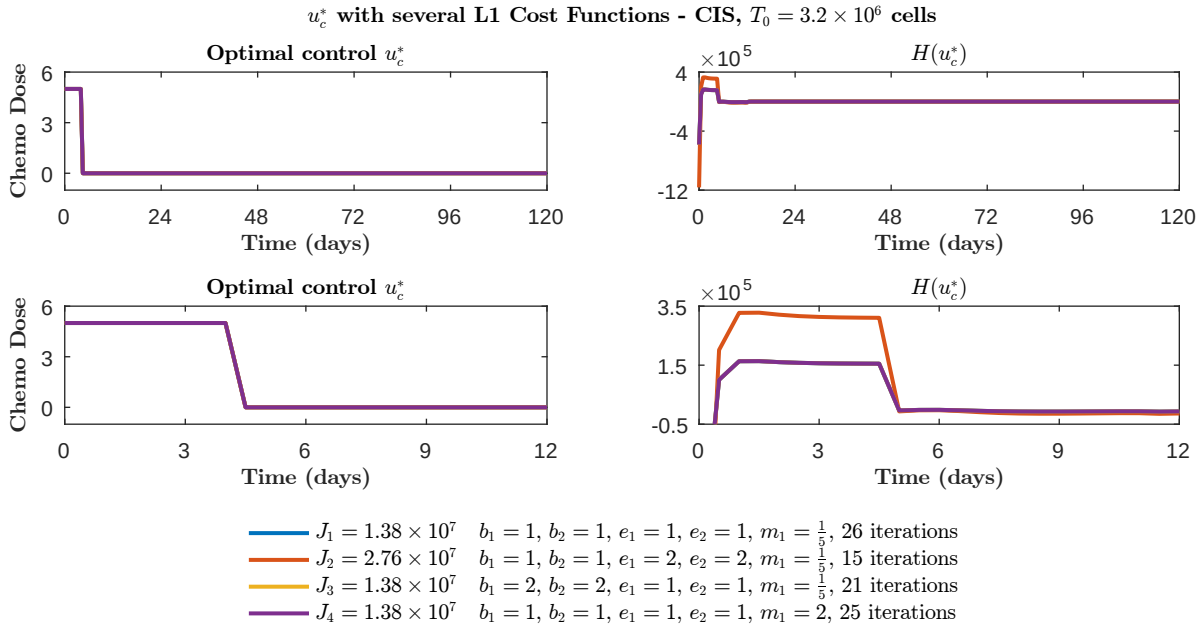

Figure 6.2: Four distinct performance indexes and their respective optimal chemotherapy (left) and, Hamiltonian (right). Second row is a zoom in of the first row. Simulation parameters: compromised IS (see (4.13)), $N_{int} = 240$, $N_s = 10$, $T = 120, T_0 = 3.2 \times 10^6, \varepsilon_1 = \varepsilon_2 = 10^{-10}, \varepsilon_3 = 0.5, \varepsilon_4 = 10, w_1 = 0.8, w_2 = 2$ except for the case of J_3, where $w_2 = 2.8$.

6.1.2.2 Initial tumor burden

An optimal chemotherapy is designed for three distinct tumor burdens, $T_0 = 7.0 \times 10^5$, $T_0 = 3.2 \times 10^6$, and $T_0 = 2.5 \times 10^7$ cells, in the case of a compromised immune system. Figure 6.3 presents the optimal control u_c^*, the system dynamics response to it and the concomitant development of chemotherapy resistance, as well as the Hamiltonian for each T_0.

Chemotherapy is able to eradicate a tumor burden of 7.0×10^5 cells and 3.2×10^6 cells but not a tumor burden of 2.5×10^7 cells. While for $T_0 = 7.0 \times 10^5$ (see figure 6.3 top) chemotherapy is administered until day 3.0, for $T_0 = 3.2 \times 10^6$ (see figure 6.3 middle) it is administered until day 4.0. Interestingly, sensitive and resistant chemotherapeutic cells are only completely eliminated some days after the end of the treatment. The elimination of these cells have occurred respectively at day 12.5 and day 12.0 for $T_0 = 7.0 \times 10^5$, and at day 18.0 and 17.5 for $T_0 = 3.2 \times 10^6$. Accordingly, chemotherapy does not need to be administered as long as tumor cells exist. Conversely, it must be administered only until the immune system of the patient is capable of eradicating the remaining tumor cells. These results highlight the importance of modeling simultaneously chemotherapy, development of chemotherapeutic resistance and immunosurveillance. If the immune response was not taken into account, chemotherapy would certainly have been given for a longer time. In both cases, the NK cells of the innate immunity increased along time while the adaptive immune T_C cells have diminished and disappeared completely. The behavior of the immune system is in accordance with what was discussed in 4.2.1. In the case of $T_0 = 7.0 \times 10^5$, tumor cells are eradicated faster comparatively with $T_0 = 3.2 \times 10^6$ and a smaller dose of chemotherapy is also given. As a result, the objective value for $T_0 = 7.0 \times 10^5$, $J(u_c^*) = 1.93 \times 10^6$, is smaller than the one obtained for $T_0 = 3.2 \times 10^6$, $J(u_c^*) = 1.38 \times 10^7$.

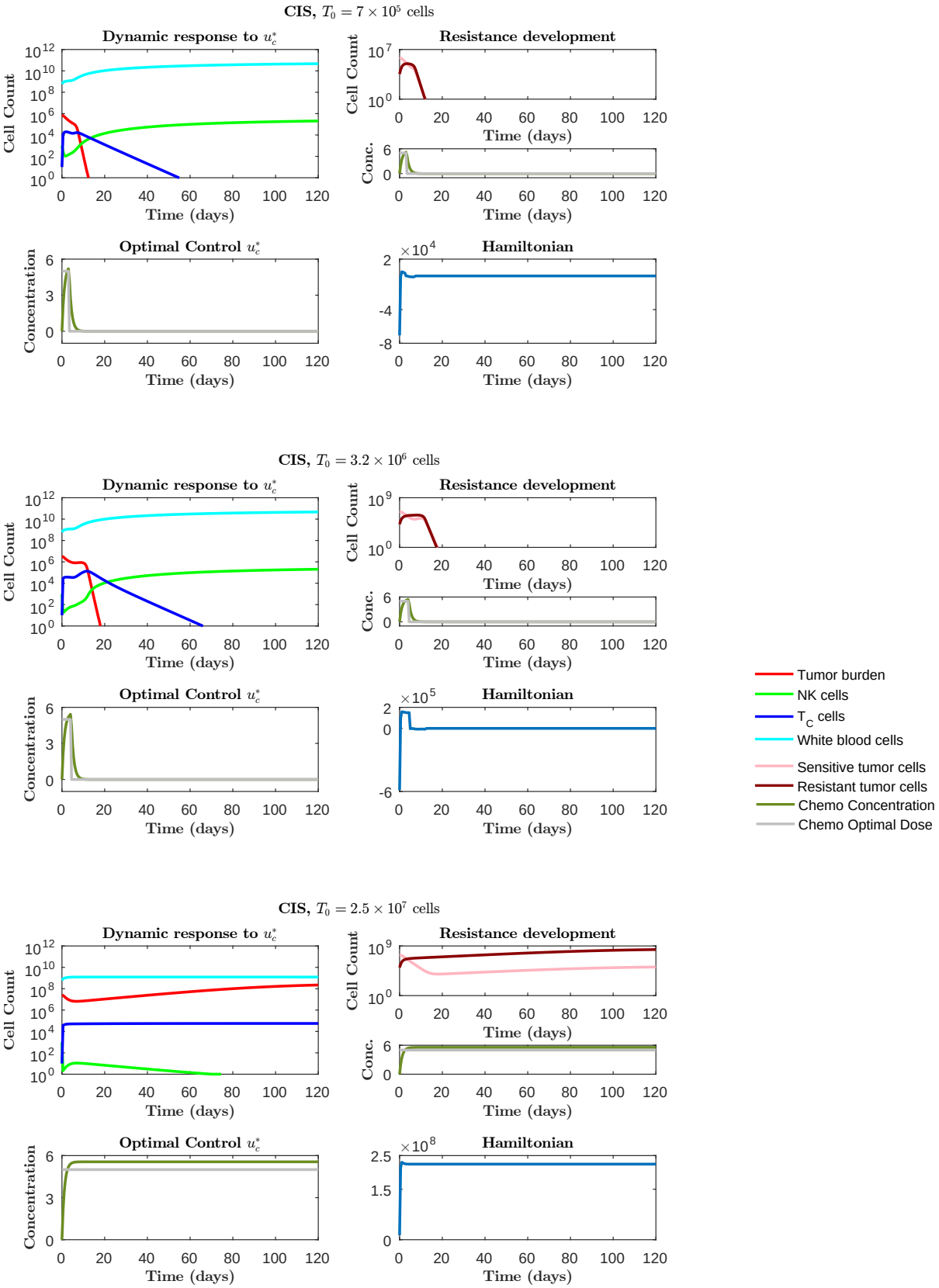

Figure 6.3: Dynamic response of model (4.11) (top left) to the optimal control (bottom left), development of resistance (top right) and the Hamiltonian (bottom right), for the linear J_4. Simulation parameters: $\varepsilon_1 = 10^{-10}$, $N_{int} = 240$, $N_s = 10$, $T = 120$, $\varepsilon_1 = \varepsilon_2 = 10^{-10}, \varepsilon_3 = 0.25, \varepsilon_4 = 10.00, w_1 = 0.80, w_2 = 2.00$ except for the case of $T_0 = 7.0 \times 10^5$where $w_2 = 2.25$. A compromised IS was considered together (see (4.13)) with J_4.

Regarding $T_0 = 2.5 \times 10^7$ (see figure 6.3 bottom), although chemotherapy is not able to eradicate the tumor, the optimal u_c^* obtained is a full dose chemotherapy along the treatment time. The toxicity of this treatment together with the incapacity of successfully minimize the number of tumor cells, both during and at the end of the treatment, has resulted in a high value for the cost function, $J(u_c^*) = 9.49 \times 10^9$. Conceding that the cost function only considered the toxicity of the treatment, chemotherapy would not be administered at any time. On the whole, in this case chemotherapy is only administered because it contributes to the minimization of tumor cells. In fact, initially the number of new sensitive cells resultant from the proliferation of the pre-existent ones is smaller than the number of sensitive cells eliminated by both chemotherapy and immune system. However, this scenario is reversed at day 18.0. As discussed in 4.2.1, the number of NK cells decreases along time and finally disappears due to the immunoevasive cancer strategies and the toxic effects of chemotherapy. In contrast, the presence of tumor cells stimulates the proliferation and activation of T_C cells in such way that neither chemotherapy nor the immunoevasive cancer strategies are capable of diminishing the T_C cells number.

The Hamiltonian of the optimal solutions must be constant over time. Notwithstanding, there are always time intervals where these requisites are not fulfilled. The reasons behind this bad behaviors of the Hamiltonian functions were already mentioned in 6.1.2.1. Concerning the time discretization, it is not possible to have a switching time at $t = 4.01$ day since the sampling interval considered was 0.5 day. However, the use of smaller sampling intervals makes the integration with *ode45* even slower. This holds particularly importance in the case of time consuming algorithms, which is the case. For example, in the cases in which the tumor is not eradicated a single iteration can take up to 3.0 hours.

In order to investigate the optimality of the solutions obtained, these were perturbed and the objective function was re-computed. Figure 6.4 illustrates the perturbation of the u_c^* (left) for $T_0 = 3.2 \times 10^6$, and the resultant Hamiltonian (right). A small perturbation of u_c^* has in fact resulted in an added cost of $1.28.0 \times 10^5$. Nevertheless, the present result does not prove that this solution is the optimal one.

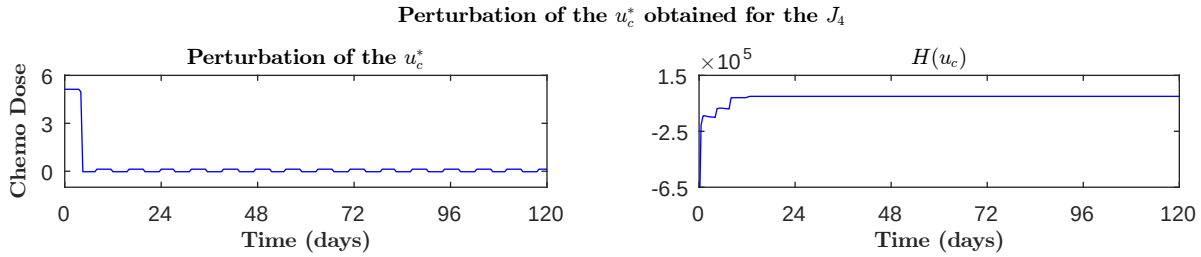

Figure 6.4: Perturbation of the optimal solution obtained for $T_0 = 3.2 \times 10^6$ and respective Hamiltonian. Simulation parameters: $u_{pert} = u_c^* + 0.08 * square(0.8 * t)' + 0.05, T = 120, J_4$.

6.1.2.3 Time horizon

Finally, an optimal chemotherapy schedule is design to a tumor burden of $T_0 = 3.2 \times 10^6$ cells considering three distinct therapy time horizons (see figure 6.5). The same discretization time - 0.5 day - is considered for every simulation. The alteration of the therapy time horizon does not change u_c^*. In all the three cases, tumor is eradicated at the same day and the systems dynamics behaves in the same way.

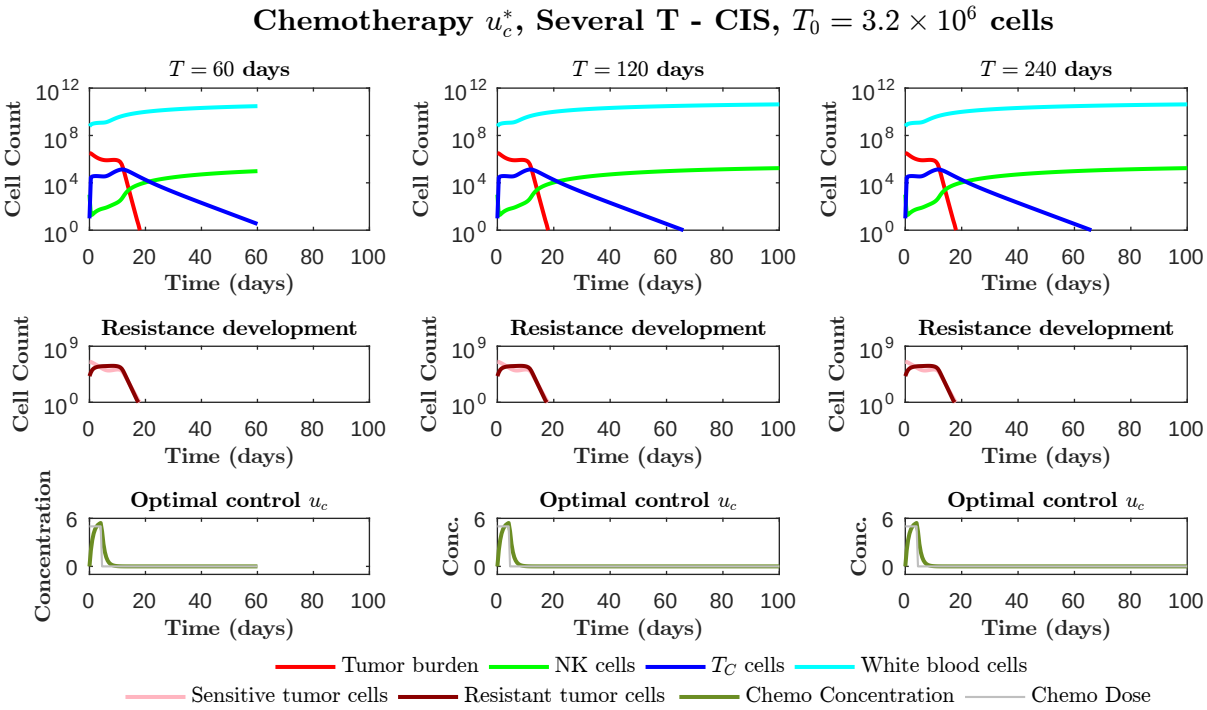

Figure 6.5: Simulation of the optimal chemotherapy for three distinct time horizons: $T = 60$ days (left), $T = 120$ days (middle), $T = 240$ days (right). Simulation parameters: $\varepsilon_1 = \varepsilon_2 = 10^{-10}$, $\varepsilon_3 = 0.25$, $\varepsilon_4 = 10.00$, $w_1 = 0.80, w_2 = 2.00$, $N_s = 10$, $N_{int} = 2T + 1$ except for $T = 60$ days, where $\varepsilon_3 = 1.00$, $\varepsilon_4 = 3.00$, $w_2 = 2.60$. A compromised IS was considered together (see (4.13)) with J_4 for a tumor burden of $T_0 = 3.2 \times 10^6$.

6.1.3 Algorithm C: L2 norm

As algorithm A, algorithm C has not converged to the u_c^*. Figure 6.6 presents the model dynamic response to the supposed u_c^* (solution 3 of figure 5.5), the development of resistance and the Hamiltonian.

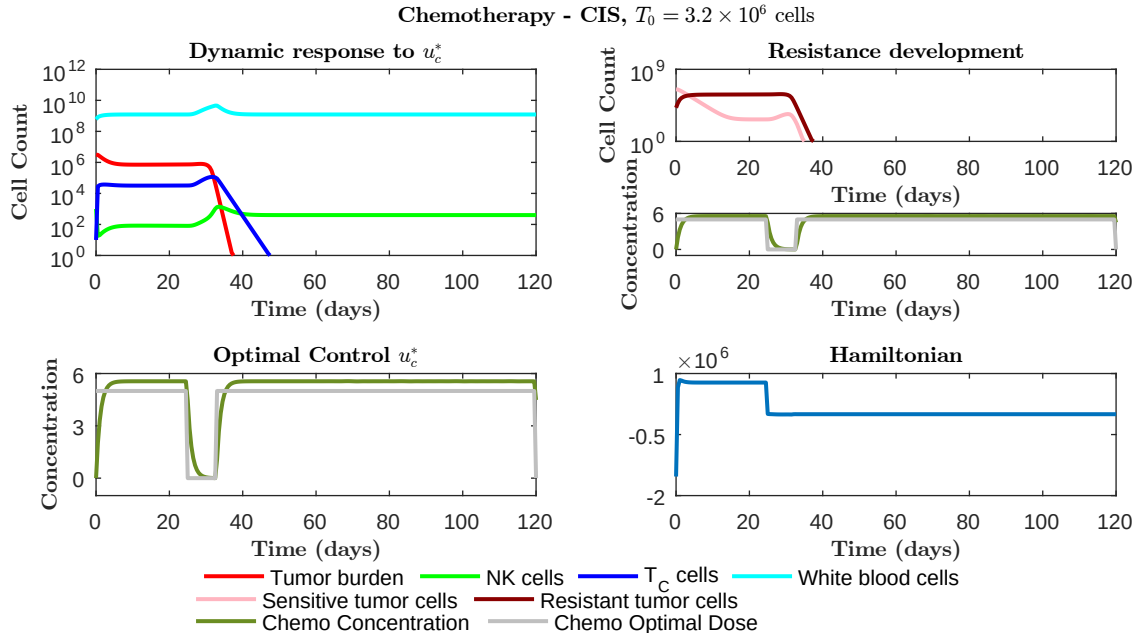

Figure 6.6: Dynamic response of model (4.11) (top left) to the supposed u_c^* (bottom left), development of resistance (top right) and the Hamiltonian (bottom right). Simulation parameters: $\varepsilon_1 = 10^{-10}$, $u_{guess} = C_{max}\, ones(1, N_{int} + 1)$, $N_{int} = 240$, $T = 120$, $T_0 = 3.2 \times 10^6$ considering a compromised IS (see (4.13)).

The control presented in figure 6.6 is not optimal. Since the minimization of the treatment toxicity is privileged by the performance index J_4, the administration of chemotherapy after the eradication of tumor cells necessarily increases the value of the cost function. Furthermore, the resulting Hamiltonian is not constant during time. Given the obvious limitations of this algorithm, it will not be applied to the remaining models.

6.1.4 Algorithm D: L2 norm

In contrast to algorithm C, algorithm D has converged to the optimal solutions.

6.1.4.1 Performance index

As before, four distinct performance indexes are simulated. Figure 6.7 presents the optimal controls u_c^* (left), and respective Hamiltonian functions (right) for an initial tumor burden of 3.2×10^6 in the case of a compromised immune system, for all the four J_1, J_2, J_3, and J_4 objective functions. Figure 6.7 bottom is a zoom of figure 6.7 top. Tumor burden is eradicated in all cases.

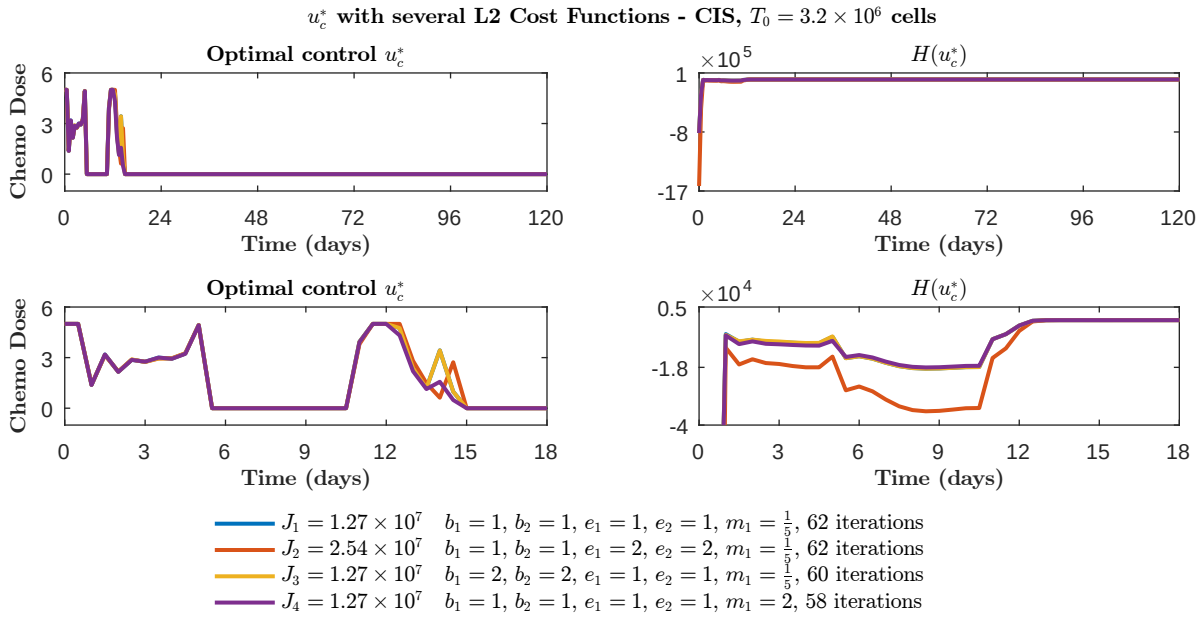

Figure 6.7: Four distinct performance indexes and their respective optimal chemotherapy (left), Hamiltonian (right). Second row is a zoom in of the first row. Simulation parameters: $N_{int} = 240$, $T = 120$, $u_{guess} = C_{max}\, ones(1, 1:15)$, $w_1 = 2.83$, $w_2 = 0.99$, $w_3 = 0.41$, $w_4 = 0.94$, $w_5 = 0.61$, $\varepsilon_1 = \varepsilon_2 = 10^{-10}$ for a compromised IS (see (4.13)) considering $T_0 = 3.2 \times 10^6$. Model (4.11).

As expected, all the four optimal solutions differ from each other (see figure 6.7 right). Nevertheless, the chemotherapy administration period is the same for all the solutions. Once again, the similarities in the period of administration between the distinct solutions may arise from the high discretization time (0.5 day) considered in Algorithm D, step **2.**. In short, $J_2 > J_4 > J_1 > J_3$, where $J_4 - J_1 = 100.67$ and $J_1 - J_3 = 108.69$. As concluded in 6.1.2.1, favouring the minimization of the tumor burden during the treatment has a higher cost than privilege its minimization at the treatment terminus or privilege the minimization of the treatment toxicity. In opposition to the results obtained in 6.1.2.1, not to privilege anything has resulted

in a greater cost than minimizing the tumor burden at the end of the treatment. According to figure 6.7 left, the solutions in which a higher dose of chemotherapy is administered are the ones that favors the minimization of the tumor burden along and at the end of the treatment. The solutions that privilege the minimization of the chemotherapy toxicity, or not privilege any measure, are the ones that have resulted in a lower dose of chemotherapy being administered. In conclusion, favouring the minimization of the tumor burden requires the administration of a higher dose of chemotherapy comparatively with the remaining solutions.

Once again, the Hamiltonian is not constant along time (see figure 6.7 left). The possible explanations for the bad behaviors of these functions were already specified in the previous section. The higher the value of the objective, the more pronounced is the bad behavior of the Hamiltonian.

In the following sections the solutions presented result from the L2-cost function J_4.

6.1.4.2 Initial tumor burden

An optimal chemotherapy is design for the same three distinct tumor burdens, $T_0 = 7.0 \times 10^5$ cells, $T_0 = 3.2 \times 10^6$ cells and $T_0 = 2.5 \times 10^7$ cells considered in 6.1.2.2, for a compromised immune system. Figure 6.8 presents the optimal control u_c^*, the system dynamics response to it and the concomitant development of chemotherapy resistance, as well as the Hamiltonian, for each T_0.

Chemotherapy is capable of eradicating a tumor burden of 7.0×10^5 cells and 3.2×10^6 cells but not a tumor burden of 2.5×10^7 cells. While for $T_0 = 7.0 \times 10^5$ (see figure 6.8 top) chemotherapy is administered without breaks until day 9.5, for $T_0 = 3.2 \times 10^6$ (see figure 6.8 middle) it is administered from day 0.0 until day 5.0 and then from day 11.0 until day 14.5. In both cases, sensitive and resistant chemotherapeutic cells are only completely eliminated some days after the end of the treatment. The elimination of these cells have occurred respectively at day 10.5 and day 11.5 for $T_0 = 7.0 \times 10^5$, and at day 16.0 and day 17.5 for $T_0 = 3.2 \times 10^6$. In conclusion, chemotherapy just needs to be administered until the immune system of the patient has the capability of eradicating the remaining tumor cells. The behavior of the NK cells and T_C cells is in accordance with what was discussed in 4.2.1. In the case of $T_0 = 7.0 \times 10^5$, tumor cells are eradicated faster comparatively with $T_0 = 3.2 \times 10^6$ and a smaller dose of chemotherapy is also given. Altogether, the objective value for $T_0 = 7.0 \times 10^5$, $J(u_c^*) = 1.89 \times 10^6$, is smaller than the one obtained for $T_0 = 3.2 \times 10^6$, $J(u_c^*) = 1.27 \times 10^7$.

Regarding $T_0 = 2.5 \times 10^7$ (see figure 6.8 bottom), chemotherapy is not able to eradicate the tumor burden. Surprisingly, a full dose chemotherapy is only obtained after day 10.5. Usually, in clinical practice, assuming a homogeneous, therapeutically sensitive tumor, chemotherapy is administered in a MTD scheme upfront (see 2.3.1) [144]. To understand if this unexpected chemotherapy schedule results either from a poor choice of the control parameters or from the tumor heterogeneous nature along with the development of resistance to chemotherapy, the cost of a full-dose regime was computed using the performance index J_4. While the value of the objective function of the chemotherapy schedule represented in figure 6.8 bottom is $J(u_c^*) = 7.93 \times 10^9$, the value obtained for a full-dose chemotherapy was $J(u_c) = 9.49 \times 10^9$. The toxicity of this treatment together with the incapacity of successfully minimize the number of tumor cells during and at the end of the treatment explains these high values.

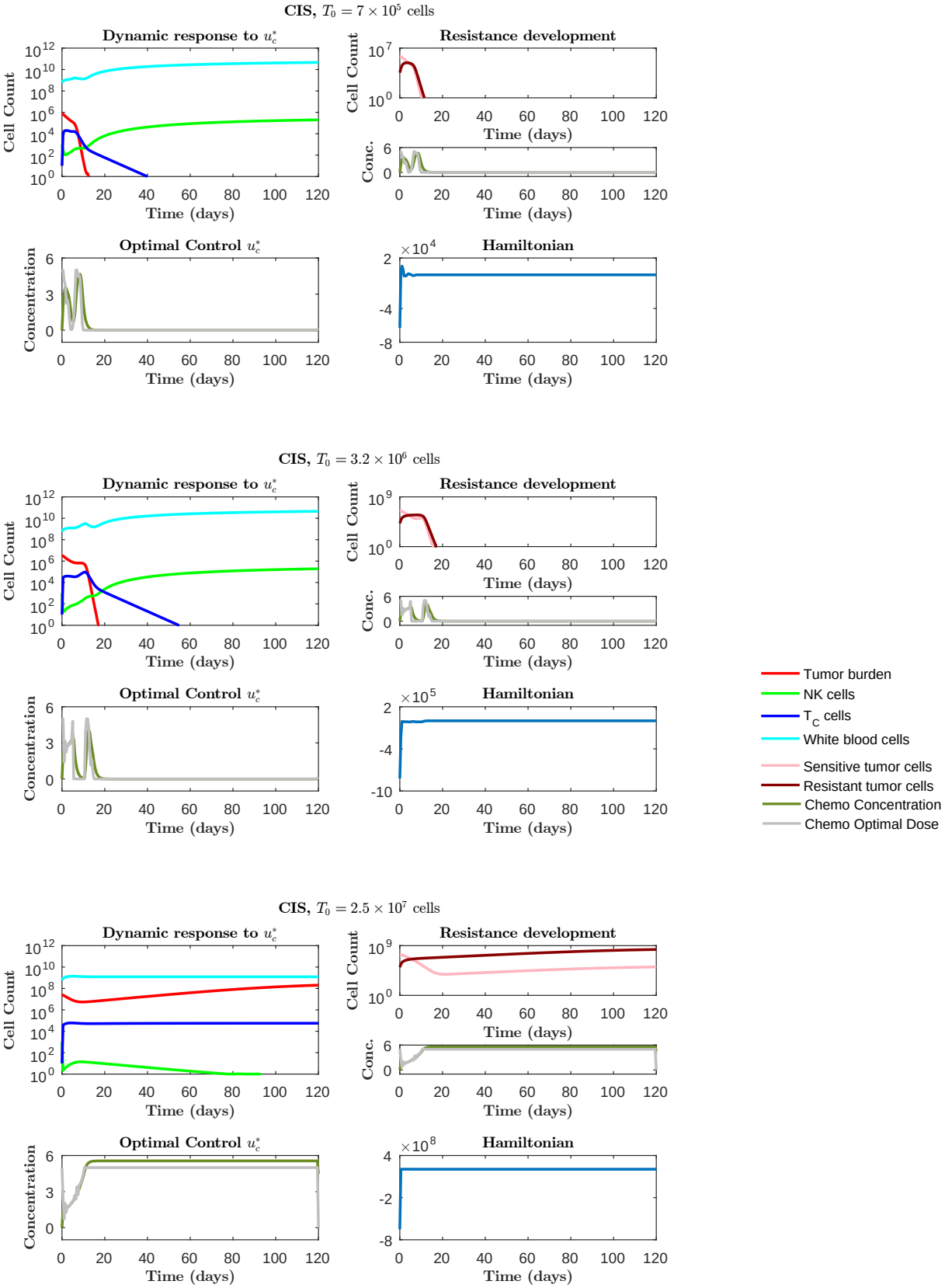

Figure 6.8: Dynamic response of model (4.11) (top left) to the optimal control (bottom left), development of resistance (top right) and the Hamiltonian (bottom right), for the quadratic J_4. Simulation parameters: $N_{int} = 240$, $T = 120$, $u_{guess} = C_{max}\, ones(1, 1 : 15)$, $w_1 = 2.83$, $w_2 = 0.99$, $w_3 = 0.41$, $w_4 = 0.94$, $w_5 = 0.61$, $\varepsilon_1 = \varepsilon_2 = 10^{-10}$ for a compromised IS (see (4.13)). Model (4.11).

Several combinations of the control parameters together with distinct initial chemotherapy guesses were tried and all of them have resulted in the chemotherapy schedule of figure 6.8 bottom. Possibly an initial administration of chemotherapy would increase the number of resistant cells at the beginning of the treatment due to development of chemotherapy resistance, resulting in a minor minimization of the tumor cells both at the end of the treatment or during it. The behavior of the immune cells is in agreement with what was discussed in 4.2.1.

Concerning the Hamiltonian functions in figure 6.8, there are always time periods in which the Hamiltonian is not constant. The higher the cost value, or by the same token, the higher the initial T_0, the more pronounced is its deviation from a constant function.

In order to investigate the optimality of the solutions obtained, these are perturbed and the objective function is recomputed. Figure 6.9 illustrates the perturbation of the u_c^* for $T_0 = 3.2 \times 10^6$, the resultant Hamiltonian. This small perturbation of u_c^* results in an added cost of 2.93×10^4. Nevertheless this does not prove that this solution is the optimal one. In all the three cases, tumor is eradicated at the same day and the systems dynamics behaves in the same way.

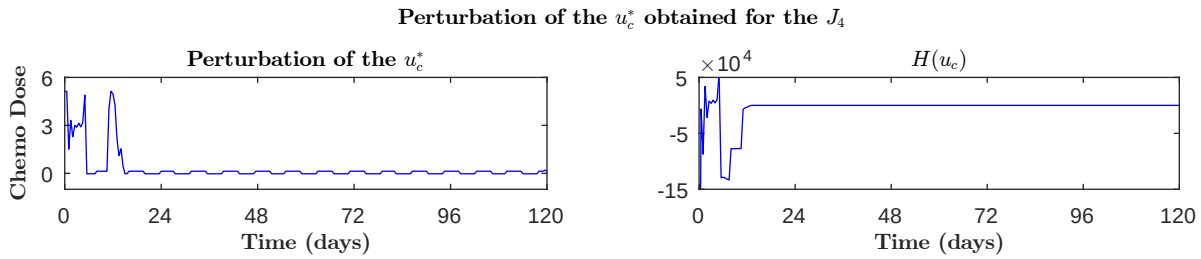

Figure 6.9: Perturbation of the optimal solution obtained for $T_0 = 3.2 \times 10^6$ and respective Hamiltonian. Simulation parameters: $u_{pert} = u_c^* + 0.08 * square(0.8 * t)' + 0.05, T = 120, J_4$.

6.1.4.3 Time horizon

At last, three different therapy time horizons, $T = 60$, $T = 120$, and $T = 240$ are considered for a tumor burden of $T_0 = 3.2 \times 10^6$ in a compromised immune system (see figure 6.10). The same discretization time - 0.5 day is considered for every simulation. Once again, the alteration of the therapy time horizon has not changed the results obtained. However, this scenario might be different if the tumor burden had been eradicated after day 60.0, or if it was not eradicated at all. Due to the high integration time of the state equation, it was not possible to design an optimal therapy schedule for high tumor burdens.

6.1.5 Comparison of the L1- and L2-norm performance indexes

The utilization of objective functions with different norms, and henceforth distinct algorithms, leads to different solutions. In this subsections the results obtained for algorithms B and D are compared and discussed.

Concerning the simulations with different performance indexes (see table 6.1), the value obtained for the linear and quadratic cost functions are of the same order of magnitude. Although the minimization of the linear performance index has resulted in smaller periods of chemotherapy administration, the

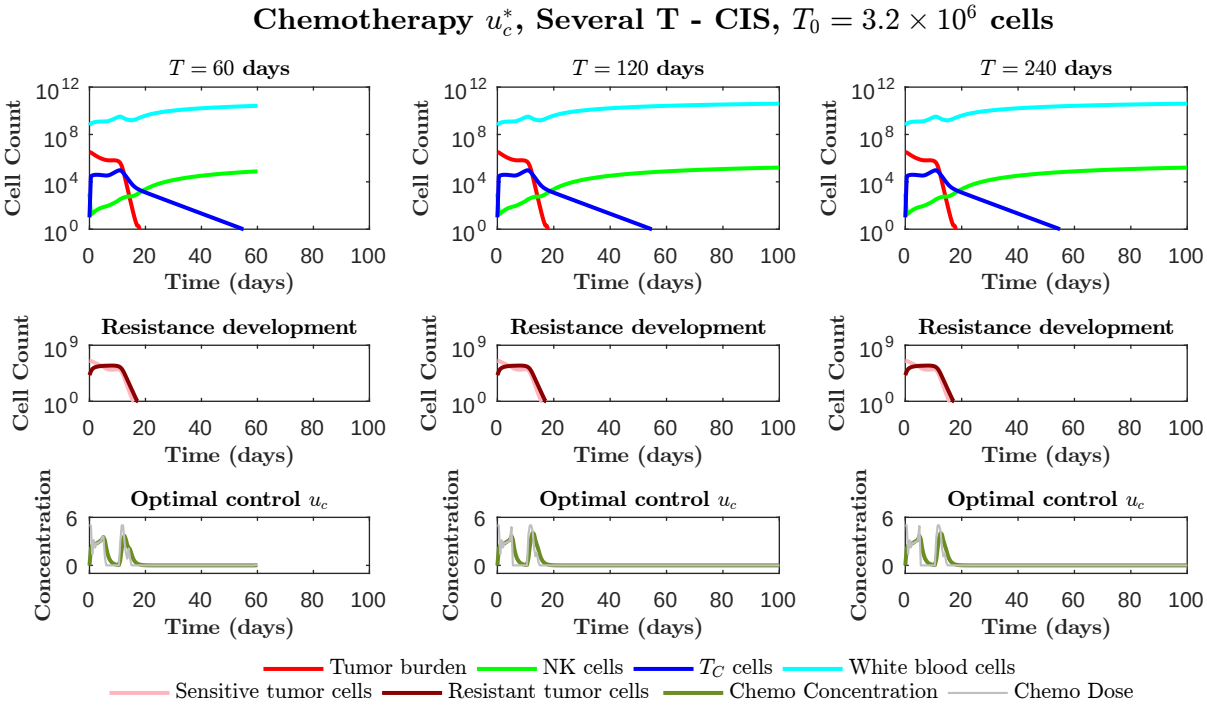

Figure 6.10: Simulation of the optimal chemotherapy for three distinct time horizons: $T = 60$ days (left), $T = 120$ days (middle), $T = 240$ days (right). Simulation parameters: $N_{int} = 240$, $T = 120$, $u_{guess} = C_{max}\, ones(1, 1:15)$, $w_1 = 2.83$, $w_2 = 0.99$, $w_3 = 0.41$, $w_4 = 0.94$, $w_5 = 0.61$, $\varepsilon_1 = \varepsilon_2 = 10^{-10}$ for a compromised IS (see (4.13)) considering $T_0 = 3.2 \times 10^6$. Model (4.11).

objective values obtained for the quadratic norm are smaller than the ones obtained for the linear one. As discussed in 5.1.2, quadratic objective favors lower drug concentrations. Accordingly, despite the higher chemotherapy administration period obtained for the L2-norm, the chemotherapy dose administered, and thus the treatment toxicity, is smaller in the case of the quadratic objective comparatively with the L1-norm. Overall, the smaller chemotherapy dose obtained for the L2-norm has resulted in smaller cost values comparatively with the L1-norm. Additionally, the added cost of favouring the minimization of the tumor burden at the end of the treatment (J_3) is higher for the linear objectives relatively to the quadratic ones. This difference may result from the different periods of chemotherapy administration. Possibly, by administrating chemotherapy twice and in lower doses, it is possible to decrease the development of

Table 6.1: Chemotherapy results for the four distinct linear and quadratic performance indexes when a compromised IS and an initial tumor burden of 3.2×10^6 are considered.

Objective Norm	**Cost function**	**Administration period** (*day*)	**Note**	**Tumor eradication**
L1	$J_1 = 1.38 \times 10^7$	$0.0 - 4.0$	$J_2 > J_4 > J_3 > J_1$	✔
	$J_2 = 2.76 \times 10^7$	$0.0 - 4.0$		✔
	$J_3 = 1.38 \times 10^7$	$0.0 - 4.0$		✔
	$J_4 = 1.38 \times 10^7$	$0.0 - 4.0$		✔
L2	$J_1 = 1.27 \times 10^7$	$0.0 - 5.0,\ 11.0 - 14.5$	$J_2 > J_4 > J_1 > J_3$	✔
	$J_2 = 2.54 \times 10^7$	$0.0 - 5.0,\ 11.0 - 14.5$		✔
	$J_3 = 1.27 \times 10^7$	$0.0 - 5.0,\ 11.0 - 14.5$		✔
	$J_4 = 1.27 \times 10^7$	$0.0 - 5.0,\ 11.0 - 14.5$		✔

resistance, resulting in a earlier tumor eradication comparatively with the linear objectives. Regardless of the performance index norm and parameters, the tumor is eradicated in all the cases.

Regarding the simulations with distinct initial tumor burdens for the performance index J_4 (see table 6.2), as before, the chemotherapy administration period is higher for the L2-norm objective than for the linear one. Once again, although in the same order of magnitude, the objective values are higher for the L1-norm cost functions relatively to the L2-norm objectives. These results arise from the L2-norm favor of lower drug concentrations, as explained before. Even though higher chemotherapy doses are administered in the case of the L1-norm and the treatments are ceased earlier comparatively with the L2-norm objective, both L1-norm sensitive and resistant tumor cells are only eliminated after the same had occurred to the L2-norm.

Accordingly to figure 6.11, these results arise from the different chemotherapy schedules obtained for these two norms. While chemotherapy is administered once for the L1-norm, in the case of the L2-norm it is administered twice. Although there is not a break in the administration of chemotherapy for $T_0 = 7.0 \times 10^5$, two peaks of chemotherapy exist. The second peak contributes for this faster elimination of sensitive cells comparatively with the resistant ones. In the final analysis, a longer and interrupted administration of chemotherapy but in lower doses results in a faster eradication of tumor cells due to the smaller development of chemotherapy resistance and the faster elimination of sensitive tumor cells.

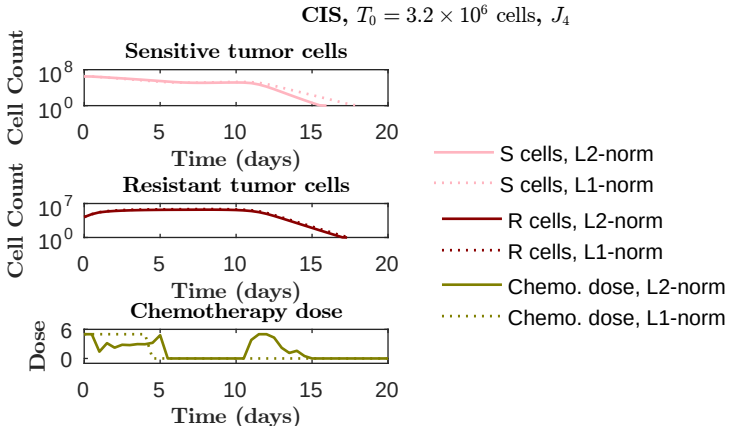

Figure 6.11: Resistance onset to two chemotherapy doses obtained for the L1- an L2-norm objective J_4, for $T_0 = 3.2 \times 10^6$ cells when a compromised IS is considered.

Table 6.2: Chemotherapy results of the minimization of the linear and quadratic performance indexes J_4 for three distinct initial tumor burdens when a compromised IS is considered.

Objective Norm	T_0	**Administration period** (*day*)	**S cells erad.** (*day*)	**R cells erad.** (*day*)	**Cost function**	**Tumor erad.**
L1	7.0×10^5	$0.0 - 3.0$	12.5	12.0	1.93×10^6	✔
	3.2×10^6	$0.0 - 4.0$	18.0	17.5	1.38×10^7	✔
	2.5×10^7	$0.0 - 120.0$	–	–	9.49×10^9	✘
L2	7.0×10^5	$0.0 - 9.5$	10.5	11.5	1.89×10^6	✔
	3.2×10^6	$0.0 - 5.0, 11.0 - 14.5$	16.0	17.5	1.27×10^7	✔
	2.5×10^7	$0.0 - 120.0$	–	–	7.93×10^9	✘

6.2 Immunotherapy

In this section, the results from the optimal control problems [OC1] (algorithm B) and [OC2] (algorithm D) are presented in the subsections 6.2.1 and 6.2.2, respectively. Since algorithms A and C are not able to converge to the the optimal solution, only the numerical simulations regarding algorithms B and D are presented. Remember that TILs are administered as bolus at day 7.0.

6.2.1 Algorithm B: L1 norm

6.2.1.1 Performance index

Figure 6.12 presents the optimal controls u_i^* (left), and respective Hamiltonians (right) for an initial tumor burden of 7.0×10^5, for a case of a compromised immune system when the four distinct objective functions J_1, J_2, J_3, and J_4 are minimized. Figure 6.12 bottom is a zoom of figure 6.12. The tumor burden is eradicated in all cases.

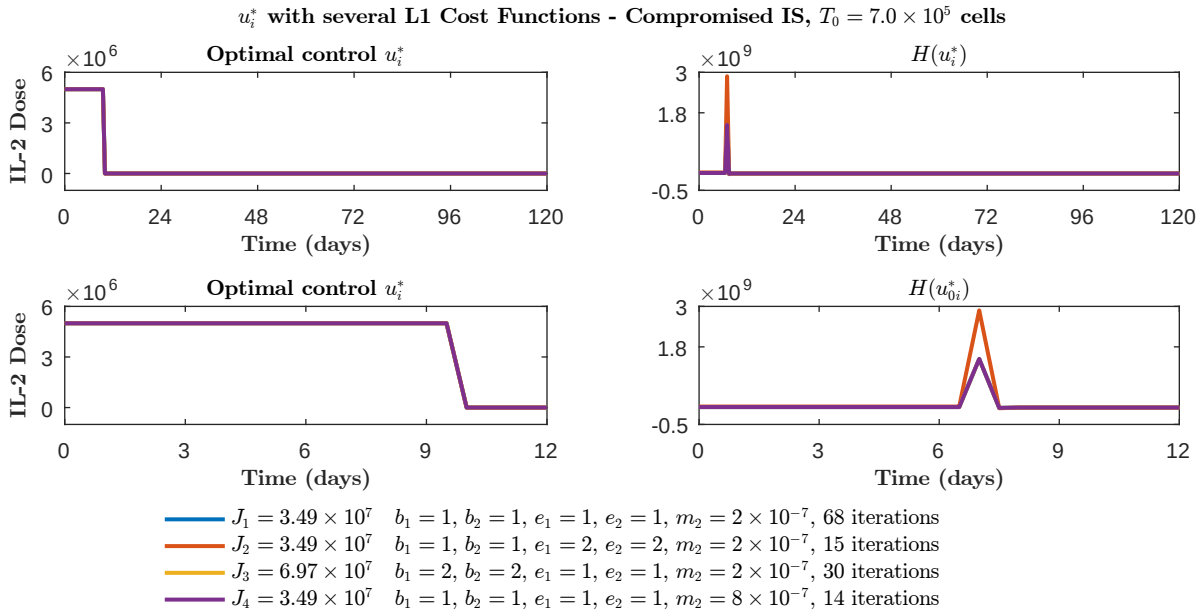

Figure 6.12: Four distinct performance indexes and their respective optimal chemotherapy (left), and Hamiltonian (right). Second row is a zoom in of the first row. Simulation parameters: compromised IS (see (4.13)), $N_{int} = 240$, $N_s = 10$ except for $N_s(J_3) = 2$, $T = 120$, $T_0 = 7.0 \times 10^5$, $\varepsilon_1 = \varepsilon_2 = 10^{-10}$, $\varepsilon_3 = 2.0$, except for $\varepsilon_3(J_2) = 1.0$ and $\varepsilon_3(J_4) = 0.25$, $\varepsilon_4 = 3$, except for J_2 and J_4, where $\varepsilon_4 = 5$, $w_1 = 0.8$, except for $w_1(J_2) = 0.5$, and $w_2 = 2.8$ except for $w_2(J_2) = 2.0$ and $w_2(J_3) = 2.5$. Model (4.10).

In the case of immunotherapy, distinct performance indexes have given rise to the same optimal solution (see figure 6.12 left), which can result from the high discretization time used - 0.5 day. Although the same solution is obtained for all the cost functions, both the objective value and the Hamiltonian are distinct. While for chemotherapy J_3 is one of the the lowest cost values, in immunotherapy it is the highest one. In brief, $J_3 > J_4 > J_1 > J_2$, where $J_4 - J_1 = 509.78$ and $J_1 > J_2 = 5.13$. Accordingly, favouring the minimization of the tumor burden at the treatment end is now the measure with highest cost associated, followed by favouring the minimization of the IL-2 toxicity and, in third place, not to privilege anything.

Interestingly, the objective J_2, which favors the minimization of the tumor burden along the treatment, is the one with lowest cost. In the case of chemotherapy, it is the one with highest cost associated. Which are the reasons behind these scenario change? In the first place, in contrast to chemotherapy, the administration of IL-2 and TILs strengths the immune system and does not affect directly the tumor cells. Forthwith, the immune system is thus capable of eliminate more cells during the treatment and, since tumor cells are not directly affected by the treatment, they not develop resistance to it. In the worst case scenario, tumor cells may develop efficient immunoevasive strategies (see 2.2.1), hampering the action of the immune system. The real challenge is then to strengthen enough the immune system so it is capable of eliminating all the tumor cells.

In contrast to the chemotherapy, the cost function which Hamiltonian has the worst behavior does not correspond to the highest cost value (see figure 6.12 right). Although the Hamiltonian is almost constant along time, there is a time period where it explodes. The reasons behind these bad behaviors were refereed in the last section.

In the following subsections, the solutions obtained result from the minimization of the linear J_4 cost function.

6.2.1.2 Initial tumor burden

In contrast to chemotherapy, only two distinct initial tumor burdens, $T_0 = 7.0 \times 10^5$ and, $T_0 = 8.0 \times 10^5$ are simulated. The simulation for a higher tumor burden ran for almost a week without results. Possibly this time-consuming computation may result from the low relative tolerance (10^{-30}) used in *ode45* in order to avoid oscillations and negative values in the solution of the dynamics. Other *ODE's* were tried without success. Figure 6.13 presents the optimal control u_i^*, the system dynamics response as well as the Hamiltonian, for each T_0, considering a compromised immune system.

Immunotherapy has succeed to control a tumor burden of 7.0×10^5 cells but not a tumor burden of 8.0×10^5. Regarding $T_0 = 7.0 \times 10^5$ cells (see figure 6.13 top), IL-2 is administered from day 0.0 until day 9.5. Note that TILs have been administered at day 7.0. As referred in 2.3.2, IL-2 promotes the expansion and long-term survival of T_C cells. Forthwith, an administration of IL-2 coincident with the administration of TILs was expected. Possibly the administration of IL-2 prior to the administration of TILs promotes the expansion of the pre-existent T_C cells. Moreover, IL-2 is not given during the whole treatment period because its toxicity would outweigh the benefits obtained concerning the tumor reduction. The tumor burden is only controlled at day 17.0. As seen for chemotherapy, immunotherapy just needs to be administered until the immune system is strong enough to be capable of eradicating the remaining tumor cells by itself. This finding highlights the importance of modeling immunotherapy together with the modulation of the immune response.

In the case of $T_0 = 8.0 \times 10^5$ (see figure 6.13 bottom), the immune system has failed to eradicate the tumor burden. IL-2 is administered from day 0.0 until day 17.5. Once again, both IL-2 and TILs administration is coincident. Although the administration of TILs and IL-2 has resulted in a prompt reduction of the tumor burden, the immune system is not capable of deal with it yet. Once the tumor burden is not eradicated and a high dose of IL-2 is administered for $T_0 = 8.0 \times 10^5$ comparatively with

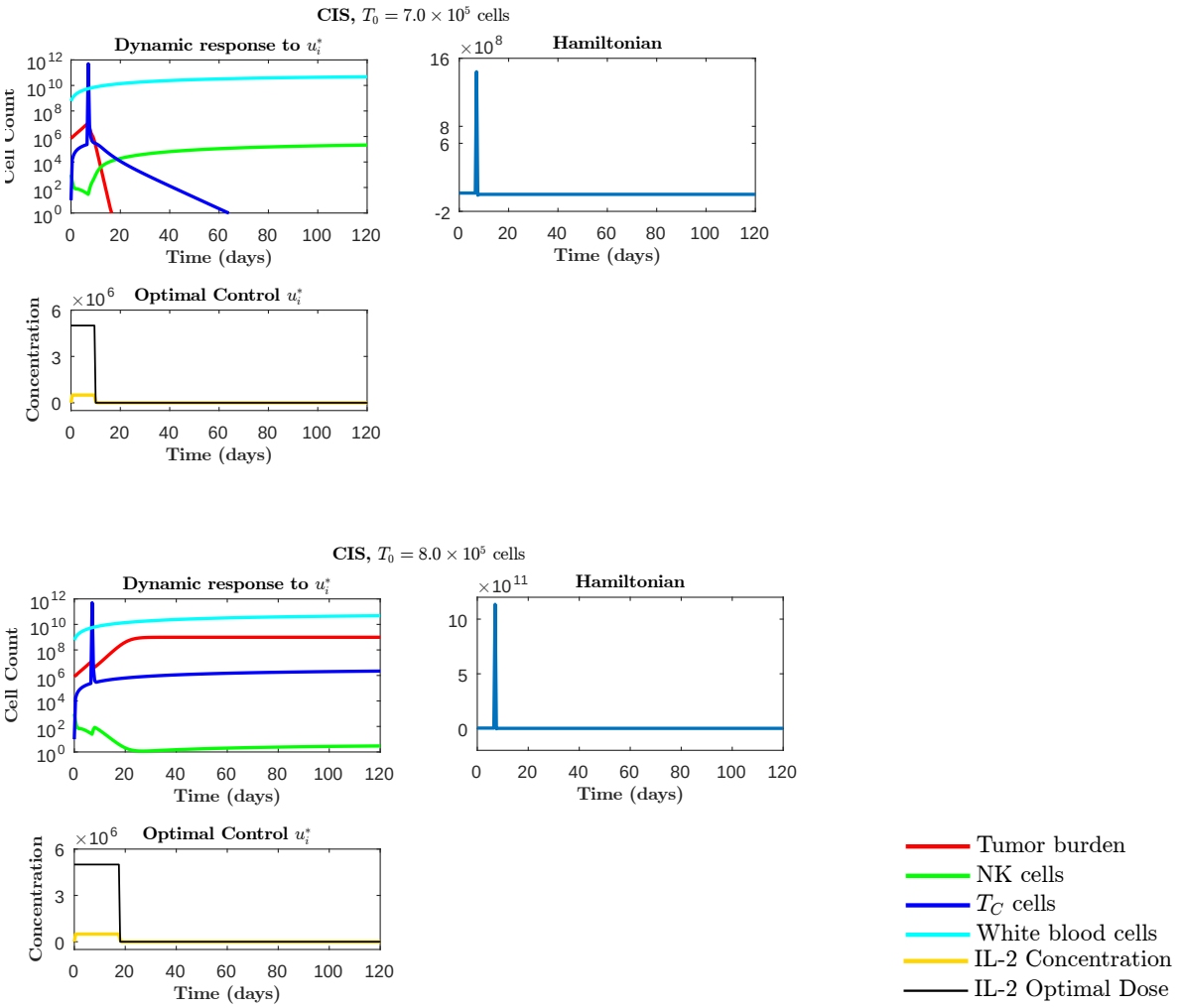

Figure 6.13: Dynamic response of model (4.10) (top left) to the optimal control (bottom left) and the Hamiltonian (top right). Simulation parameters: A compromised IS was considered together (see (4.13)) with J_4. $N_{int} = 240$, $N_s = 10$, $T = 120$, $\varepsilon_1 = \varepsilon_2 = 10^{-10}$, $\varepsilon_3 = 0.25$, $\varepsilon_4 = 5$, $w_1 = 0.8$, and $w_2 = 2.8$. Model (4.10).

$T_0 = 7.0 \times 10^5$, a higher cost value is also obtained for the higher tumor burden ($J(u_i^*) = 9.82 \times 10^{10}$) relatively to the smaller one ($J(u_i^*) = 3.49 \times 10^7$).

Concerning the Hamiltonian functions in figure 6.13, in all the cases the Hamiltonian is almost constant along time with the exception of a little time subinterval in which it explodes. Once again, the higher the initial tumor burden, and therefore the cost value, the higher is the peak observed for the Hamiltonian.

In order to study the optimality of the solutions obtained, these are perturbed and the objective function is recomputed. Since the perturbation is too small comparatively with the order of magnitude of the IL-2 dose administered, no alterations in the solution, and Hamiltonian are visible to the naked eye. However, the perturbation of the u_c^* for $T_0 = 7.0 \times 10^5$ has resulted in an added cost of 8.51.

6.2.1.3 Time horizon

Three distinct therapy time horizons, $T = 60$, $T = 120$, and $T = 240$ are considered for a tumor burden of $T_0 = 3.2 \times 10^6$ in a compromised immune system (see figure 6.14). The same discretization time - 0.5

days is considered for every simulation. Once again, the alteration of the therapy time horizon has not changed the results obtained.

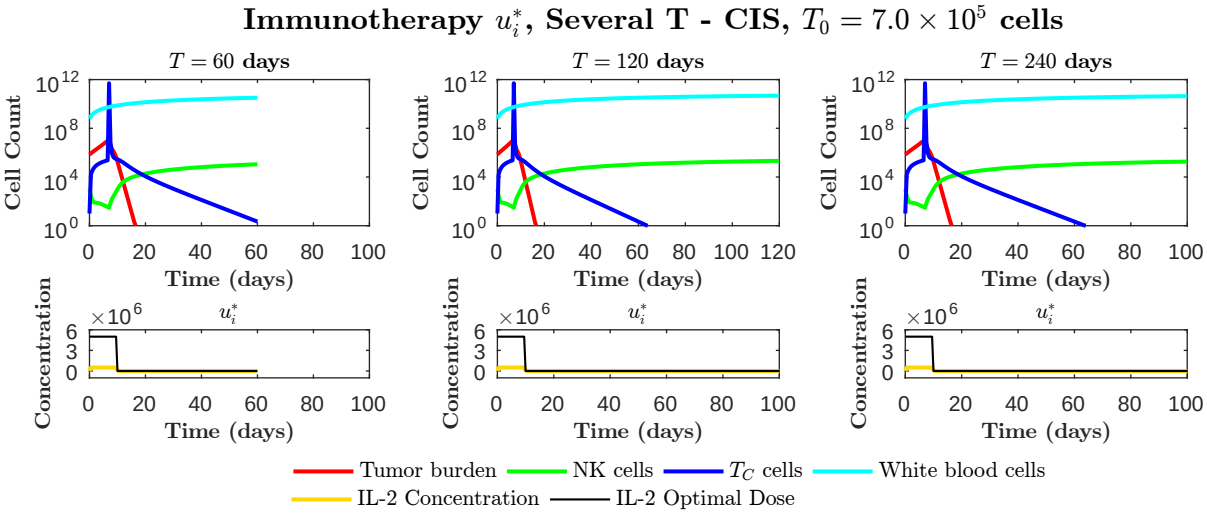

Figure 6.14: Simulation of the optimal chemotherapy for three distinct time horizons: $T = 60$ days (left), $T = 120$ days (middle), $T = 240$ days (right). Simulation parameters: compromised IS (see (4.13)), $N_{int} = 240$, $N_s = 10$, $T = 120, T_0 = 7.0 \times 10^5, \varepsilon_1 = \varepsilon_2 = 10^{-10}, \varepsilon_3 = 0.25, \varepsilon_4 = 5, w_1 = 0.8, w_2 = 2.8$ except for the case of $T = 60$, where $N_s = 10$, $w_1 = 0.4$, $w_2 = 2.5$. Model (4.10).

6.2.2 Algorithm D: L2 norm

6.2.2.1 Performance index

In figure 6.15, the optimal controls u_i^* (left), respective Hamiltonian functions (right) are presented for an initial tumor burden of 7.0×10^5, in a case of a compromised immune system, when the four distinct quadratic objective functions J_1, J_2, J_3, and J_4 are minimized. The bottom of figure 6.15 is simply a zoom of its top 6.12. The tumor burden is eradicated in all cases.

Distinct performance indexes do have given rise to different optimal solutions (see figure 6.15 left). In short, $J_2 > J_3 > J_1 > J_4$, where $J_3 - J_1 = 1.16$ and $J_1 - J_4 = 504.00$. In contrast to 6.2.1.1 but similarly to chemotherapy, the privilege of the minimization of the tumor burden during the treatment is the measure with highest cost. Since it corresponds to the solution with highest dose of IL-2 administered, probably the highest cost obtained comes from the inherent toxicity of this solution. The second highest performance index favors the minimization of the tumor burden at the treatment terminus and its value is close to the cost of not favouring any measure. Accordingly, the number of cancer cells in the end of the treatment is basically the same. Provided that the tumor is eradicated in all cases, the difference between these performance indexes arise from the slightly different dose of IL-2 administered. Finally, the favor of the minimization of the treatment toxicity is the measure with the lowest cost associated and also the one with the smallest quantity of IL-2 being administered.

As seen previously, the Hamiltonian is not constant along time (see figure 6.15 right). The solution with highest cost value - J_3 - is the one with the worst behavior of the respective Hamiltonian. The possible explanations for this unexpected bad behavior were already specified. Briefly, they may come from the high temporal discretization considered - 0.5 day, a poor selection of the controls parameters,

and the optimal solution may not be a solution of the dynamics or it does not comply with the constraints imposed.

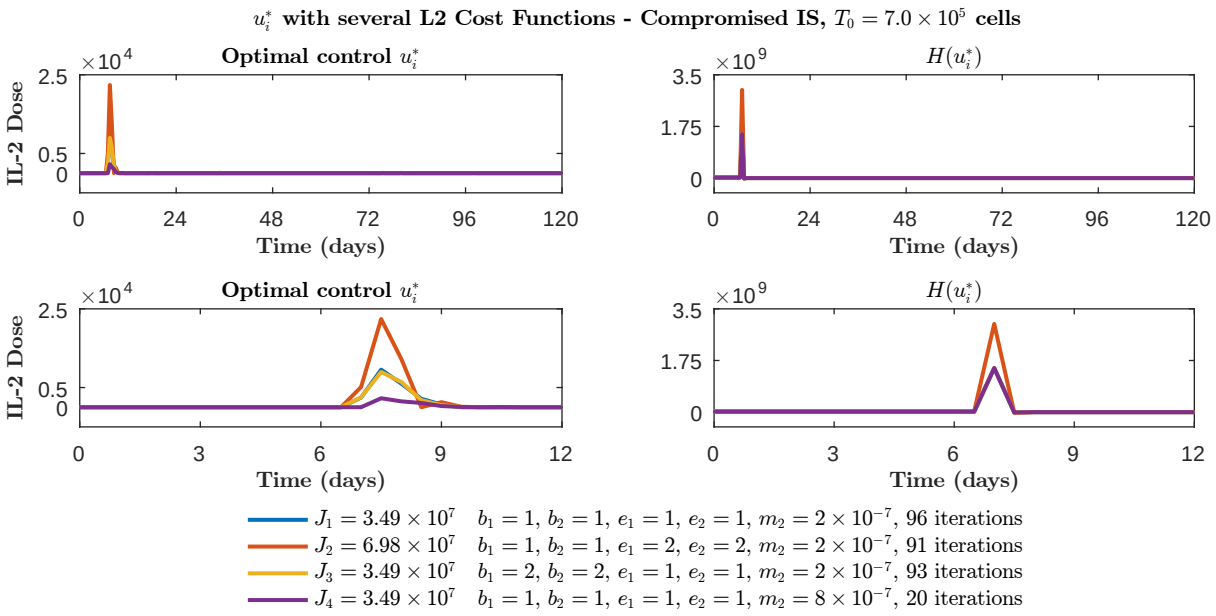

Figure 6.15: Five distinct performance indexes and their respective optimal chemotherapy (left), Hamiltonian (right). Second row is a zoom in of the first row. Simulation parameters: compromised IS (see (4.13)), $N_{int} = 240$, $T = 120, T_0 = 7.0 \times 10^5$, $u_{guess} = u_{max}\, ones(1, 1:15)$, $varepsilon_1 = \varepsilon_2 = 10^{-10}$, $w_1 = 1.2$, except for J_4 where $w_1 = 2.83$, $w_2 = 0.99$, $w_3 = 0.41$, $w_4 = 0.61$ except for J_4 where $w_4 = 0.35$, for a compromised IS (see (4.13)) considering $T_0 = 7.0 \times 10^5$. Model (4.10).

In the following subsections, the solutions obtained result from the minimization of the quadratic J_4 objective.

6.2.2.2 Initial tumor burden

For the reasons mentioned in 6.2.1.2 , it is not possible to design the optimal immunotherapy for a high tumor burden. Two optimal immunotherapies are designed for two distinct tumor burdens, $T_0 = 7.0 \times 10^5$ cells and $T_0 = 8.0 \times 10^5$, in the case of a compromised immune system. Figure 6.16 presents the optimal control u_c^*, the system dynamics response to it as well as the Hamiltonian functions.

Immunotherapy is able to eradicate a tumor burden of 7.0×10^5 cells but not one of 8.0×10^5 cells (see figure 6.16 top and bottom). The administration of IL-2 starts at day 6.5 for both solutions and coincides with the TILs administration. However, the administration period of this cytokine is longer for $T_0 = 8.0 \times 10^5$ than it is for $T_0 = 7.0 \times 10^5$ cells. The treatment seems to end at day 11.0 and day 16.5 for $T_0 = 7.0 \times 10^5$ and $T_0 = 8.0 \times 10^5$ cells, respectively. Due to the residual administration of IL-2 is difficult to determine the exact day. The tumor burden is fully eradicated in day 16.5 in the case of $T_0 = 7.0 \times 10^5$. Once again, immunotherapy only needs to be administered until the immune system of the patient has the capability of eradicating the remaining tumor cells. Nonetheless, the major difference between these two solutions focuses in the dose administered. A higher dose of IL-2 is administered in the case of $T_0 = 8.0 \times 10^5$ compared with $T_0 = 7.0 \times 10^5$ (see the difference between the order of magnitude of the IL-2 peak in figures 6.16 top and bottom). The fact that the tumor is not eradicated and a high dose

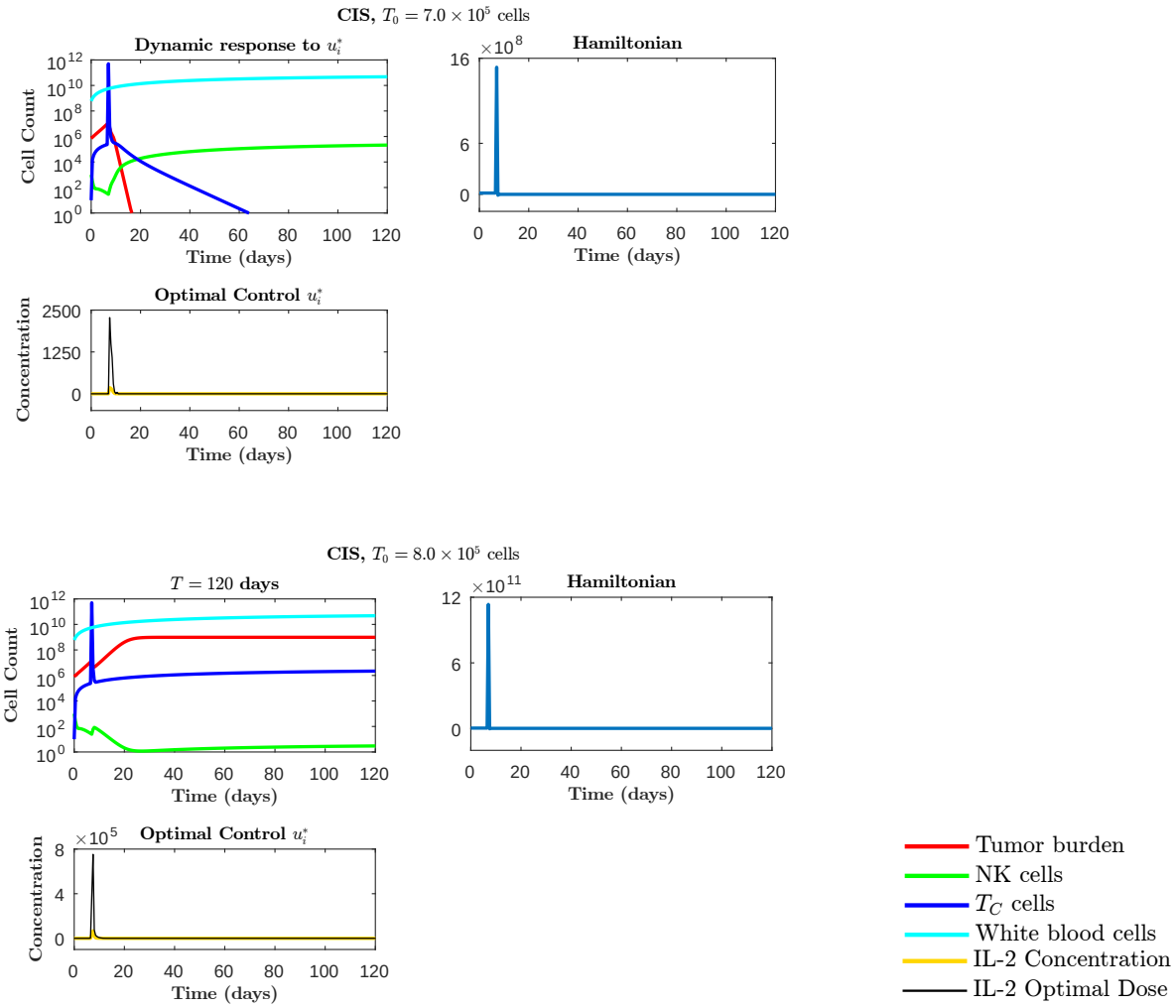

Figure 6.16: Dynamic response of model (4.10) (top left) to the optimal control (bottom left) and the Hamiltonian (top right) in the case of $T_0 = 7.0 \times 10^5$ and $T_0 = 8.0 \times 10^5$. Simulation parameters: A compromised IS (see (4.13)) was considered together (see (4.13)) with J_4. Simulation parameters: $N_{int} = 240$, $T = 120, u_{guess} = u_{max}\, ones(1, 1:15)$, $w_1 = 2.83$, $w_2 = 0.99$, $w_3 = 0.41$, $w_4 = 0.35$, $\varepsilon_1 = \varepsilon_2 = 10^{-10}$.

of IL-2 is administered explains the higher cost value obtained ($J(u_i^*) = 9.82 \times 10^{10}$) for $T_0 = 8.0 \times 10^5$ compared with $T_0 = 7.0 \times 10^5$ ($J(u_i^*) = 3.49 \times 10^7$).

Regarding the Hamiltonians in figure 6.16, there are always time periods in which the Hamiltonian is not constant. The higher the cost value, or by the same token, the higher the initial tumor burden, the more pronounced is the deviation from a constant function in the case of the Hamiltonian.

At last, the optimal solutions are perturbed. Once again, the alterations in the solutions and in the Hamiltonian functions are not visible to the naked eye and therefore are not presented. Concerning the $T_0 = 7.0 \times 10^5$, the perturbation of the solution has in fact resulted in an added cost of 511.47. Note that this result does not prove that the solution obtained is the optimal one.

6.2.2.3 Time horizon

Three distinct therapy time horizons, $T = 60$, $T = 120$, and $T = 240$ are considered for a tumor burden of $T_0 = 7.0 \times 10^5$ in a compromised immune system (see figure 6.17). The same discretization time - 0.5 day is considered for every simulation. Once again, the profile of the IL-2 administration is almost the

same between the different time horizons. In this case the slightly differences observed may arise from the control parameters chosen rather than a distinct optimal solution.

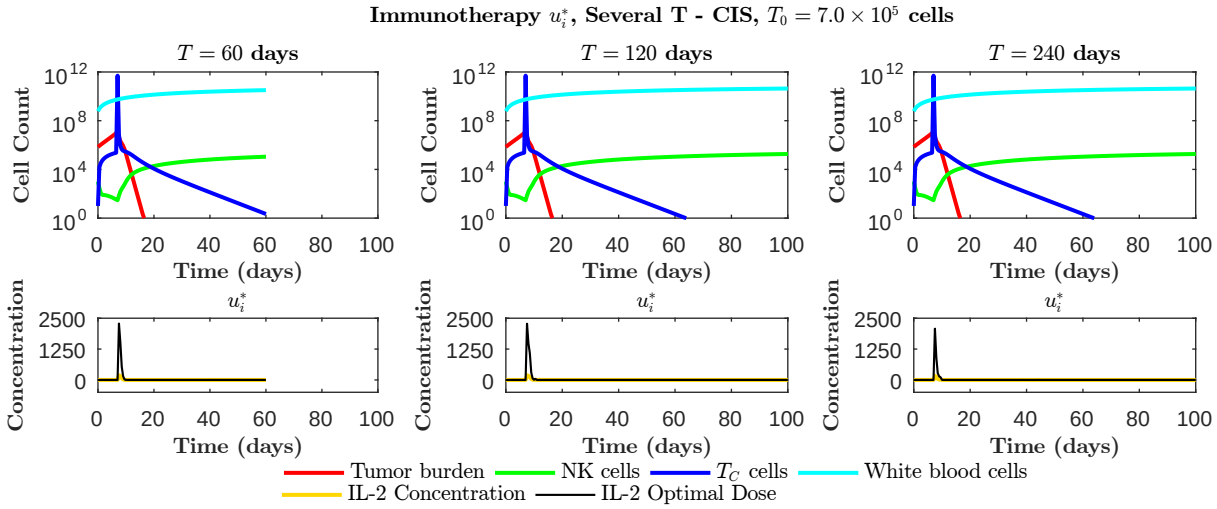

Figure 6.17: Simulation of the optimal chemotherapy for three distinct time horizons: $T = 60$ days (left), $T = 120$ days (middle), $T = 240$ days (right). Simulation parameters: compromised IS (see (4.13)), $N_{int} = 240, T_0 = 7.0 \times 10^5$, $u_{guess} = u_{max}\, ones(1, 1:15)$, $w_1 = 2.83$, $w_2 = 0.99$, $w_3 = 0.41$, $w_4 = 0.35$, $\varepsilon_1 = \varepsilon_2 = 10^{-10}$ except for $T = 240$, where $w_1 = 1.2$, and $w_4 = 0.61$. Model (4.10).

6.2.3 Comparison of the L1- and L2-norm performance indexes

Once again, the minimization of objectives with linear and quadratic dependence on the control, which in this case is the IL-2, has lead to distinct optimal solutions. In this subsection the results obtained for both algorithms B and D are compared and analyzed.

Regarding the minimization of the four different performance indexes (see table 6.3), they all have the same order of magnitude. However, in contrast to what was observed for chemotherapy, the value of the quadratic objectives are in fact higher than the linear ones, with the exception of J_3. In fact, quadratic objectives favor the administration of lower drug doses (see the administration period in table 6.3), explaining why the objective that favors the minimization of the treatment toxicity - J_4 - is the quadratic objective with lowest value. However, this lower dose administration obtained for the L2-norm

Table 6.3: Optimal immunotherapy results of algorithm B and C for four distinct performance indexes when a compromised IS and an initial tumor burden of 7.0×10^5 are considered.

Objective Norm	Cost function	Administration period (*day*)	Note	Tumor eradication
L1	$J_1 = 3.49 \times 10^7$	$0.0 - 9.5$	$J_3 > J_4 > J_1 > J_2$	✔
	$J_2 = 3.49 \times 10^7$	$0.0 - 9.5$		✔
	$J_3 = 6.97 \times 10^7$	$0.0 - 9.5$		✔
	$J_4 = 3.49 \times 10^7$	$0.0 - 9.5$		✔
L2	$J_1 = 3.49 \times 10^7$	$6.5 - 9.5$	$J_2 > J_3 > J_1 > J_4$	✔
	$J_2 = 6.98 \times 10^7$	$6.5 - 10.0$		✔
	$J_3 = 3.49 \times 10^7$	$6.5 - 10.0$		✔
	$J_4 = 3.49 \times 10^7$	$6.5 - 11.0$		✔

cost functions, and thus smaller drug toxicity, results in a lower minimization of the tumor cells along the treatment. Accordingly, the sequence of the objectives organized in descending order of its value (see column *Note* in table 6.3) changes almost completely between these two objective norms. Nonetheless, why is the administration period so different between these two algorithms? Possibly the difference regarding the first day of IL-2 administration between the L1- and L2-norm performance indexes arises from the initial guesses considered for the IL-2. In algorithm B, the initial guess for both chemo- and immunotherapy is considered to start in their maximum value (see figure 5.1). The results may have been different if the IL-2 initial guess started in its minimum value.

Regardless of the performance index norm and parameters, the tumor burden is eradicated for all the cases.

Concerning the simulations with distinct initial tumor burdens for the performance index J_4 (see table 6.4), in contrast to chemotherapy, the administration period is smaller for the L2-norm objective than for the linear one. Once again, although in the same order of magnitude, the objective values are higher for the L2-norm cost function relatively to the L1-norm objective. With regards to $T_0 = 7.0 \times 10^5$, despite a lower IL-2 dose has been administered in the case of the L2-norm and the treatment is ceased earlier comparatively with the L1-norm objective, tumor cells are eradicated at the same day for both norms. However, the L1-norm objective has resulted in a higher minimization of the the tumor cells along the treatment which outweighs the added cost of the treatment toxicity. Regarding $T_0 = 8.0 \times 10^5$, the IL-2 administrations has ceased earlier for the L2-norm objective than for the L1 one. Once again, the lower toxicity of the IL-2 administered with the L2-norm does not compensate the lower minimization of tumor cells along the treatment.

Table 6.4: Optimal immunotherapy results of algorithm B and C for three distinct initial tumor burdens when a compromised IS the performance index J_4 are considered.

Objective Norm	T_0	**Administration period** (*day*)	**T cells erad.** (*day*)	**Cost function**	**Tumor erad.**
L1	7.0×10^5	$0.0 - 9.5$	16.5	3.49×10^7	✔
	8.0×10^5	$0.0 - 17.5$	$-$	9.82×10^{10}	✘
L2	7.0×10^5	$6.5 - 11.0$	16.5	3.49×10^7	✔
	8.0×10^5	$6.5 - 16.5$	$-$	9.82×10^{10}	✘

6.3 Combination therapy

In this section, the results from the optimal control problems [OC5] (algorithm B) and [OC6] (algorithm D) are presented in the subsections 6.3.1 and 6.3.2, respectively, for two distinct tumor burdens, $T_0 = 3.2 \times 10^6$ and $T_0 = 4.0 \times 10^7$. Finally, a comparison of the results obtained for [OC5] and [OC6] is made in 6.3.3.

6.3.1 Algorithm B: L1 norm

Once again, for the reasons mentioned before, it is not possible to design the optimal combination therapy for a high tumor burden. Figure 6.18 presents the optimal controls u_c^* and u_i^*, the system dynamics response to them, as well as the Hamiltonian functions and the evolution of the controls towards optimality, for the above mentioned T_0, considering a compromised immune system.

As seen in 6.1.2, chemotherapy is capable of eradicating a tumor burden of $T_0 = 3.2 \times 10^6$ by itself. In turn, immunotherapy is not able to eradicate such a burden of tumor cells. Henceforth, the combination therapy, *i.e.* the combination of both therapies, is expected to eradicate the tumor earlier than chemotherapy does by itself. According to with figure 6.18 top, combination therapy is in fact successful to eradicate $T_0 = 3.2 \times 10^6$ cells. Chemotherapy is administered between day 0.0 and day 8.5. At the same time, IL-2 is administered from day 0.0 to day 5.0. Since TILs have been administered at day 7.0, there is not a simultaneously administration of the IL-2 and TILs. Sensitive and resistant chemotherapeutic cells are eradicated at day 11.0 and day 13.0, respectively. As seen until now, both chemo- and immunotherapy just need to be administered until the immune system has the full capacity to eradicate the tumor burden.

Table 6.5 summarizes the results obtained for the minimization of the L1-norm cost function J_4, in the case of $T_0 = 3.2 \times 10^6$, for both chemotherapy and combination therapy. Surprisingly, the combination therapy has resulted in a higher period of chemotherapy administration, and therefore, in a higher dose been administered, comparatively with chemotherapy by itself. This higher chemotherapeutic dose must result in a higher onset of chemotherapeutic resistance and a higher toxicity. However, both sensitive and resistant tumor cells are eliminated earlier in the combination therapy than in chemotherapy by itself. Furthermore, the value of the objective for the combination therapy is lower than the one obtained for chemotherapy. Possibly, due to the administration of TILs and IL-2, the strengthened immune system is now capable of killing a higher number of tumor cells, inclusively the ones that have become resistant to chemotherapy. In other words, immunotherapy may subvert the chemotherapy-induced immunosuppression. These results match the clinical benefits of the combination therapy discussed in 2.3.3.

With regards to $T_0 = 4.0 \times 10^7$, neither immunotherapy nor chemotherapy are able to eradicate the tumor by itself. Nonetheless, combination therapy is capable of doing so (see figure 6.18 bottom). In this case, chemotherapy and IL-2 are administered between day 0.0 and day 10.0, and day 0.0 and day 7.0, respectively. Once again, there is not a simultaneous administration of IL-2 and TILs. The sensitive and the resistant chemotherapeutic cells are eradicated at day 12.0 and day 14.5, respectively. As expected, a higher period of therapy administration is obtained for $T_0 = 4.0 \times 10^7$ comparatively with

Table 6.5: Results of the minimization of the linear performance index J_4 for $T_0 = 3.2 \times 10^6$, for both chemo- and combination therapy, when a compromised IS is considered.

Cancer therapy	**Chemo. Administration period** (*day*)	**S cells erad.** (*day*)	**R cells erad.** (*day*)	**Cost function**	**Tumor erad.**
Chemotherapy	$0.0 - 4.0$	18.0	$17.5.0$	1.38×10^7	✔
Combination	$0.0 - 8.5$	11.0	13.0	1.04×10^7	✔

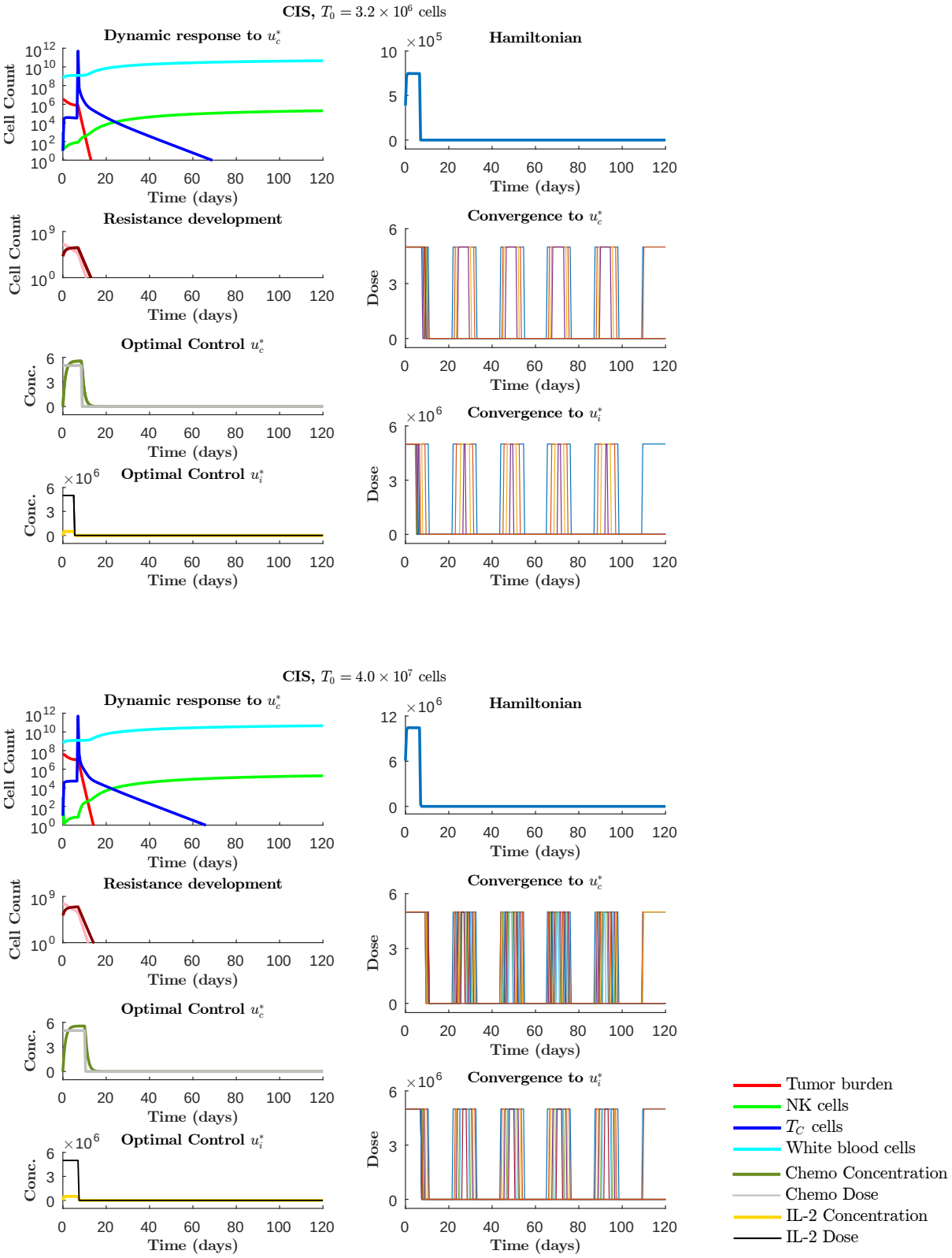

Figure 6.18: Left side: Dynamic response of model (4.5), resistance onset when the optimal control for chemotherapy and IL-2 are administered for $T_0 = 3.2 \times 10^6$ and $T_0 = 4.0 \times 10^7$. Right side: the Hamiltonian and evolution of the controls towards optimality. Simulation parameters: A compromised IS was considered together (see (4.13)) with the linear J_4. $N_{int} = 240$, $N_s = 10$, $T = 120$, $\varepsilon_1 = \varepsilon_2 = 10^{-10}$, $\varepsilon_4 = 10$, $w_1 = 0.8$ for both u_c and u_i. For u_c and $T_0 = 3.2 \times 10^6$, $\varepsilon_3 = 4$ and $w_2 = 4$. For u_c and $T_0 = 4.0 \times 10^7$, $\varepsilon_3 = 0.5$ and $w_2 = 1.5$. For u_i and $T_0 = 3.2 \times 10^6$, $\varepsilon_3 = 1$ and $w_2 = 2$. For u_i and $T_0 = 4.0 \times 10^7$, $\varepsilon_3 = 1$ and $w_2 = 0.9$. Model (4.5).

$T_0 = 3.2 \times 10^6$. Moreover, tumor cells are first eradicated in the case of $T_0 = 3.2 \times 10^6$ relatively to $T_0 = 4.0 \times 10^7$. Forthwith, the value of the objective ($J(u^*) = 1.31 \times 10^8$) is higher for $T_0 = 4.0 \times 10^7$ than it is $T_0 = 3.2 \times 10^6$ ($J(u^*) = 1.04 \times 10^7$). Over again, both chemo- and immunotherapy are only administered until the patient immune system has the full capacity to eradicate the remaining tumor burden.

The Hamiltonian functions are not constant in the subintervals corresponding to the first 10 days. The higher the tumor burden, by the same token, the higher the cost function, the more prominent is the bad behavior of the Hamiltonian, specially for chemotherapy. The reason behind these behaviors were already mention in the previous sections.

At last, figure 6.18 *Convergence to* u_i^* and 6.18 *Convergence to* u_c^*, top and bottom, are a reflex of the control parameters considered for each case. See the caption of figure 6.18 for more informations. In all these images, it is evident that the control is converging towards optimality.

6.3.2 Algorithm D: L2 norm

Figure 6.19 presents the optimal controls u_c^* and u_i^*, the system dynamics response to them, as well as the Hamiltonian functions and the evolution of the controls towards optimality, for $T_0 = 3.2 \times 10^6$ and $T_0 = 4.0 \times 10^7$, considering a compromised immune system. A higher tumor burden is not simulated due to the *ode45* time-consuming integrations.

As observed in 6.1.4, chemotherapy by itself eradicates a tumor burden of $T_0 = 3.2 \times 10^6$. However, the same cannot be said regarding immunotherapy. Accordingly, the combination of these two therapies is also expected to eradicate this tumor burden, but in a more effective way. As anticipated, combination therapy does eliminate an initial tumor burden of $T_0 = 3.2 \times 10^6$ (see figure 6.19 top). Chemotherapy is administered from day 0.0 until day 12.0. However, an insignificant interruption on the chemotherapy administration seems to occur between day 10.5 and day 11.5. Meanwhile, IL-2 is given between day 7.0 and day 12.0. The TILs and IL-2 administration coincides in time. A residual administration of IL-2 exists almost during the 120 day. Sensitive and resistant chemotherapeutic cells are eradicated at day 11.5 and day 13.0, respectively.

In table 6.6, the results obtained for both chemo- and combination therapy, regarding the minimization of the quadratic objective J_4 for $T_0 = 3.2 \times 10^6$, are summarized. As seen in 6.3.1, the chemotherapy administration period is higher for the combination therapy (12.0 day counting with that insignificant interruption) comparatively with chemotherapy alone (9.5 day). Despite the probable higher chemotherapy resistance onset, both sensitive and resistant tumor cells are eliminated earlier in the combination therapy than they are in chemotherapy by itself. In addition, the objective function is lower for combination therapy comparatively to chemotherapy alone. As previously mentioned, immunotherapy strengths the immune system that may be capable of eliminating a higher number of tumor cells, even the ones that have become resistant to chemotherapy. As before, these results are in accordance with the clinical benefits of the combination therapy presented in 2.3.3.

While immunotherapy and chemotherapy alone cannot eradicate a tumor burden of $T_0 = 4.0 \times 10^7$ cells, combination therapy is capable of doing so (see figure 6.19 bottom). Chemotherapy and IL-2

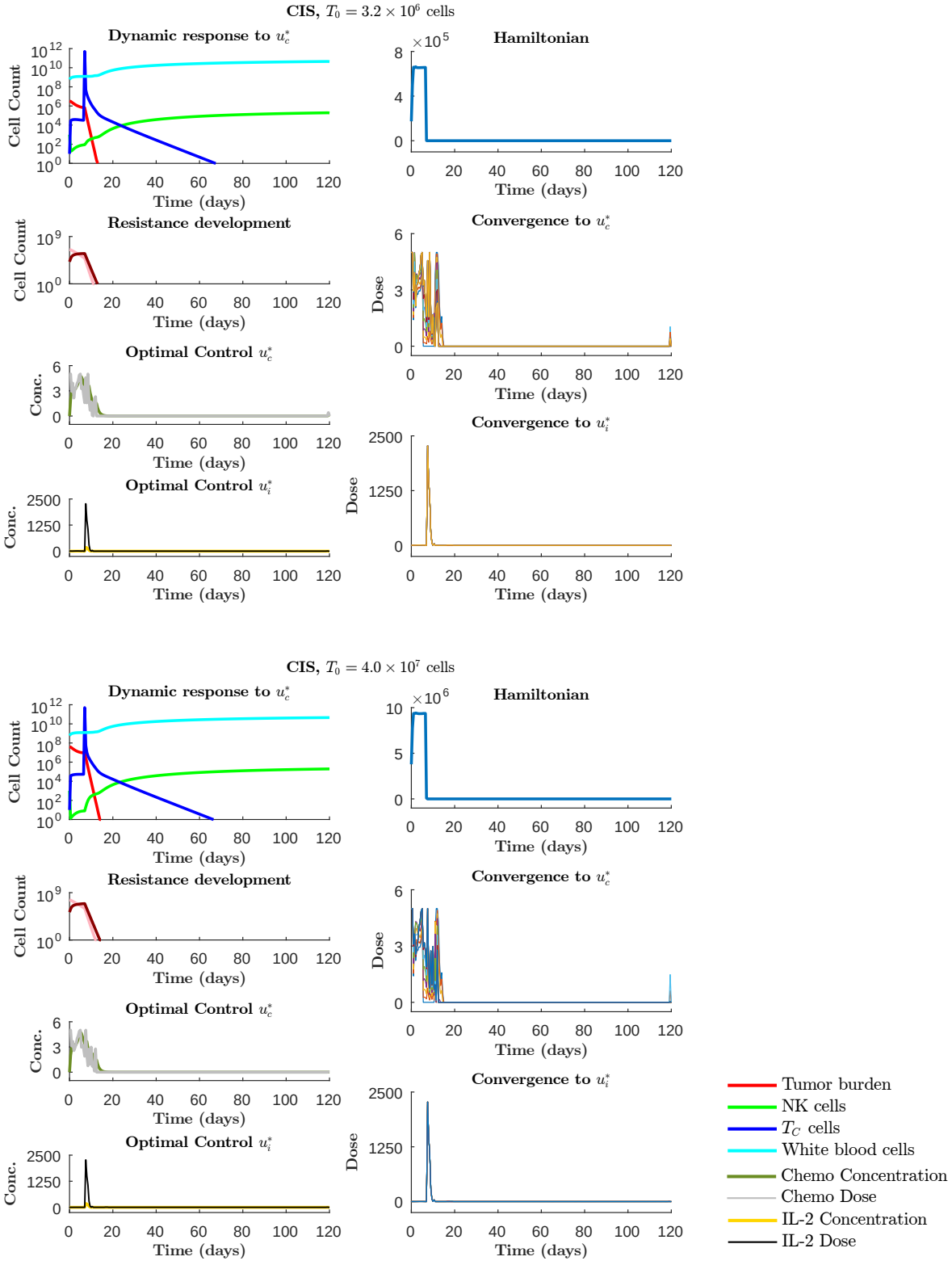

Figure 6.19: Left side: Dynamic response of the model (4.5), resistance onset when the optimal control for chemotherapy and IL-2 are administered for $T_0 = 3.2 \times 10^6$ and $T_0 = 4.0 \times 10^7$. Right side: the Hamiltonian and the evolution of the controls towards optimality. Simulation parameters: $N_{int} = 240$, $T = 120$, $w_1 = 1.2$, $w_2 = 0.99$, $w_3 = 0.41$, $w_4 = 0.94$, $w_5 = 0.61$, except for immunotherapy where $w_5 = 0.35\, \varepsilon_1 = \varepsilon_2 = 10^{-10}$. For u_i and $T_0 = 4.0 \times 10^7$, $w_4 = 0.83$. Compromised IS (see (4.13)) with the quadratic J_4. Model (4.5).

Table 6.6: Results of the minimization of the quadratic performance index J_4 for $T_0 = 3.2 \times 10^6$, for both chemo- and combination therapy, when a compromised IS is considered.

Cancer therapy	**Chemo. Administration period** (*day*)	**S cells erad.** (*day*)	**R cells erad.** (*day*)	**Cost function**	**Tumor erad.**
Chemotherapy	$0.0 - 5.0, 11.0 - 14.5$	16.0	17.5	1.27×10^7	✔
Combination	$0.0 - 12.0$	11.5	13.0	1.02×10^7	✔

are administered between day 0.0 and day 12.0, and day 7.5 and day 10.5, respectively. Sensitive and resistant chemotherapeutic cells are eradicated at day 12.5 and day 14.5, respectively. Accordingly, a higher therapy administration period is obtained for $T_0 = 4.0 \times 10^7$ relatively to $T_0 = 3.2 \times 10^6$. In addition, tumor cells are first eradicated for $T_0 = 3.2 \times 10^6$ than for $T_0 = 4.0 \times 10^7$. Consequently, the value of the performance index ($J(u^*) = 1.29 \times 10^8$) is higher than the one obtained for $T_0 = 3.2 \times 10^6$ ($J(u^*) = 1.02 \times 10^7$).

The Hamiltonian functions are not constant in the beginning of the time axis. Once again, the higher the initial tumor burden, and therefore the higher the cost functions, the more pronounced is the bad behavior of the Hamiltonian functions.

Finally, figures 6.19 *Convergence to* u_i^* and 6.19 *Convergence to* u_c^*, top and bottom, reflect the control parameters considered for each T_0. For more information, please see the caption of figure 6.19. The initial guesses considered for the chemotherapy and IL-2 controls, for both tumor burdens, are the optimal solutions obtained in 6.1.4 for $T_0 = 3.2 \times 10^6$, and in 6.2.2 for $T_0 = 7.5 \times 10^5$, respectively. According with these results, the initial guess considered for the IL-2 is almost the optimal control.

6.3.3 Comparison of the L1- and L2-norm performance indexes

Considering the results obtained for the two initial tumor burdens with the linear and quadratic performance indexes J_4 (see table 6.7), as seen before in 6.1.5, the chemotherapy administration period is higher for the L2-norm cost function than for the linear one. Interestingly, the opposite occurs for the immunotherapy administration period. As explained in 6.2.3, these higher IL-2 administration periods, obtained for the L1-norm objective, may result from the way in which algorithm B is implemented (see 5.3.2). In fact, the initial time t_0 was not considered to be a switching time (it is fixed), and the initial guesses for the controls are considered to begin in their maximum admissible value.

Table 6.7: Combination therapy optimal results of the minimization of the linear and quadratic performance indexes J_4 for two initial tumor burdens when a compromised IS is considered.

J Norm	T_0	**Chemo. admin. period** (*day*)	**Immuno. admin. period** (*day*)	**S cells erad.** (*day*)	**R cells erad.** (*day*)	**Cost function**	**Tumor erad.**
L1	3.2×10^6	$0.0 - 8.5$	$0.0 - 5.0$	11.0	13.0	1.04×10^7	✔
	4.0×10^7	$0.0 - 10.0$	$0.0 - 7.0$	12.0	14.5	1.31×10^8	✔
L2	3.2×10^6	$0.0 - 12.0$	$7.0 - 10.5$	11.5	13.0	1.02×10^7	✔
	4.0×10^7	$0.0 - 12.0$	$7.5 - 10.5$	12.5	14.5	1.29×10^8	✔

Despite having the same order of magnitude, the performance indexes are higher for the L1-norm rel-

atively to the L2-norm objectives, which favor lower drug concentrations. Even though higher chemotherapy doses are administered in the case of the L1-norm and the treatments are ceased earlier comparatively with the L2-norm objective, both sensitive and resistant tumor cells are first eradicated for the L2-objective. However, for $T_0 = 4.0 \times 10^7$, the resistant tumor cells are eliminated in the same day, regardless the objective norm considered. Provided that a lower discretization time was used, resistant tumor cells would have been eradicated in different time subintervals. Interestingly, sensitive tumor cells are first eradicated than the resistant ones, even in the case of the L1-norm. In fact, when the L1-objective was considered for the chemotherapy alone, resistant tumor cells are first eradicated than the sensitive ones (see table 6.2).

Chapter 7

Conclusions

In this final chapter, the most important conclusions regarding the work performed are summarized. Subsequently, the achievements and limitations of the master thesis are clarified and discussed. Finally, some advices and suggestions are made regarding future work.

The simulations for the chemotherapy, immunotherapy and combination therapy models, made in 4.2, not only confirm that the immune system has a key role in the efficacy of chemotherapy, but also show that the same is true for the case of immunotherapy and combination therapy. Indeed, a compromised immune system only eradicates a fraction of the cells eliminated by a healthy one, regardless of the therapy considered.

Moreover, chemotherapy was shown to be more effective than immunotherapy as an anticancer treatment. These results are in agreement with the literature. In fact, the beneficial effects of immunotherapy are more evident for both compromised immune systems and small tumors. However, the combination of both therapies enables the eradication of tumor burdens that are not possible to eliminate by none of these therapies *per se*. Immunotherapy seems to subvert the chemotherapy-induced immunosuppression, as proposed in the literature.

Rather than administering chemotherapy, immunotherapy or the combination of both as longer as tumor cells exist, these therapies only need to be applied until the patient immune system is capable of eradicating the remaining tumor cells. In other words, chemotherapy, immunotherapy and combination therapy do not aim at fully eradicate the tumor burden, but instead intend to restore the equilibrium of the immunosurveillance mechanism. These results highlight the importance of modeling anticancer therapies together with the immunosurveillance mechanism. Otherwise, the optimal treatment schedules would result in higher drug doses being administered and therefore, higher therapeutic toxicity. Furthermore, disregarding the onset of chemotherapy resistance would lead to the design of inaccurate drug schedules that in the long run could result in a worst prognosis for the patient, due to the highly genomically unstable resistant tumor cells created.

Regarding the optimal control problems formulated in this master thesis, only the indirect gradient-based algorithms B and D were able to converge to the optimal solution. In addition, the minimization of L1-or L2-type objectives leads to optimal solutions with distinct mathematical characteristics. Besides

favouring the administration of lower drug doses relatively to L1- cost functions, L2-objectives also privilege higher therapeutic administration periods. Accordingly, all these solutions must not be used as a mathematical replacement or approximation of the other [144]. Moreover, even when the same objective dependence on the control is considered, distinct set of weights give rise to different optimal solutions. It is up to medical practitioners to decide which solutions best fit the specific patient biological situation and whether any of the results can be used for practical implementation [144].

Whenever optimal therapies schedules were designed, there were always time subintervals in which the Hamiltonian functions were not constant over time, which is a sign of non-optimality. This unexpected behavior may result from numerical errors, a high discretization time considered in the numerical algorithms and poor selection of the control parameters. Furthermore, the optimal control may not be a solution of the dynamics or it does not comply with the constraints imposed during the formulation of the optimal control problem.

These behaviors may come from numerical errors, a high discretization time $(0.5$ day) considered in algorithm B and D step **1.**, or even a poor selection of the control parameters. Moreover, the optimal solution that would give rise to a constant Hamiltonian may not be a solution of the dynamics or it does not comply with the constraints imposed. Furthermore, a high time discretization and a poor selection of the control parameters may result in a solution distinct of the optimal one.

In the final analysis, the development of predictive pre-clinical models of human cancer may not only reduce the expense of drug development, but also provide "personalized molecular medicine" at affordable cost in a near future [1]. Only these type of approaches will enable the administration of therapies in an optimal way, balancing the therapeutic benefits of treatment with its side effects.

7.1 Achievements and limitations

For the first time in the literature, an ODE model combining chemotherapy, chemotherapy resistance, immunotherapy and a realistic immune response is proposed. Although this model was born as a combination of the de Pillis et al. [10] and Hahnfeldt et al. [14] models, some novelties are introduced. Unlike anything seen so far, the onset of chemotherapeutic resistance is modeled as being proportional to the chemotherapy blood concentration. Moreover, a modified version of the Norton-Simon hypothesis is proposed in 4.2.3.

With regards to optimal control, the linear Duda [11] algorithm is modified and improved, giving rise to Algorithm B (see 5.3.2). Concerning the L2 objective function, a backpropagation algorithm for neural networks (Silva and Almeida [12, 13]) is adapted and modified, resulting in algorithm D (see 5.3.4). In both algorithms, the stopping criteria are evaluated after the computation of the new performance index, in order to avoid unnecessary steps. In addition, the step size in algorithm B and the initial step size in algorithm D, are considered as a function of $\frac{\partial H}{\partial u}$ for each time subinterval.

Despite the aforementioned achievements, there are several limitations that deserve to be addressed.

With respect to the model (4.5), to begin with, it was impossible to use the modified Norton-Simon hypothesis proposed in 4.2.3 due to the additional computational cost that this assumption would bring to

the model. As a consequence, chemotherapy is assumed to kill a fraction of tumor cells and not only the ones actively dividing. Secondly, the cell equations on the model are "forced" (by means of *if* conditions) to be positive and whenever the cell number becomes less than one, it is considered to be zero. In the same fashion, drug bloodstream concentrations are also "forced' to be positive. If these considerations had not been taken into account, complex numbers and NaNs would be obtained during the integration with *ode45* or would result in unrealistic model behaviors. For instance, tumor cells whose number had fallen beyond one were able to recover and give rise to a considerable tumor burden. These undesirable model behaviors were not introduced by the alterations proposed in this master thesis, but were rather inherited from de Pillis et al. [10] model. Finally, although de Pillis et al. [10] claim having used human parameter values, most of the values in table 4.4 came from murine experiments or were from unknown origin [146]. This limitation has also affected the model developed here. Moreover, since the values of these parameters varies between patients and cancer types and most of the parameters are not human data, the model proposed here is not suitable for generating treatment schedules useful in the clinical practice [146].

Regarding the optimal control, singular control arcs were not considered as optimal candidates. However, in this field singular controls cannot be ruled out [146]. As a matter of fact, they might be the prime candidates to optimality with bang-bang controls only arising where singular control arcs are either inadmissible or inexistent [147]. Furthermore, the algorithms implemented have some drawbacks. In the first place an exhaustive search is required to chose the several optimal control parameters. Second, in the case of algorithm B, the initial time t_0 is not considered to be a switching time. Unexpectedly, the Hamiltonians correspondent to the optimal solutions found present high value discontinuities, rather than being constant over time, a fact due to numerical approximations. Finally, is not possible to optimal therapies for high tumor burden due to the *ode45* time-consuming integrations.

7.2 Future Work

In this section some suggestions are made concerning the direction of the future work. Regarding the model:

- The re-sensitization of resistant tumor cells should also depend on chemotherapy bloodstream concentration. In other words, the smaller the bloodstream concentration of chemotherapy, the more probable resistant cells are of becoming sensitive to this drug. This can be achieved by replacing $P_{RS}R$ in (4.5) with $\left(1 - \frac{C}{C_{max}}\right) P_{RS}R$.
- Besides considering the administration of chemotherapy, IL-2 and TILs in model (4.5), it would be interesting to consider the further administration of chemotherapeutic re-sensitizations drugs, which are now being discussed in the literature. For more information see for instance [148, 149].
- Consider other scenarios of drug resistance. As mentioned before, there are several levels of drug resistance. Therefore, it would be interesting to include more tumor cell populations representative of those distinct levels. Moreover, in some cancers, the phenotypically distinct sub-

populations of cells within the tumor may act symbiotically [1]. Rather than directly competing with one another $\left(\text{term } \frac{S+R}{T_{max}} \text{ in the growth model of tumor populations, model (4.5)}\right)$, they support the growth and survival of one another [1]. With this in mind, a positive term modeling the interactions between tumor populations could be added.

- Model (4.5) should account for the role of inflammation in tumor progression. In fact, inflammatory cells recruited into tissues (e.g. macrophages and neutrophils) are rich sources of reactive species of oxygen and nitrogen, which may fuel mutagenesis [1].This can be done by adding a positive term in tumor cell equations proportional to a portion of the white blood cells W.

- More recently, it has been discussed the possibility that tumor growth may be driven by minority populations of tumorigenic cells, while most of cancer cells have little or no capacity to contribute to disease progression (cancer stem cell model) [150]. Accordingly, durables remissions and cures are only observed for therapeutic strategies that are able to kill those minority populations of tumorigenic cells [1]. Therefore, it would be interesting to adapt model (4.5) to the cancer stem cell model and compare it with the clinical reality.

Finally, regarding the optimal control:

- Singular control arcs must be considered. Indeed, they correspond to time-varying administrations of the drug agent at intermediate and often significantly lower dose rates than typical MTD chemotherapy [147]. Therefore, by considering these solutions, small drug doses would be privileged. As discussed in 2.3.1, the administration of smaller doses of chemotherapy (metronomic chemotherapy) has several advantages.

- The administration of TILs must be explored as a third control.

- Other cost functions could be experimented.

- Algorithm B must be modified so the initial time t_0 can also be considered as a switching time.

Bibliography

[1] W. R. *The Biology of Cancer, Second Edition*. Taylor & Francis Group, 2^{nd} edition, 2013. ISBN:978-1317963462.

[2] W. H. Organization. The top 10 causes of death 2017. http://gco.iarc.fr/today/data/pdf/fact-sheets/cancers/cancer-fact-sheets-29.pdf, 2 2017. Online; accessed 14-08-2017.

[3] J. Ferlay, I. Soerjomataram, R. Dikshit, S. Eser, C. Mathers, M. Rebelo, D. M. Parkin, D. Forman, and F. Bray. Cancer incidence and mortality worldwide: Sources, methods and major patterns in globocan 2012. *International Journal of Cancer*, 136(5):E359–E386, 2015. ISSN 1097-0215. doi:10.1002/ijc.29210.

[4] R. S. Kerbel. A cancer therapy resistant to resistance. *Nature*, 390(6658):335–336, 1997. doi:10.1038/36978.

[5] C. R. Parish. Cancer immunotherapy: the past, the present and the future. *Immunology and cell biology*, 81(2):106, 2003. doi:10.1046/j.0818-9641.2003.01151.x.

[6] G. Liu, K. L. Black, and J. S. Yu. Sensitization of malignant glioma to chemotherapy through dendritic cell vaccination. *Expert Review of Vaccines*, 5(2):233–247, 2006. doi:10.1586/14760584.5.2.233.

[7] M. E. Dudley, J. R. Wunderlich, P. F. Robbins, J. C. Yang, P. Hwu, D. J. Schwartzentruber, S. L. Topalian, R. Sherry, N. P. Restifo, A. M. Hubicki, M. R. Robinson, M. Raffeld, P. Duray, C. A. Seipp, L. Rogers-Freezer, K. E. Morton, S. A. Mavroukakis, D. E. White, and S. A. Rosenberg. Cancer regression and autoimmunity in patients after clonal repopulation with antitumor lymphocytes. *Science*, 298(5594):850–854, 2002. ISSN 0036-8075. doi: 10.1126/science.1076514. doi:10.1126/science.1076514.

[8] F. Michor and K. Beal. Improving cancer treatment via mathematical modeling: Surmounting the challenges is worth the effort. *Cell*, 163(5):1059 – 1063, 2015. ISSN 0092-8674. doi:10.1016/j.cell.2015.11.002.

[9] H. Schättler and U. Ledzewicz. Cancer and tumor development: Biomedical background. In *Optimal Control for Mathematical Models of Cancer Therapies: An Application of Geometric Methods*, chapter 1, pages 1–40. Springer New York, 2015. doi:10.1007/978-1-4939-2972-6_1.

[10] L. G. de Pillis, W. Gu, and A. E. Radunskaya. Mixed immunotherapy and chemotherapy of tumors: modeling, applications and biological interpretations. *Journal of theoretical biology*, 238(4):841–862, 2006. doi:10.1016/j.jtbi.2005.06.037.

[11] Z. Duda. A gradient method for application of chemotherapy protocols. *Journal of Biological Systems*, 3(01):3–11, 1995. doi:10.1142/S0218339095000022.

[12] F. M. Silva and L. B. Almeida. Acceleration techniques for the backpropagation algorithm. In L. B. Almeida and C. J. Wellekens, editors, *Neural Networks: EURASIP Workshop 1990 Sesimbra, Portugal, February 15–17, 1990 Proceedings*, pages 110–119. Springer Berlin Heidelberg, Berlin, Heidelberg, 1990. ISBN 978-3-540-46939-1. doi:10.1007/3-540-52255-7_32.

[13] F. M. Silva and L. B. Almeida. Speeding up backpropagation. In E. Rolf, editor, *Advanced Neural Computers*, pages 151–158. North-Holland, Amsterdam, 2014. ISBN 978-0-444-88400-8. doi:10.1016/B978-0-444-88400-8.50022-4.

[14] P. Hahnfeldt, J. Folkman, and L. Hlatky. Minimizing long-term tumor burden: The logic for metronomic chemotherapeutic dosing and its antiangiogenic basis. *Journal of Theoretical Biology*, 220 (4):545–554, 2003. ISSN 0022-5193. doi:10.1006/jtbi.2003.3162.

[15] H. Shen and P. Laird. Interplay between the cancer genome and epigenome. *Cell*, 153(1):38 – 55, 2013. ISSN 0092-8674. doi:10.1016/j.cell.2013.03.008.

[16] S. J. Elledge. Cell cycle checkpoints: preventing an identity crisis. *Science*, 274(5293):1664–1672, 1996. doi:10.1126/science.274.5293.1664.

[17] D. P. Tabassum and K. Polyak. Tumorigenesis: it takes a village. *Nature Reviews. Cancer*, 15(8): 473, 2015. doi:10.1038/nrc3971.

[18] E. Vivier, E. Tomasello, M. Baratin, T. Walzer, and S. Ugolini. Functions of natural killer cells. *Nature immunology*, 9(5):503, 2008. doi:10.1038/ni1582.

[19] L. Zamai, C. Ponti, P. Mirandola, G. Gobbi, S. Papa, L. Galeotti, L. Cocco, and M. Vitale. Nk cells and cancer. *The Journal of Immunology*, 178(7):4011–4016, 2007. ISSN 0022-1767. doi:10.4049/jimmunol.178.7.4011.

[20] L. Galluzzi, A. Buqué, O. Kepp, L. Zitvogel, and G. Kroemer. Immunological effects of conventional chemotherapy and targeted anticancer agents. *Cancer Cell*, 28(6):690 – 714, 2015. ISSN 1535-6108. doi:10.1016/j.ccell.2015.10.012.

[21] G. A. Rabinovich, D. Gabrilovich, and E. M. Sotomayor. Immunosuppressive strategies that are mediated by tumor cells. *Annual Review of Immunology*, 25(1):267–296, 2007. doi:10.1146/annurev.immunol.25.022106.141609.

[22] V. T. DeVita and E. Chu. A history of cancer chemotherapy. *Cancer Research*, 68(21):8643–8653, 2008. ISSN 0008-5472. doi:10.1158/0008-5472.CAN-07-6611.

[23] B. A. Chabner and T. G. Roberts Jr. Chemotherapy and the war on cancer. *Nature reviews. Cancer*, 5(1):65, 2005. doi:10.1038/nrc1529.

[24] M. S. Nars and R. Kaneno. Immunomodulatory effects of low dose chemotherapy and perspectives of its combination with immunotherapy. *International journal of cancer*, 132(11):2471–2478, 2013. doi:10.1002/ijc.27801.

[25] C. L. Mackall, T. A. Fleisher, M. R. Brown, M. P. Andrich, C. C. Chen, I. M. Feuerstein, I. T. Magrath, L. H. Wexler, D. S. Dimitrov, and R. E. Gress. Distinctions between cd8+ and cd4+ t-cell regenerative pathways result in prolonged t-cell subset imbalance after intensive chemotherapy. *Blood*, 89(10):3700–3707, 1997. ISSN:0006-4971.

[26] E. Azuma, M. Nagai, J. Qi, M. Umemoto, M. Hirayama, T. Kumamoto, S. Hiratake, Y. Komada, and M. Sakurai. Cd4+ t-lymphocytopenia in long-term survivors following intensive chemotherapy in childhood cancers. *Pediatric Blood & Cancer*, 30(1):40–45, 1998. doi:10.1002/(SICI)1096-911X(199801)30:1¡40::AID-MPO11¿3.0.CO;2-C.

[27] S. Alanko, T. T. Salmi, and T.-T. Pelliniemi. Recovery of natural killer cells after chemotherapy for childhood acute lymphoblastic leukemia and solid tumors. *Pediatric Blood & Cancer*, 24(6): 373–378, 1995. doi:10.1002/mpo.2950240607.

[28] H. Nakashima, A. Tasaki, M. Kubo, H. Kuroki, K. Matsumoto, M. Tanaka, M. Nakamura, T. Morisaki, and M. Katano. Effects of docetaxel on antigen presentation-related functions of human monocyte-derived dendritic cells. *Cancer Chemotherapy and Pharmacology*, 55(5):479–487, May 2005. ISSN 1432-0843. doi:10.1007/s00280-004-0918-7.

[29] S. Ferrari, B. Rovati, C. Porta, P. E. Alessandrino, A. Bertolini, E. Collovà, A. Riccardi, and M. Danova. Lack of dendritic cell mobilization into the peripheral blood of cancer patients following standard- or high-dose chemotherapy plus granulocyte-colony stimulating factor. *Cancer Immunology, Immunotherapy*, 52(6):359–366, Jun 2003. ISSN 1432-0851. doi:10.1007/s00262-002-0365-4.

[30] N. Andre, M. Carre, and E. Pasquier. Metronomics: towards personalized chemotherapy? *Nature reviews Clinical oncology*, 11(7):413–431, 2014. doi:10.1007/s00262-002-0365-4.

[31] B. Bonavida. *Molecular Mechanisms of Tumor Cell Resistance to Chemotherapy: Targeted Therapies to Reverse Resistance*. Resistance to Targeted Anti-Cancer Therapeutics. Springer New York, 2013. ISBN:9781461470700.

[32] G. L. Klement and B. A. Kamen. Nontoxic, fiscally responsible, future of oncology: could it be beginning in the third world? *Journal of pediatric hematology/oncology*, 33(1):1–3, 2011. doi:910.1097/MPH.0b013e3182024918.

[33] R. Kaneno, G. V. Shurin, I. L. Tourkova, and M. R. Shurin. Chemomodulation of human dendritic cell function by antineoplastic agents in low noncytotoxic concentrations. *Journal of Translational Medicine*, 7(1):58, 2009. doi:10.1186/1479-5876-7-58.

[34] F. Ghiringhelli, C. Menard, P. E. Puig, S. Ladoire, S. Roux, F. Martin, E. Solary, A. Le Cesne, L. Zitvogel, and B. Chauffert. Metronomic cyclophosphamide regimen selectively depletes cd4+ cd25+ regulatory t cells and restores t and nk effector functions in end stage cancer patients. *Cancer immunology, immunotherapy*, 56(5):641–648, 2007. doi:10.1007/s00262-006-0225-8.

[35] C. Banissi, F. Ghiringhelli, L. Chen, and A. F. Carpentier. Treg depletion with a low-dose metronomic temozolomide regimen in a rat glioma model. *Cancer Immunology, Immunotherapy*, 58(10): 1627–1634, Oct 2009. ISSN 1432-0851. doi:10.1007/s00262-009-0671-1.

[36] J. Zhao, Y. Cao, Z. Lei, Z. Yang, B. Zhang, and B. Huang. Selective depletion of cd4+cd25+foxp3+ regulatory t cells by low-dose cyclophosphamide is explained by reduced intracellular atp levels. *Cancer Research*, 70(12):4850–4858, 2010. ISSN 0008-5472. doi:10.1158/0008-5472.CAN-10-0283.

[37] S. Kan, S. Hazama, K. Maeda, Y. Inoue, S. Homma, S. Koido, M. Okamoto, and M. Oka. Suppressive effects of cyclophosphamide and gemcitabine on regulatory t-cell induction in vitro. *Anticancer research*, 32(12):5363–5369, 2012. PMID:23225438.

[38] S. R. Sierro, A. Donda, R. Perret, P. Guillaume, H. Yagita, F. Levy, and P. Romero. Combination of lentivector immunization and low-dose chemotherapy or pd-1/pd-l1 blocking primes self-reactive t cells and induces anti-tumor immunity. *European journal of immunology*, 41(8):2217–2228, 2011. doi:10.1002/eji.201041235.

[39] S. M. Geary, C. D. Lemke, D. M. Lubaroff, and A. K. Salem. The combination of a low-dose chemotherapeutic agent, 5-fluorouracil, and an adenoviral tumor vaccine has a synergistic benefit on survival in a tumor model system. *PloS one*, 8(6):e67904, 2013. doi:10.1371/journal.pone.0067904.

[40] M. Todaro, S. Meraviglia, N. Caccamo, G. Stassi, and F. Dieli. Combining conventional chemotherapy and $\gamma\delta$ t cell-based immunotherapy to target cancer-initiating cells. *OncoImmunology*, 2(9): e25821, 2013. doi:10.4161/onci.25821.

[41] R. A. Gatenby. A change of strategy in the war on cancer. *Nature*, 459(7246):508–509, 2009. doi:10.1038/459508a.

[42] N. André, S. Banavali, Y. Snihur, and E. Pasquier. Has the time come for metronomics in low-income and middle-income countries? *The Lancet Oncology*, 14(6):e239 – e248, 2013. ISSN 1470-2045. doi:10.1016/S1470-2045(13)70056-1.

[43] U. Emmenegger, G. Francia, A. Chow, Y. Shaked, A. Kouri, S. Man, and R. S. Kerbel. Tumors that acquire resistance to low-dose metronomic cyclophosphamide retain sensitivity to maximum tolerated dose cyclophosphamide. *Neoplasia*, 13(1):40 – 48, 2011. ISSN 1476-5586. doi:10.1593/neo.101174.

[44] N. C. Institute. Biological therapies for cancer. http://gco.iarc.fr/today/data/pdf/fact-sheets/cancers/cancer-fact-sheets-29.pdf, 12 2013. URL https://www.cancer.gov/about-cancer/treatment/types/immunotherapy/bio-therapies-fact-sheet. Online; accessed 11-11-2017.

[45] W. Blahd. Immunotherapy: What are the types? http://www.webmd.com/cancer/immunotherapy-treatment-types#2, 2017. Online; accessed 12-09-2017.

[46] https://www.cancer.gov/about-cancer/treatment/types/immunotherapy#1, 2017. Online; accessed 12-09-2017.

[47] S. A. Rosenberg, N. P. Restifo, J. C. Yang, R. A. Morgan, and M. E. Dudley. Adoptive cell transfer: a clinical path to effective cancer immunotherapy. *Nature reviews. Cancer*, 8(4):299, 2008. doi:10.1038/nrc2355.

[48] D. A. Morgan, F. W. Ruscetti, R. Gallo, et al. Selective in vitro growth of t lymphocytes from normal human bone marrows. *Science*, 193(4257):1007–1008, 1976. doi:10.1126/science.181845.

[49] S. A. Rosenberg. Il-2: The first effective immunotherapy for human cancer. *The Journal of Immunology*, 192(12):5451–5458, 2014. ISSN 0022-1767. doi:10.4049/jimmunol.1490019.

[50] M. Lenardo, F. K.-M. Chan, F. Hornung, H. McFarland, R. Siegel, J. Wang, and L. Zheng. Mature t lymphocyte apoptosis—immune regulation in a dynamic and unpredictable antigenic environment. *Annual Review of Immunology*, 17(1):221–253, 1999. doi:10.1146/annurev.immunol.17.1.221.

[51] J. C. Rathmell, M. G. Heiden, M. H. Harris, K. A. Frauwirth, and C. B. Thompson. In the absence of extrinsic signals, nutrient utilization by lymphocytes is insufficient to maintain either cell size or viability. *Molecular Cell*, 6(3):683 – 692, 2000. ISSN 1097-2765. doi:10.1016/S1097-2765(00)00066-6.

[52] S. A. Rosenberg, M. T. Lotze, L. M. Muul, S. Leitman, A. E. Chang, S. E. Ettinghausen, Y. L. Matory, J. M. Skibber, E. Shiloni, J. T. Vetto, C. A. Seipp, C. Simpson, and C. M. Reichert. Observations on the systemic administration of autologous lymphokine-activated killer cells and recombinant interleukin-2 to patients with metastatic cancer. *New England Journal of Medicine*, 313 (23):1485–1492, 1985. doi:10.1056/NEJM198512053132327.

[53] S. A. Rosenberg, J. C. Yang, D. E. White, and S. M. Steinberg. Durability of complete responses in patients with metastatic cancer treated with high-dose interleukin-2: identification of the antigens mediating response. *Annals of surgery*, 228(3):307, 1998. doi:10.1016/S0022-5347(05)68669-7.

[54] L. MT, C. AE, S. CA, S. C, V. JT, and R. SA. High-dose recombinant interleukin 2 in the treatment of patients with disseminated cancer: Responses, treatment-related morbidity, and histologic findings. *JAMA*, 256(22):3117–3124, 1986. doi:10.1001/jama.1986.03380220083027.

[55] S. L. Gaffen and K. D. Liu. Overview of interleukin-2 function, production and clinical applications. *Cytokine*, 28(3):109 – 123, 2004. ISSN 1043-4666. doi:10.1016/j.cyto.2004.06.010.

[56] U. S. Kammula, D. E. White, and S. A. Rosenberg. Trends in the safety of high dose bolus interleukin-2 administration in patients with metastatic cancer. *Cancer*, 83(4):797–805, 1998. doi:10.1002/(SICI)1097-0142(19980815)83:4¡797::AID-CNCR25¿3.0.CO;2-M.

[57] G. Liu, K. L. Black, and J. S. Yu. Sensitization of malignant glioma to chemotherapy through dendritic cell vaccination. *Expert Review of Vaccines*, 5(2):233–247, 2006. doi:10.1586/14760584.5.2.233.

[58] L. Galluzzi, A. Buqué, O. Kepp, L. Zitvogel, and G. Kroemer. Immunological effects of conventional chemotherapy and targeted anticancer agents. *Cancer Cell*, 28(6):690 – 714, 2015. ISSN 1535-6108. doi:10.1016/j.ccell.2015.10.012.

[59] R. A. Lake and B. W. Robinson. Opinion: Immunotherapy and chemotherapy–a practical partnership. *Nature reviews. Cancer*, 5(5):397, 2005. doi:10.1038/nrc1613.

[60] R. Ramakrishnan, S. Antonia, and D. I. Gabrilovich. Combined modality immunotherapy and chemotherapy: a new perspective. *Cancer Immunology, Immunotherapy*, 57(10):1523–1529, 2008. doi:10.1007/s00262-008-0531-4.

[61] A. K. Nowak, R. A. Lake, A. L. Marzo, B. Scott, W. R. Heath, E. J. Collins, J. A. Frelinger, and B. W. S. Robinson. Induction of tumor cell apoptosis in vivo increases tumor antigen cross-presentation, cross-priming rather than cross-tolerizing host tumor-specific cd8 t cells. *The Journal of Immunology*, 170(10):4905–4913, 2003. ISSN 0022-1767. doi:10.4049/jimmunol.170.10.4905.

[62] R. J. North and D. P. Kirstein. T-cell-mediated concomitant immunity to syngeneic tumors. i. activated macrophages as the expressors of nonspecific immunity to unrelated tumors and bacterial parasites. *Journal of Experimental Medicine*, 145(2):275–292, 1977. ISSN 0022-1007. doi:10.1084/jem.145.2.275.

[63] A. K. Nowak, B. W. S. Robinson, and R. A. Lake. Synergy between chemotherapy and immunotherapy in the treatment of established murine solid tumors. *Cancer Research*, 63(15): 4490–4496, 2003. ISSN 0008-5472. PMID:12907622.

[64] L. Polak and J. Turk. Reversal of immunological tolerance by cyclophosphamide through inhibition of suppressor cell activity. *Nature*, 249(5458):654–656, 1974. doi:10.1038/249654a0.

[65] F. Ghiringhelli, N. Larmonier, E. Schmitt, A. Parcellier, D. Cathelin, C. Garrido, B. Chauffert, E. Solary, B. Bonnotte, and F. Martin. Cd4+ cd25+ regulatory t cells suppress tumor immunity but are sensitive to cyclophosphamide which allows immunotherapy of established tumors to be curative. *European journal of immunology*, 34(2):336–344, 2004. doi:10.1002/eji.200324181.

[66] S. M. Kaech, J. T. Tan, E. J. Wherry, B. T. Konieczny, C. D. Surh, and R. Ahmed. Selective expression of the interleukin 7 receptor identifies effector cd8 t cells that give rise to long-lived memory cells. *Nature immunology*, 4(12):1191, 2003. doi:10.1038/ni1009.

[67] E. S. Bergmann-Leitner and S. I. Abrams. Treatment of human colon carcinoma cell lines with anti-neoplastic agents enhances their lytic sensitivity to antigen-specific cd8+ cytotoxic t lymphocytes. *Cancer Immunology, Immunotherapy*, 50(9):445–455, Nov 2001. ISSN 1432-0851. doi:10.1007/s002620100229.

[68] S. Yang and F. G. Haluska. Treatment of melanoma with 5-fluorouracil or dacarbazine in vitro sensitizes cells to antigen-specific ctl lysis through perforin/granzyme- and fas-mediated pathways. *The Journal of Immunology*, 172(7):4599–4608, 2004. ISSN 0022-1767. doi:10.4049/jimmunol.172.7.4599.

[69] L. Liu, P. A. Mayes, S. Eastman, H. Shi, S. Yadavilli, T. Zhang, J. Yang, L. Seestaller-Wehr, S.-Y. Zhang, C. Hopson, L. Tsvetkov, J. Jing, S. Zhang, J. Smothers, and A. Hoos. The braf and mek inhibitors dabrafenib and trametinib: Effects on immune function and in combination with immunomodulatory antibodies targeting pd-1, pd-l1, and ctla-4. *Clinical Cancer Research*, 21(7): 1639–1651, 2015. ISSN 1078-0432. doi:10.1158/1078-0432.CCR-14-2339.

[70] S. Park, Z. Jiang, E. D. Mortenson, L. Deng, O. Radkevich-Brown, X. Yang, H. Sattar, Y. Wang, N. K. Brown, M. Greene, Y. Liu, J. Tang, S. Wang, and Y.-X. Fu. The therapeutic effect of anti-her2/neu antibody depends on both innate and adaptive immunity. *Cancer Cell*, 18(2):160 – 170, 2010. ISSN 1535-6108. doi:10.1016/j.ccr.2010.06.014.

[71] R. Eftimie, J. L. Bramson, and D. J. Earn. Interactions between the immune system and cancer: A brief review of non-spatial mathematical models. *Bulletin of Mathematical Biology*, 73(1):2–32, Jan 2011. ISSN 1522-9602. doi:10.1007/s11538-010-9526-3.

[72] R. Martin and K. L. Teo. Basic concepts. In *Optimal Control of Drug Administration in Cancer Chemotherapy*, chapter 1, pages 2–4. WORLD SCIENTIFIC, 1993. doi:10.1142/9789812832542_0001.

[73] D. Barbolosi, J. Ciccolini, B. Lacarelle, F. Barlési, and N. André. Computational oncology [mdash] mathematical modelling of drug regimens for precision medicine. *Nature Reviews Clinical Oncology*, 13(4):242–254, 2016. doi:10.1038/nrclinonc.2015.204.

[74] J. T. Oden, E. E. Prudencio, and A. Hawkins-Daarud. Selection and assessment of phenomenological models of tumor growth. *Mathematical Models and Methods in Applied Sciences*, 23(07): 1309–1338, 2013. doi:10.1142/S0218202513500103.

[75] H. Murphy, H. Jaafari, and H. M. Dobrovolny. Differences in predictions of ode models of tumor growth: a cautionary example. *BMC Cancer*, 16(1):163, 2016. ISSN 1471-2407. doi:10.1186/s12885-016-2164-x.

[76] J. Folkman and M. Hochberg. Self-regulation of growth in three dimensions. *Journal of Experimental Medicine*, 138(4):745–753, 1973. ISSN 0022-1007. doi:10.1084/jem.138.4.745.

[77] S. Benzekry, C. Lamont, A. Beheshti, A. Tracz, J. M. L. Ebos, L. Hlatky, and P. Hahnfeldt. Classical mathematical models for description and prediction of experimental tumor growth. *PLoS Comput Biol*, 10(8):1–19, 08 2014. doi:10.1371/journal.pcbi.1003800.

[78] P. Gerlee. The model muddle: In search of tumor growth laws. *Cancer Research*, 73(8):2407–2411, 2013. ISSN 0008-5472. doi:10.1158/0008-5472.CAN-12-4355.

[79] N. Hartung, S. Mollard, D. Barbolosi, A. Benabdallah, G. Chapuisat, G. Henry, S. Giacometti, A. Iliadis, J. Ciccolini, C. Faivre, and F. Hubert. Mathematical modeling of tumor growth and metastatic spreading: Validation in tumor-bearing mice. *Cancer Research*, 74(22):6397–6407, 2014. ISSN 0008-5472. doi:10.1158/0008-5472.CAN-14-0721.

[80] V. G. Vaidya and F. J. Alexandro. Evaluation of some mathematical models for tumor growth. *International journal of bio-medical computing*, 13(1):19–35, 1982. ISSN 0020-7101. doi:10.1016/0020-7101(82)90048-4.

[81] L. Simpson-Herren and H. H. Lloyd. Kinetic parameters and growth curves for experimental tumor systems. *Cancer chemotherapy reports*, 54(3):143, 1970. PMID:5527016.

[82] L. A. Dethlefsen, J. M. S. Prewitt, and M. L. Mendelsohn. Analysis of tumor growth curves2. *JNCI: Journal of the National Cancer Institute*, 40(2):389–405, 1968. doi:10.1093/jnci/40.2.389.

[83] A. K. Laird. Dynamics of tumour growth. *British journal of cancer*, 18(3):490, 1964. doi:10.1038/bjc.1964.55.

[84] A. K. Laird. Dynamics of tumour growth: comparison of growth rates and extrapolation of growth curve to one cell. *British Journal of Cancer*, 19(2):278, 1965. doi:10.1038/bjc.1965.32.

[85] R. Sachs, L. Hlatky, and P. Hahnfeldt. Simple ode models of tumor growth and anti-angiogenic or radiation treatment. *Mathematical and Computer Modelling*, 33(12):1297–1305, 2001. ISSN 0895-7177. doi:10.1016/S0895-7177(00)00316-2.

[86] R. Bocu, S. Tabirca, and Y. J. Chen. Fister-panetta upper bound for cancer growth. some computational remarks. In *2008 International Conference on Biocomputation, Bioinformatics, and Biomedical Technologies*, pages 17–22. IEEE, June 2008. doi:10.1109/BIOTECHNO.2008.7.

[87] S. Benzekry, E. Pasquier, D. Barbolosi, B. Lacarelle, F. Barlési, N. André, and J. Ciccolini. Metronomic reloaded: Theoretical models bringing chemotherapy into the era of precision medicine. In *Seminars in cancer biology*, volume 35, pages 53 – 61. Elsevier, 2015. doi:10.1016/j.semcancer.2015.09.002.

[88] M. Schwab. *Encyclopedia of Cancer*. Sage reference. Springer-Verlag Berlin Heidelberg, 3ed. edition, 2011. ISBN:978-3-642-16483-5.

[89] H. E. Skipper. On mathematical modeling of critical variables in cancer treatment (goals: Better understanding of the past and better planning in the future). *Bulletin of Mathematical Biology*, 48 (3):253 – 278, 1986. ISSN 0092-8240. doi:10.1016/S0092-8240(86)90027-3.

[90] L. Norton and R. Simon. Tumor size, sensitivity to therapy, and design of treatment schedules. *Cancer treatment reports*, 61(7):1307, 1977. PMID:589597.

[91] J. Goldie and A. Coldman. A mathematic model for relating the drug sensitivity of tumors to their spontaneous mutation rate. *Cancer treatment reports*, 63(11-12):1727–1733, 1979. ISSN 0361-5960. PMID:526911.

[92] L. Norton and R. Simon. The norton-simon hypothesis revisited. *Cancer treatment reports*, 70(1): 163, 1986. PMID:3510732.

[93] J. J. Westman, B. R. Fabijonas, D. L. Kern, and F. B. Hanson. Probabilistic rate compartment cancer model: Alternate versus traditional chemotherapy scheduling. In B. Pasik-Duncan, editor, *"Stochastic Theory and Control: Proceedings of a Workshop held in Lawrence, Kansas"*, pages 491–506. Springer Berlin Heidelberg, 2002. ISBN 978-3-540-48022-8. doi:10.1007/3-540-48022-6_33.

[94] L. E. Harnevo and Z. Agur. Drug resistance as a dynamic process in a model for multistep gene amplification under various levels of selection stringency. *Cancer Chemotherapy and pharmacology*, 30(6):469–476, Nov 1992. ISSN 1432-0843. doi:10.1007/BF00685599.

[95] M. Kimmel and D. Axelrod. *Branching Processes in Biology*, volume 19 of *Interdisciplinary Applied Mathematics*. Springer-Verlag New York, 2^{nd} edition, 2015. ISBN 9781493915590. doi:10.1007/978-1-4939-1559-0.

[96] J. Goldie and A. Coldman. *Drug Resistance in Cancer: Mechanisms and Models*. Cambridge University Press, 1998. ISBN:9780521482738.

[97] M. Kimmel, A. Swierniak, and A. Polanski. Infinite-dimensional model of evolution of drug resistance of cancer cells. *Journal of Mathematical Systems Estimation and Control*, 8(1):1–16, 01 1998.

[98] A. Swierniak and J. Smieja. Cancer chemotherapy optimization under evolving drug resistance. *Nonlinear Analysis: Theory, Methods & Applications*, 47(1):375–386, 2001. ISSN 0362-546X.

[99] A. Lorz, T. Lorenzi, M. E. Hochberg, J. Clairambault, and B. Perthame. Populational adaptive evolution, chemotherapeutic resistance and multiple anti-cancer therapies. *ESAIM: Mathematical Modelling and Numerical Analysis*, 47(2):377–399, 2013. doi:10.1051/m2an/2012031.

[100] A. Lorz, T. Lorenzi, J. Clairambault, A. Escargueil, and B. Perthame. Modeling the effects of space structure and combination therapies on phenotypic heterogeneity and drug resistance in solid tumors. *Bulletin of Mathematical Biology*, 77(1):1–22, 2015. ISSN 1522-9602. doi:10.1007/s11538-014-0046-4.

[101] J. Greene, O. Lavi, M. M. Gottesman, and D. Levy. The impact of cell density and mutations in a model of multidrug resistance in solid tumors. *Bulletin of Mathematical Biology*, 76(3):627–653, 2014. ISSN 1522-9602. doi:10.1007/s11538-014-9936-8.

[102] O. Lavi, J. M. Greene, D. Levy, and M. M. Gottesman. The role of cell density and intratumoral heterogeneity in multidrug resistance. *Cancer Research*, 73(24):7168–7175, 2013. ISSN 0008-5472. doi:10.1158/0008-5472.CAN-13-1768.

[103] U. Ledzewicz, S. Wang, H. Schattler, N. Andre, M. A. Heng, and E. Pasquier. On drug resistance and metronomic chemotherapy: A mathematical modeling and optimal control approach. *Mathematical biosciences and engineering: MBE*, 14(1):217–235, February 2017. ISSN 1547-1063. doi:10.3934/mbe.2017014.

[104] L. G. de Pillis and A. E. Radunskaya. Modeling tumor–immune dynamics. In A. Eladdadi, P. Kim, and D. Mallet, editors, *Mathematical Models of Tumor-Immune System Dynamics*, pages 59–108. Springer New York, New York, NY, 2014. ISBN 978-1-4939-1793-8. doi:10.1007/978-1-4939-1793-8_4.

[105] K. P. Wilkie. A review of mathematical models of cancer–immune interactions in the context of tumor dormancy. In H. Enderling, N. Almog, and L. Hlatky, editors, *Systems Biology of Tumor Dormancy*, pages 201–234. Springer New York, New York, NY, 2013. ISBN 978-1-4614-1445-2. doi:10.1007/978-1-4614-1445-2_10.

[106] N. Stepanova. Course of the immune reaction during the development of a malignant tumor. *Biophysics*, 24(1):220–235, 1980.

[107] S. Michelson, B. Miller, A. Glicksman, and J. Leith. Tumor micro-ecology and competitive interactions. *Journal of Theoretical Biology*, 128(2):233 – 246, 1987. ISSN 0022-5193. doi:10.1016/S0022-5193(87)80171-6.

[108] S. Michelson and J. T. Leith. Growth factors and growth control of heterogeneous cell populations. *Bulletin of Mathematical Biology*, 55(5):993 – 1011, 1993. ISSN 0092-8240. doi:10.1016/S0092-8240(05)80200-9.

[109] H. P. de Vladar and J. A. González. Dynamic response of cancer under the influence of immunological activity and therapy. *Journal of Theoretical Biology*, 227(3):335 –348, 2004. ISSN 0022-5193. doi:10.1016/j.jtbi.2003.11.012.

[110] U. Foryś, J. Waniewski, and P. Zhivkov. Anti-tumor immunity and tumor anti-immunity in a mathematical model of tumor immunotherapy. *Journal of Biological Systems*, 14(01):13–30, 2006. doi:10.1142/S0218339006001702.

[111] V. A. Kuznetsov, I. A. Makalkin, M. A. Taylor, and A. S. Perelson. Nonlinear dynamics of immunogenic tumors: Parameter estimation and global bifurcation analysis. *Bulletin of Mathematical Biology*, 56(2):295 – 321, 1994. ISSN 0092-8240. doi:10.1016/S0092-8240(05)80260-5.

[112] M. Gałach. Dynamics of the tumor-immune system competition—the effect of time delay. *International Journal of Applied Mathematics and Computer Science*, 13(3):395–406, 2003. doi:10.1.1.390.3004.

[113] O. Sotolongo-Costa, L. M. Molina, D. R. Pérez, J. Antoranz, and M. C. Reyes. Behavior of tumors under nonstationary therapy. *Physica D: Nonlinear Phenomena*, 178(3):242 –253, 2003. ISSN 0167-2789. doi:10.1016/S0167-2789(03)00005-8.

[114] L. D. Pillis and A. Radunskaya. A mathematical tumor model with immune resistance and drug therapy: an optimal control approach. *Computational and Mathematical Methods in Medicine*, 3 (2):79–100, 2001. doi:10.1080/10273660108833067.

[115] L. G. De Pillis and A. Radunskaya. The dynamics of an optimally controlled tumor model: A case study. *Mathematical and Computer Modelling*, 37(11):1221–1244, 2003. ISSN 0895-7177. doi:10.1016/S0895-7177(03)00133-X.

[116] M. R. Owen and J. A. Sherratt. Modelling the macrophage invasion of tumours: effects on growth and composition. *Mathematical Medicine and Biology: A Journal of the IMA*, 15(2):165–185, 1998. doi:10.1093/imammb/15.2.165.

[117] D. Kirschner and J. C. Panetta. Modeling immunotherapy of the tumor–immune interaction. *Journal of Mathematical Biology*, 37(3):235–252, Sep 1998. ISSN 1432-1416. doi:10.1007/s002850050127.

[118] J. Arciero, T. Jackson, and D. Kirschner. A mathematical model of tumor-immune evasion and sirna treatment. *Discrete and Continuous Dynamical Systems – Series B*, 4(1):39–58, 2004. ISSN 1531-3492. doi:10.3934/dcdsb.2004.4.39.

[119] L. de Pillis and A. Radunskaya. A mathematical model of immune response to tumor invasion. pages 1661 – 1668, 2003. doi:10.1016/B978-008044046-0.50404-8.

[120] L. G. de Pillis, A. E. Radunskaya, and C. L. Wiseman. A validated mathematical model of cell-mediated immune response to tumor growth. *Cancer Research*, 65(17):7950–7958, 2005. ISSN 0008-5472. doi:10.1158/0008-5472.CAN-05-0564.

[121] N. Kronik, Y. Kogan, V. Vainstein, and Z. Agur. Improving alloreactive ctl immunotherapy for malignant gliomas using a simulation model of their interactive dynamics. *Cancer Immunology, Immunotherapy*, 57(3):425–439, 2008. ISSN 1432-0851. doi:10.1007/s00262-007-0387-z.

[122] A. Cappuccio, M. Elishmereni, and Z. Agur. Cancer immunotherapy by interleukin-21: Potential treatment strategies evaluated in a mathematical model. *Cancer Research*, 66(14):7293–7300, 2006. ISSN 0008-5472. doi:10.1158/0008-5472.CAN-06-0241.

[123] F. Castiglione and B. Piccoli. Cancer immunotherapy, mathematical modeling and optimal control. *Journal of Theoretical Biology*, 247(4):723–732, 2007. ISSN 0022-5193. doi:10.1016/j.jtbi.2007.04.003.

[124] R. J. De Boer, P. Hogeweg, H. F. Dullens, R. A. De Weger, and W. Den Otter. Macrophage t lymphocyte interactions in the anti-tumor immune response: a mathematical model. *The Journal of Immunology*, 134(4):2748–2758, 1985. ISSN 0022-1767. PMID:3156189.

[125] M. Villasana and A. Radunskaya. A delay differential equation model for tumor growth. *Journal of Mathematical Biology*, 47(3):270–294, 2003. ISSN 1432-1416. doi:10.1007/s00285-003-0211-0.

[126] A. Diefenbach, E. R. Jensen, A. M. Jamieson, and D. H. Raulet. Rae1 and h60 ligands of the nkg2d receptor stimulate tumour immunity. *Nature*, 413(6852):165–171, 2001. doi:10.1038/35093109.

[127] A. E. Bryson. Optimal control-1950 to 1985. *IEEE Control Systems*, 16(3):26–33, Jun 1996. ISSN 1066-033X. doi:10.1109/37.506395.

[128] H. J. Sussmann and J. C. Willems. 300 years of optimal control: from the brachystochrone to the maximum principle. *IEEE Control Systems*, 17(3):32–44, Jun 1997. ISSN 1066-033X. doi:10.1109/37.588098.

[129] A. V. Rao. A survey of numerical methods for optimal control. *Advances in the Astronautical Sciences*, 135(1):497–528, 2009. doi:10.1.1.661.6337.

[130] H. Schättler and U. Ledzewicz. *Geometric Optimal Control: Theory, Methods and Examples*, volume 38 of *Interdisciplinary Applied Mathematics*. Springer New York, 1^{nd} edition, 2012. ISBN 978-1-4614-3834-2. doi:10.1007/978-1-4614-3834-2.

[131] H. Schättler and U. Ledzewicz. The pontryagin maximum principle: From necessary conditions to the construction of an optimal solution. In *Geometric Optimal Control: Theory, Methods and Examples*, pages 83–194. Springer New York, New York, NY, 2012. ISBN 978-1-4614-3834-2. doi:10.1007/978-1-4614-3834-2_2.

[132] H. Schättler and U. Ledzewicz. Optimal control for problems with a quadratic cost functional on the therapeutic agents. In *Optimal Control for Mathematical Models of Cancer Therapies: An Application of Geometric Methods*, chapter 4, pages 141–170. Springer New York, 2015. doi:10.1007/978-1-4939-2972-6_4.

[133] H. Robbins. A generalized legendre-clebsch condition for the singular cases of optimal control. *IBM Journal of Research and Development*, 11(4):361–372, 1967. doi:10.1147/rd.114.0361.

[134] H. S. Rodrigues, M. T. T. Monteiro, and D. F. Torres. Optimal control and numerical software: an overview. In F. Miranda, editor, *Systems Theory: Perspectives, Applications and Developments*, chapter 6. Nova Science Publishers, 2014. ISBN:978-1-63117-876-4.

[135] A. Bryson. *Applied Optimal Control: Optimization, Estimation and Control*. Halsted Press book'. Taylor & Francis. ISBN 9780891162285. ISBN:9780891162285.

[136] X. Wang. Solving optimal control problems with matlab — indirect methods. pages 1–21, 11 2017. here.

[137] A. Yates and R. Callard. Cell death and the maintenance of immunological memory. *Discrete and Continuous Dynamical Systems - Series B*, 1(1):43–60, 2001. ISSN 1531-3492. doi:10.3934/dcdsb.2001.1.43.

[138] A. Lanzavecchia and F. Sallusto. Dynamics of t lymphocyte responses: Intermediates, effectors, and memory cells. *Science*, 290(5489):92–97, 2000. ISSN 0036-8075. doi:10.1126/science.290.5489.92.

[139] M. Perry. *The Chemotherapy Source Book*. Lippincott Williams & Wilkins, 2001. ISBN:9780781723633.

[140] P. Calabresi and P. Schein. *Medical Oncology: Basic Principles and Clinical Management of Cancer*. Medical Oncology: Basic Principles and Clinical Management of Cancer. McGraw-Hill, Health Professions Division, 1993. ISBN:9780071054089.

[141] J. V. Frangioni. New technologies for human cancer imaging. *Journal of clinical oncology*, 26(24): 4012–4021, 2008. doi:10.1200/JCO.2007.14.3065.

[142] A. Ghaffari and N. Naserifar. Optimal therapeutic protocols in cancer immunotherapy. *Computers in Biology and Medicine*, 40(3):261 – 270, 2010. ISSN 0010-4825. doi:10.1016/j.compbiomed.2009.12.001.

[143] E. M. Voisin, M. Ruthsatz, J. M. Collins, and P. C. Hoyle. Extrapolation of animal toxicity to humans: Interspecies comparisons in drug development. *Regulatory Toxicology and Pharmacology*, 12(2): 107 – 116, 1990. ISSN 0273-2300. doi:10.1016/S0273-2300(05)80052-2.

[144] H. Schättler and U. Ledzewicz. Cell cycle specific cancer chemotherapy for homogeneous tumors. In *Optimal Control for Mathematical Models of Cancer Therapies: An Application of Geometric Methods*, chapter 2, pages 41–114. Springer New York, 2015. doi:10.1007/978-1-4939-2972-6_2.

[145] L. B. Almeida. Multilayer perceptrons. In E. Fiesler and R. Beale, editors, *Handbook of Neural Computation*, The Computational Intelligence Library. Institute of Physics and Oxford University Press, New York, New York, 1996. ISBN 0-7503-0312–3 and 0-7503-0413-8. Available here.

[146] M. Engelhart, D. Lebiedz, and S. Sager. Optimal control for selected cancer chemotherapy ode models: a view on the potential of optimal schedules and choice of objective function. *Mathematical Biosciences*, 229(1):123–134, 2011. ISSN 0025-5564. doi:10.1016/j.mbs.2010.11.007.

[147] H. Schättler and U. Ledzewicz. Optimal control: A review of main results and concepts. In *Optimal Control for Mathematical Models of Cancer Therapies: An Application of Geometric Methods*, chapter A, pages 385–422. Springer New York, 2015. doi:10.1007/978-1-4939-2972-6.

[148] T. Reid, S. Dad, R. Korn, B. Oronsky, S. Knox, and J. Scicinski. Two case reports of resensitization to previous chemotherapy with the novel hypoxia-activated hypomethylating anticancer agent rrx-001 in metastatic colorectal cancer patients. *Case reports in oncology*, 7(1):79–85, 2014. doi:10.1159/000358382.

[149] M. S. I. Abaza, K. Y. Orabi, E. Al-Quattan, and R. J. Al-Attiyah. Growth inhibitory and chemosensitization effects of naringenin, a natural flavanone purified from thymus vulgaris, on human

breast and colorectal cancer. *Cancer Cell International*, 15(1):46, Apr 2015. ISSN 1475-2867. doi:10.1186/s12935-015-0194-0.

[150] C. E. Meacham and S. J. Morrison. Tumour heterogeneity and cancer cell plasticity. *Nature*, 501 (7467):328–337, 2013. doi:10.1038/nature12624.

Appendix A

Validation of Algorithm B and D

In this appendix, the results from the validation of algorithms B and D, discussed in 5.3, are presented together with the correspondent solution found in the literature.

A.1 Algorithm B

The application of algorithm B to the optimal control problem formulated in Schättler and Ledzewicz [144, p.48–65], has resulted in figure A.1.

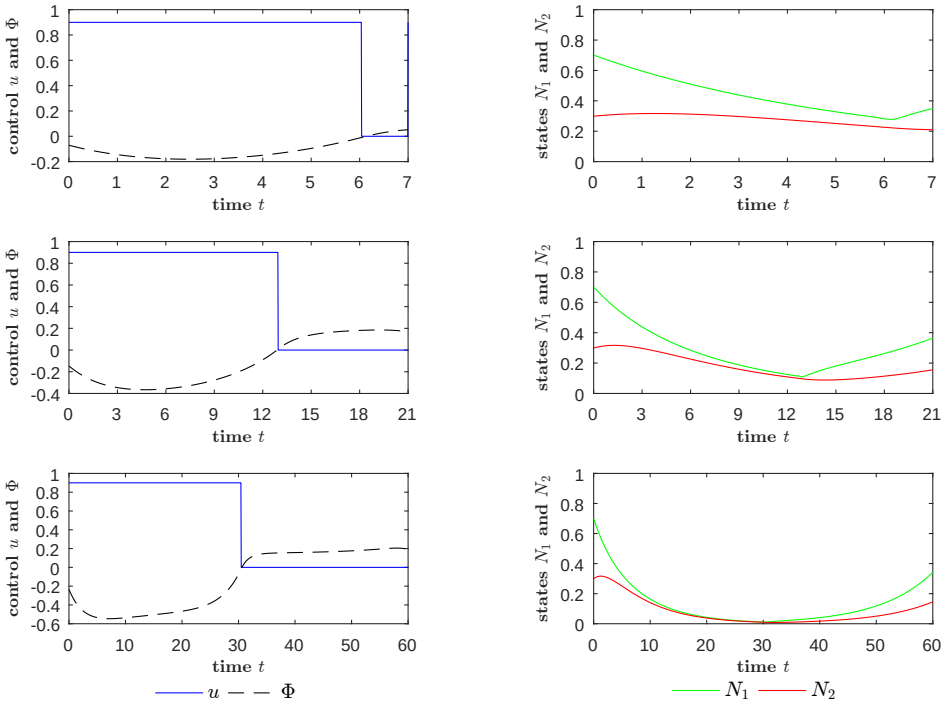

Figure A.1: Validation of the algorithm B using three known optimal solutions [144, p.48–65]. Control parameters: $N_{int} = 1000$, $w_2 = 0.225$, $\varepsilon_1 = \varepsilon_2 = 10^{-10}$. First row: $N_s = 15$, $w_1 = 0.95$, $\varepsilon_3 = \varepsilon_4 = 0.25$. Second row: $N_s = 30$, $w_1 = 0.8$, $\varepsilon_3 = \varepsilon_4 = 0.50$. Third row:$N_s = 60$, $w_1 = 0.8$, $\varepsilon_3 = \varepsilon_4 = 0.50$.

Figure A.2 represents the solution presented in the literature for the same optimal control problem.

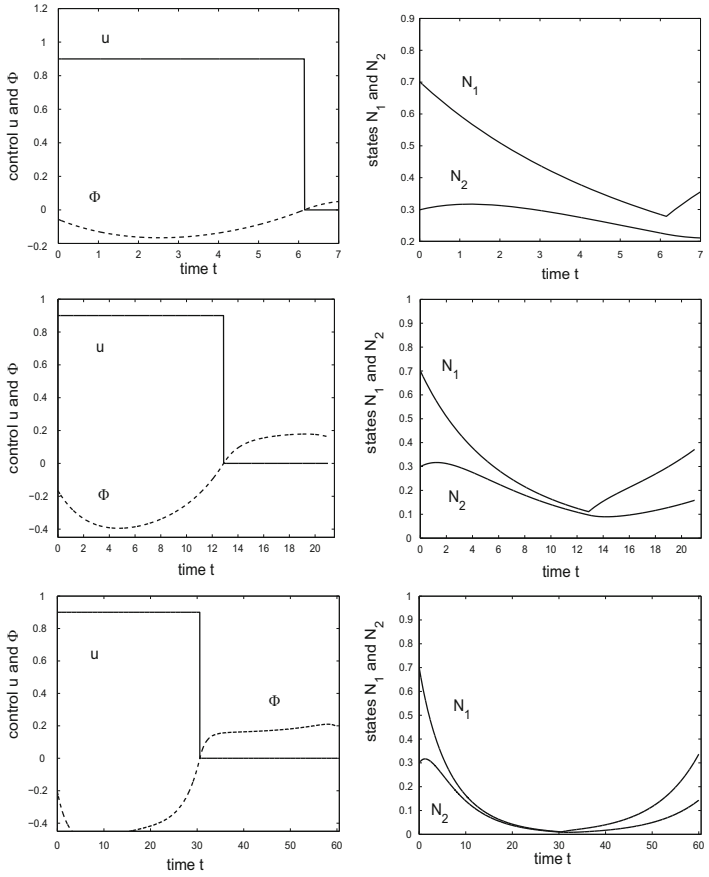

Fig. 2.4 Examples of locally optimal controls (left) and their corresponding trajectories (right) for $T = 7$ (top), $T = 21$ (middle) and $T = 60$ (bottom) from the steady-state solution (2.6) for the parameter values given in Table 2.1.

Figure A.2: Literature solution of the optimal control problem formulated in Schättler and Ledzewicz [144, p.48–65] presented in the literature [144].

A.2 Algorithm D

Algorithm D was also applied to a control problem formulated in [132, p.158–161], resulting in figure A.3. The solution presented in [132, p.159] and [132, p.160] is given by figures A.4 and A.4 left side. The right side concerns the minimization of a linear objective.

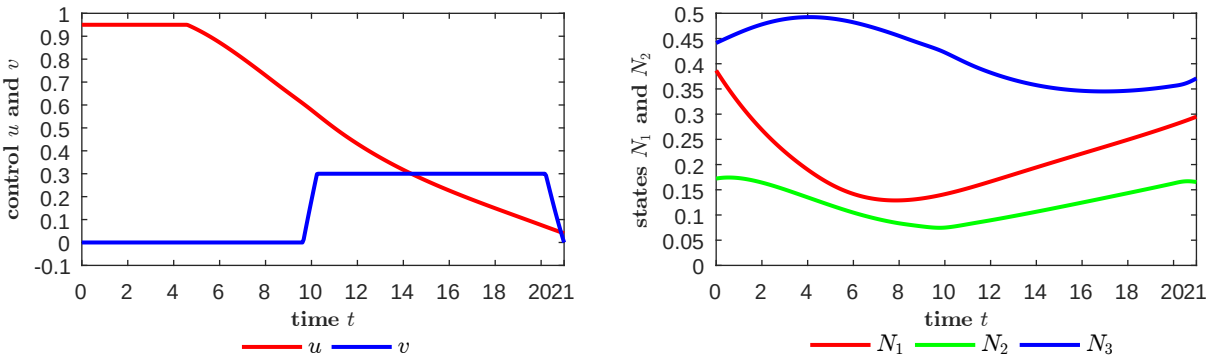

Figure A.3: Validation of the algorithm D using a known optimal solution [132, p.158–160]. Control parameters: $N_{int} = 400$, $w_1 = 1.20$, $w_2 = 0.95$, $w_3 = 0.98$, $w_4 = 9 \times 10^{-4}$, $\varepsilon_1 = \varepsilon_2 = \varepsilon_3 = 10^{-10}$.

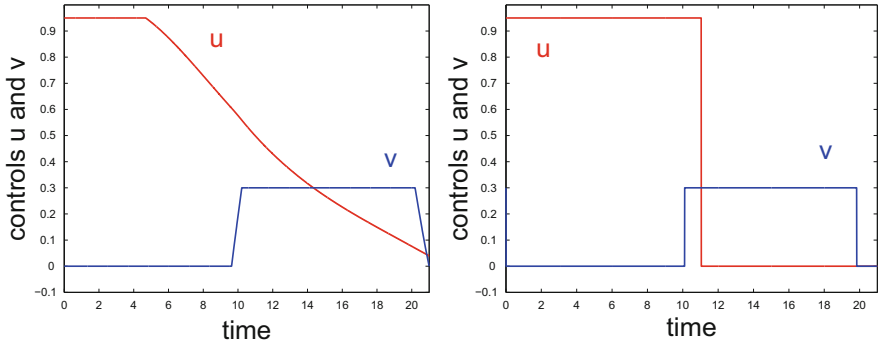

Fig. 4.1 Locally optimal controls (with the cytotoxic agent u shown in red and the cytostatic agent v shown in blue) for the objectives J_2 (left) and J_1 (right)

Figure A.4: Literature solution of the optimal control problem formulated in [132, p.158–160] (left side).

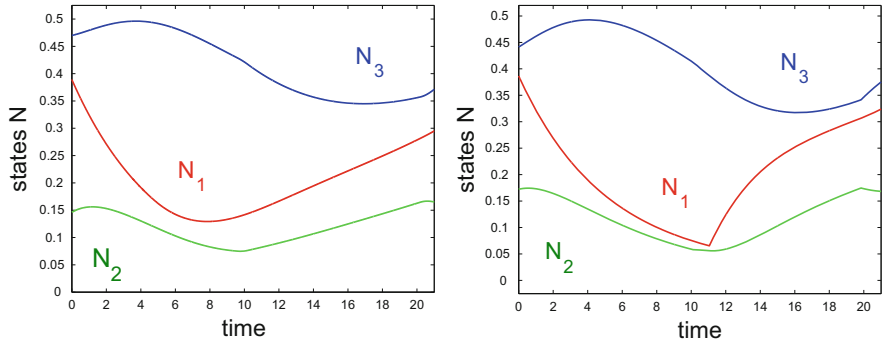

Fig. 4.2 Locally optimal controlled trajectories for the objectives J_2 (left) and J_1 (right)

Figure A.5: Dynamic response to the literature solution of the optimal control problem (left side) formulated in [132, p.158–160]

.